MOUNTAIN-PLAINS CONSORTIUM

MPC 21-436 | C. Pantelides and D. Thapa

Self-Centering Bridge Bent for Accelerated Bridge Construction

MOUNTAIN-PLAINS CONSORTIUM REGION 8

A University Transportation Center sponsored by the U.S. Department of Transportation serving the Mountain-Plains Region. Consortium members:

Colorado State University
North Dakota State University
South Dakota State University
University of Colorado Denver
University of Denver
University of Utah
Utah State University
University of Wyoming

Technical Report Documentation Page

1. Report No.	2. Government Accession No.	3. Recipient's Catalog No.
MPC-545		

4. Title and Subtitle	5. Report Date
Self-Centering Bridge Bent for Accelerated Bridge Construction	July 2021
	6. Performing Organization Code

7. Author(s)	8. Performing Organization Report No.
C.P. Pantelides D. Thapa	MPC 21-436

9. Performing Organization Name and Address	10. Work Unit No. (TRAIS)
University of Utah Salt Lake City, UT 84112	11. Contract or Grant No.

12. Sponsoring Agency Name and Address	13. Type of Report and Period Covered
Mountain-Plains Consortium North Dakota State University PO Box 6050, Fargo, ND 58108	Final Report
	14. Sponsoring Agency Code

15. Supplementary Notes

Supported by a grant from the US DOT, University Transportation Centers Program

16. Abstract

Precast concrete construction has been proven to be very efficient in bridge engineering, especially in accelerated bridge construction (ABC), where precast concrete components are connected to save time and minimize disruption of traffic. Post-tensioned (PT) concrete structural elements when combined with energy dissipators (ED) create a hybrid system which ensures self-centering, energy dissipation, and minimum residual drift. The present study investigates the connection of precast concrete elements with unbonded post-tensioned bars and stretch length anchors (SLA) and their seismic performance. This study consists of the construction of a precast concrete bridge bent consisting of two footings, two columns, and a cap beam; the bridge bent was tested under quasi-static cyclic load. The scaled bridge bent is a 42% scale model of the Riverdale Bridge, located over I-80 in Utah. Post-tensioned bars connect the cap-beam, columns, and footings, whereas the SLAs connect the cap-beam to the columns, and the columns to the footings. The SLAs are not part of the existing bridge.

The tested bridge bent performed very well under cyclic loads with good re-centering, minimum residual displacement, good energy dissipation, and minimal damage to the structure. SLAs yielded early and displayed good energy dissipation. Initially stressed post-tensioned bars played an important role in self-centering of the bridge bent and only yielded at the end of the test. Gap opening in the precast bridge bent avoided damage of concrete in the plastic hinge region.

17. Key Word	18. Distribution Statement
bents, bridge construction, columns, earthquake resistant design, posttensioning, seismicity	Public distribution

19. Security Classif. (of this report)	20. Security Classif. (of this page)	21. No. of Pages	22. Price
Unclassified	Unclassified	95	n/a

SELF-CENTERING BRIDGE BENT FOR ACCELERATED BRIDGE CONSTRUCTION

Chris P. Pantelides
Professor

Dipendra Thapa
Graduate Student

Department of Civil and Environmental Engineering
The University of Utah

July 2021

Acknowledgments

The authors acknowledge the financial support provided by the Mountain-Plains Consortium (MPC) under project MPC-545.

Disclaimer

ABSTRACT

Precast concrete construction has been proven to be very efficient in bridge engineering, especially in accelerated bridge construction (ABC), where precast concrete components are connected to save time and minimize disruption of traffic. Post-tensioned (PT) concrete structural elements, when combined with energy dissipators (ED), create a hybrid system that ensures self-centering, energy dissipation, and minimum residual drift. This study investigates the connection of precast concrete elements with unbonded post-tensioned bars and stretch length anchors (SLA) and their seismic performance. This study consists of the construction of a precast concrete bridge bent, consisting of two footings, two columns, and a cap beam; the bridge bent was tested under quasi-static cyclic load. The scaled bridge bent is a 42% scale model of the Riverdale Bridge, located over I-80 in Utah. Post-tensioned bars connect the cap-beam, columns, and footings, whereas the SLAs connect the cap-beam to the columns, and the columns to the footings. The SLAs are not part of the existing bridge.

The tested bridge bent performed well under cyclic loads with good recentering, minimum residual displacement, good energy dissipation, and minimal damage to the structure. SLAs yielded early and displayed good energy dissipation. Initially, stressed post-tensioned bars played an important role in self-centering of the bridge bent and only yielded at the end of the test. Gap opening in the precast bridge bent avoided damage of concrete in the plastic hinge region.

A computational model was developed and validated with the experimental results to investigate further the application of such a system in full-scale bridges. An elastic perfectly plastic gap material was used to simulate the gap opening phenomenon in the precast post-tensioned system. A force-based beam-column element with fiber sections was used to model the columns, whereas the cap-beam was assumed to remain elastic. SLAs were modeled as tension only bilinear material. Based on the lateral strength, energy dissipation capacity, self-centering capability, and minimum residual drift, the bridge structure was found to be a promising application in high-seismic regions.

TABLE OF CONTENTS

LIST OF FIGURES

LIST OF TABLES

EXECUTIVE SUMMARY

The research addresses a new hybrid bridge system for accelerated bridge construction in seismic regions. An experiment was carried out of a 42% scale precast, unbonded post-tensioned two-column bridge bent, with external energy dissipators to evaluate its seismic and rocking behavior. The external energy dissipators were SLAs attached from the footings to the columns and the columns to the cap-beam. The specimen displayed good lateral strength under the given quasi-static cyclic loads and the hysteresis curves were stable and symmetric. Column rocking was controlled without large rotations or stability problems. Steel chairs holding the SLAs performed elastically and were not damaged. The SLAs yielded in tension and bending and elongated. The combination of axial load and post-tensioning forces was able to re-center the bridge bent; the residual drift ratio was 1.1%. Three of the post-tensioning bars yielded by the last drift ratio of 6.0% imposed in the experiment. The bridge system experienced little damage. Concrete spalling over the bottom of both columns was observed but it was not significant and did not compromise strength. By comparing the experimental results with the analytical model developed, it is evident that the analytical model was capable of capturing the initial stiffness, lateral strength, hysteretic energy dissipation, and post-tensioned bar forces with good accuracy. This is the first time unbonded post-tensioned bars are combined with SLAs in a hybrid bridge system. The replaceable feature of the SLAs makes the system seismically resilient which means that the bridge can recover after an earthquake and be functional quickly. Given the observed residual displacement, lateral strength, hysteretic energy dissipation, and minimal damage, it is recommended that the hybrid bridge bent can be used in accelerated construction of bridges in seismic zones.

LIST OF ACRONYMS

AASHTO	American Association of State Highway and Transportation Officials
ABC	Accelerated Bridge Construction
ACI	American Concrete Institute
ASTM	American Society of Testing and Materials
FHWA	Federal Highway Administration
PBES	Prefabricated Bridge Element and Systems
SEI	Structural Engineering Institute
IAT	Industrial Assessment Team
SLA	Stretch Length Anchor
GSS	Grouted Splice Sleeve Connectors
PRESS	Precast Seismic Structural System
DFRCC	Ductile Fiber Reinforced Cement based Concrete
PT	Post-tension
ED	Energy Dissipators
CFT	Concrete Filled Tube
HSR	Hybrid Sliding Rocking
MDCR	Multi Performance Dissipative Controlled Rocking
DCR	Damaged Controlled Rocking
PU	Polyurethane
LVDT	Linear Variable Differential Transducer
OpenSeeS	Open System for Earthquake Engineering Simulation
UDOT	Utah Department of Transportation

1. INTRODUCTION

Accelerated bridge construction (ABC) refers to the bridge construction method that uses innovative technologies, materials, and construction methods to ensure cost-effectiveness and work-zone safety by reducing construction time with minimal traffic disruption when building new bridges (WisDOT 2019). Accelerated bridge construction promotes innovative bridge design and construction, increases the quality of construction work, minimizes weather-related delays, and reduces impact on the environment, especially when construction is over waterways. One of the five methods emphasized for ABC by the Federal Highway Administration (FHWA) is Prefabricated Bridge Elements and Systems (PBES), where the structural components of the bridge or bridge system are constructed off-site, or near the bridge site and are transported for installation; this effectively reduces construction time and disturbance to traffic mobility. Construction of bridges using ABC is completed within hours, days, or weeks, depending on the nature of the ABC technique employed; whereas, conventional methods of bridge construction take months to years for completion. The number of on-site construction activities, including the tying of reinforcing steel, formwork preparation, concrete casting, and curing of different bridge components, can be carried out off-site (Wacker et al. 2005). Furthermore, the construction of precast elements such as bridge piers, concrete deck panels, girders, abutments, pier caps, and other substructure/superstructure components is performed off-site in a more controlled environment, which enhances the quality of construction. Accelerated construction of bridges often results in an increased initial cost of the project, but this cost can be offset by minimizing repair and maintenance costs over the long run (WisDOT 2019).

Many bridges in the United States are constructed or rehabilitated using ABC techniques. The same is true in Utah. The I-80 Eastbound bridge at Atkinson Canyon, the Summit Park Bridge over I-80, the bridge over Weber River at Echo Junction, the SR-66 bridge over Weber River in Morgan City, the Pioneer Crossing in Lehi, the South Layton Interchange over I-15, the Proctor Lane over I-15, the F-762 bridge on US-6 at approximately MP 220, and the Sam White Lane Bridge over I-15, etc. are a few of the bridges constructed using ABC methodologies (UDOT).

The connection between precast elements is critical and plays a significant role in the bridge's performance in seismic zones. Various research efforts are ongoing to configure different connection details, their effectiveness, and usability. Ductility, reparability, and lateral load capacity are three significant acceptance criteria for any bridge located in a seismic region (Ameli 2016). Typical connection types include: grouted reinforcing splice couplers, grouted post-tensioning (PT) ducts, grouted voids, traditional post-tensioning (PT), welded connections, bolted connections, and cast-in-place concrete closure pours that are commonly used in concrete elements (Culmo 2009).

1.1 Development of Stretch Length Anchors (SLAs)

Steel anchorage in the form of all-threaded rods and SLAs is used for providing ductility for non-building structures, including tanks, chimneys, braced frames, and vertical vessels. Observations from post-earthquake investigations by the Structure Engineering Institute (SEI) Industrial Assessment Team (IAT) showed that in the 2010 Maule earthquake in Chile, prominent

structural, foundation, and connection damage was attributed to anchor fracture (Soules et al. 2016). However, the IAT also noticed that base connections incorporating SLAs did not experience bolt fracture and showed substantial inelastic deformation without failure. The stretch length provided in these systems ranged from eight to 16 bolt diameters. Based on the good performance of industrial structures having SLAs in significant historical earthquakes, ACI 318 requires the minimum stretch length to be at least eight times the bolt diameter. However, this value is not based on theoretical or analytical basis (Parks et al. 2019).

The stretch length of an anchor refers to the length along which plastic deformation is expected to occur. Bolts enhance the ductility of the system and are more useful in those structures where ductility and energy dissipation cannot be easily integrated (Trautner et al. 2017). ACI 318-14 requires tensile elongation of at least 14%, load reduction of at least 30%, and meeting the requirements of ASTM A307 for a steel element to be considered ductile. Trautner et al. (2014) studied the effect of various stretch lengths (3.5 to 8.0 bar diameter) for anchors at the column base of a seismic force-resisting system, where debonding was provided either by debonding the length inside the concrete or in the chairs above the concrete surface, made of steel plates. It was found that the rotation capacity of the structure increased by 30% when the stretch length of the anchorage increased from 3.5 to 8.0 bar diameters. Trautner et al. (2017) performed more than 90 tension tests on headed and all-threaded anchors to determine the relationship between stretch length and anchor deformation capacity and found that a more ductile material experiences a large increase in deformation capacity as the stretch length increases. Furthermore, they developed a rational framework for designing stretch length as an alternative to ACI 318-14 requirements.

Parks et al. (2019) performed extensive research on SLAs and examined and tested the cyclic performance of 34 individual ductile anchor bolts with stretch lengths of four, six, and eight-bar diameters under combined tension and shear loads. The single anchor tests were performed with varying anchor stretch length, shear-to-tension displacement ratio, and thickness of steel chair (elastic and yielding chairs); the results were compared with hex-headed conventional anchors. The bolts had a ¾ in. diameter and were made with ASTM F1554 Grade 36 steel. Even though the ultimate tensile force and shear force capacity of the bolts were similar to conventional bolts, tensile displacement capacity of the anchor at failure increased 2.2 times compared to conventional anchors with elastic chairs and 1.9 times compared to conventional bolts with yielding chairs. This significantly increased the ductility of the bolts and connection without compromising shear or tension capacity. In addition, the smooth shank of the bolt encouraged yielding to spread more efficiently and improve effectiveness of stretch length bolts; this is unlike conventional anchors where the free shank of the bolt is threaded. Parks et al. (2019) studied the effect of elastic and yielding chairs for SLAs and found that yielding steel chairs increase the tensile displacement capacity due to bending of the top/bottom steel plate. The bending of the plates damages the yielding steel chairs permanently and requires their replacement after a seismic event. At a higher ratio of shear-to-tension force, the tensile failure displacement was reduced.

1.2 Common ABC Connections in Seismic Zones

Various types of connections have been developed for ABC in seismic zones: grouted duct, pocket, socket, grouted splice sleeve, and bonded/unbonded post-tensioning with energy dissipators are some of the most commonly used connection types.

The grouted duct connection is one of the viable options for precast concrete connections. In the grouted duct connection, corrugated steel ducts are accommodated within the footing or cap-beam, and the projected column reinforcement is inserted and grouted inside the ducts. Raynor et al. (2002) investigated the bond-slip behavior of reinforcing bars grouted in ducts. Similarly, investigation of different embedment depths of galvanized steel in plastic tubes found that the duct material has an effect on failure of the specimens (Brenes et al. 2006). Experimental and analytical studies recommended using the anchorage length of six to 10 times the bar diameter to achieve bar yielding and fracture, respectively (Steuck et al. 2009). Similarly, Pang et al. (2010) investigated four 40% scale precast cap beam-to-column connections using grouted ducts and studied their cyclic response: they had a slightly lower energy dissipation capacity compared to a similar monolithic specimen, partial debonding was found to be ineffective, and bar fracture occurred in all four specimens. Ultra-high-performance concrete was used as the grout for duct connections with partial debonding of rebar. This specimen was better than cast-in-place in terms of strength, displacement capacity, and hysteretic performance (Tazarv and Saiidi 2015).

Another type of precast connection method is the pocket connection in which a circular corrugated steel duct is accommodated inside the cap beam to form the pocket, and the projected column bars are inserted in the pocket, which is filled with concrete. The pocket connection displayed good seismic performance. Motaref et al. (2011) performed shake table tests of a 30% scale precast two-column bent. The columns of the bent were embedded into footings using pocket connections. The embedment length of the column was equal to 1.5 times the column diameter. The specimen was tested to failure, and the connection developed the full moment capacity without damage to the connection. Research on pocket connections with octagonal pockets and embedment depths of 1.5 times the column diameter displayed satisfactory performance and behaved as a monolithic connection (Mehrsoroush 2014).

A socket connection is a new concept developed for connecting a spread footing to precast bridge columns where a precast column is first erected, and the reinforced concrete footing is cast around it (Haraldsson et al. 2013). Khaleghi et al. (2012) studied the precast socket connection under cyclic lateral load and found that it performed well, even better than a comparable cast-in-place system. Haraldsson et al. (2013) studied a 42% scale of the prototype bridge with socket connections where varying parameters of footing reinforcement and socket depths were studied. All three specimens behaved well compared to the cast-in-place specimen, and these connections were recommended. Similar research has been performed by Wang et al. (2019) who studied, both experimentally and numerically, seismic performance of socket and pocket connections and compared them with their cast-in-place (CIP) counterparts. Damage development and the failure mechanism were similar to the CIP specimen and had the same or even better seismic performance as CIP construction by using the high-strength-mortar-filled shear key connection. White (2014) carried out an investigation of two half-scale high damage connection specimens.

The precast column and precast footing were connected with a socket connection; one of the columns was tested under uniaxial and the other under biaxial lateral loading; both specimens performed well achieving more than 6% ultimate drift ratio, well-distributed flexural cracks, concrete spalling, and buckling of column bars.

Different rebar splicing devices, including grouted splice sleeve connectors (GSS), are considered effective connection types in ABC. GSS is a type of reinforcing bar splice composed of a ductile iron sleeve and high strength grout to connect two bars. Enhanced construction tolerance is one of the main advantages of these connectors (Ameli and Pantelides 2017). Jansson (2008) conducted a test on different available grout filled splices and studied their performance during slip, fatigue, ultimate load, and creep testing. Haber et al. (2015) performed a series of tests on the headed connector (HC) and the GSS connectors under monotonic load to investigate the stress-strain behavior of the spliced bars and found that strain capacity of the GSS connector was 35% that of the spliced bar — the bar fractured away from the coupler region. Ameli et al. (2015) conducted research on precast column-to-cap beam joints using GSS and compared their performance with an identical cast-in-place column-to-cap beam joints. The specimens with GSS and CIP had comparable strength capacity, but the displacement capacity of the GSS specimens was lower because of bar pullout due to excessive bond-slip; nevertheless, it exceeded the drift demand expected of such bridges in large earthquakes. The precast specimens achieved good ductility and curvature distribution that closely emulates CIP construction. In another study by (Ameli et al. 2016) and Ameli and Pantelides (2017), GSS was used to connect the column and footing with debonded bars in the footing. Test results showed that the precast system with debonded bars was ductile and had a longer performance life up to an 8% drift ratio, which was close to that of a similar CIP specimen.

2. POST-TENSIONED BRIDGE SYSTEMS

2.1 Precast Post-tensioned Bridge Bents

Transportation systems are the backbone of the national economy of any country. Bridges play an even more critical role in the interstate transportation system by connecting roads. Transportation systems are vulnerable during major earthquakes and are designed to prevent collapse during catastrophic events. Bridge piers are expected to undergo large inelastic deformations during strong earthquakes, which can result in permanent residual displacements. Irreparable damage due to inelastic behavior has been allowed to prevent collapse. Monolithic conventional bridges that sustain large residual displacements after earthquakes can lose their functionality (Bowman 2016). Bridges designed using a ductile design philosophy depend on plastic hinging of the bridge pier to dissipate energy. Most bridges will undergo moderate to severe damage in plastic hinge regions accompanied by residual displacement. A typical bridge may undergo minor traffic disruption up to complete demolition of the structure, depending upon the severity and extent of damage following an earthquake. Repair of the bridge pier will cost money, time, and resources with interruption of traffic for a long time; the problems get worse in busy urban roads (Cheng et al. 2017).

New construction of CIP concrete bridges requires a long period, which generally causes traffic disruption. Attention has been given to research, development, and application of precast bridge elements and systems for highway bridges over the past decade to minimize this problem. In precast system construction, activities are shifted away from the construction site to the precast yard, where quality control can be assured effectively. Elements such as slabs, girders, and piers can be transported to the construction site after they gain sufficient strength and can be assembled for faster construction, which also will ensure worker safety. Though precast construction has high initial cost during transportation of structural members from the precast factory to the construction site, the increased cost may not be crucial if the advantages of precast systems can be used correctly (Ou 2007). Engineers are reluctant to use precast technology until there is sufficient research done in any method of precast bridge construction and connection details. Therefore, it is vital to carry out rigorous research to ensure that this new technology performs better over the lifetime of a bridge and is more efficient in the long run.

Most applications of the precast system in bridges are limited to relatively low seismic zones. However, there are few precast bridge piers found in areas of high seismicity due to the concern related to their efficiency under earthquakes. The development of the connections between precast concrete components for use in seismic regions is limited. The connections between precast elements hold the utmost importance because the success of the precast concrete system in seismic areas rests on the performance of these connections and their reliability. Connection design and detailing can affect the speed of erection, structure stability, performance over time, strength, and ductility (Wacker et al. 2005).

It is essential to minimize the residual displacement of the structure to ensure its functionality after an earthquake. There are different techniques used to reduce and even eliminate residual

displacement. Seismic isolation is one of the most widely employed methods used for this purpose. Elastomeric or friction pendulum bearings isolate the response of the bridge superstructure from the support structure by concentrating the demand in the isolation plane. The pads are designed to remain elastic and re-center after removal of the load. However, this technology has a high cost and is often not economical for widespread use. Another unique yet inexpensive technique is the design of structural members that rock at the interfaces during an earthquake, i.e., at beam-column, column-footing, and footing-soil interfaces. This technique helps to eliminate residual displacement and avoids damage caused by inelastic deformation of the structure itself, i.e., plastic hinging in concrete structures (Trono 2014). Unbonded post-tensioning bars are used in precast bridge piers to re-center them after an earthquake, but the energy dissipation of such a hybrid system is very low. The use of an energy dissipator connected at the bottom of the pier ensures energy dissipation during seismic events. Several types of energy dissipation devices are being used to improve the seismic performance of bridge piers. Among these are internal mild steel bars, external replaceable energy dissipaters (Guerrini et al. 2015), high-performance steel bars, shape memory alloy bars (Chowdhury 2018), and steel angles or braces (ElGawady and Sha'lan 2010); these are used with the precast post-tensioned bridge piers to dissipate energy along with ensuring minimal residual displacement.

Traditional, bonded post-tensioning requires injection of a noncorrosive grout mix into the post-tensioning duct after tensioning, which results in the post-tensioning (PT) bar experiencing a similar amount of strain as the concrete. If the localized strain in the PT bar exceeds the yield strain, then the bar will undergo permanent elongation. Even though the yielding of a PT bar will increase its ductility by dissipating energy, the bridge pier will lose moment capacity and, eventually, its ability to re-center (Currie 2009). Unlike bonded PT bars where the PT bar is bonded to the column through grouting over its entire length, unbonded post-tensioned bars are unbonded throughout their length and are connected only at the ends. The mechanism ensures uniform distribution of strain along the bar's length, allowing the bar to remain elastic over large deformations with very little or no localization of strain. A significant drawback of unbonded PT is the large deflection and brittle failure due to the mechanism lacking the damping or hysteretic energy (Currie 2009).

2.2 Previous Research on Post-tensioned System

A different form of precast bridge system has been used worldwide for more than two decades to serve the purpose of accelerated bridge construction. The precast system has achieved massive success by shifting the work from the construction site to the prefabrication plant where mass production can be achieved, ensuring the highest quality. There has been significant research on the development, testing, and numerical simulation and validation of precast bridge systems over the past decade. The primary issue with the conventional method of constructing bridge piers is the inelastic deformation at the plastic hinge region and high residual displacements after a seismic event, which makes it difficult to use the bridge following an earthquake. Mild steel reinforcement is not continuous throughout the joint and thus will contribute less toward strength (Ou et al. 2009). One of the innovative methods to mitigate residual displacement in bridges is by providing self-centering of the piers. One of the types of self-centering system of bridges involves allowing for the controlled rocking of the piers under

lateral loading with motion-controlled by PT or other passive energy-dissipating systems (Lee and Billington 2009).

El-Sheikh et al. (1999) studied the behavior of two six-story unbonded post-tensioned frames under non-linear pushover static analysis and time-history dynamic analysis, and the displacement of these frames was found to be larger with low energy dissipation and minimal residual displacement. PRESS (Precast Seismic Structural System) started a program in 1990, which consisted of a number of studies over a decade including testing of a five-story precast PT frame under simulated seismic conditions at the University of California, San Diego (Priestley et al. 1999). Research led to recognition of this innovative technique and was adopted in seismic design provisions in the United States. Following that, Priestley et al. (1996) found that the use of partially bonded and unbonded PT tendons in precast frames sustained substantial lateral displacement with very low residual deformation and little permanent structural damage.

The combined system incorporating both self-centering properties of unbonded tendons and energy dissipation characteristics provided by internal mild steel bars or other forms of passive dissipators is referred to as the hybrid system (Stanton et al. 1997). Mander and Cheng (1997) constructed and tested a near full-scale precast PT bridge pier with a steel-steel rocking interface, incorporating damage avoidance design, which behaved in a bilinear elastic fashion without permanent damage. High stress concentrated at the rocking toe during rocking motion was effectively mitigated by using a steel-steel rocking interface together with a high degree of confinement at the end region. The self-centering bridge pier showed no strength or stiffness deterioration after hundreds of rocking cycles. Energy dissipation was more significant when rubber pads were inserted between steel plates at the interface.

Precast concrete segmental bridge columns with unbonded PT were investigated under lateral earthquake loading at the University of California, San Diego (Hewes and Priestley 2002); they used a steel jacket of different thickness to confine concrete in the plastic hinge region; residual drift was found to be minimal, with low damage in general. This type of column was useful for resisting lateral earthquake forces and is capable of undergoing large non-linear displacements without experiencing a sudden loss of strength. Billington and Yoon (2004) conducted cyclic tests of four short and three tall precast segmental columns that used unbonded PT to join precast elements with an option of using a ductile fiber-reinforced cement-based composite (DFRCC) in the precast segments at the potential plastic hinge region. All columns with unbonded PT reached higher drift levels of 9% with minimal residual displacement. The use of DFRCC exhibited more energy dissipation than the corresponding specimen constructed with plain concrete.

Two unbonded, each with and without external energy dissipators, PT precast concrete-filled tube (CFT) segmental bridge columns scaled to one-fifth of the original dimension were tested under lateral cyclic loading (Chou and Chen 2006). All column segments were encased in a steel tube to minimize spalling and concrete crushing at the base. Both specimens reached a 6%

drift ratio with minimal strength degradation and residual displacement; however, equivalent viscous damping was more significant for the specimen with external energy dissipators.

Palermo et al. (2007), designed and tested at 1:3 scale, two PT only specimens, two Hybrid (PT and internal unbonded mild steel dissipators grouted in metallic sleeves), and one equivalent monolithic reinforced concrete specimen; they used a varying combination of mild steel and PT reinforcement and initial prestressing load. The PT only specimen with a different configuration of PT bars and PT forces re-centered with minimal residual displacement. The hybrid specimen displayed stable hysteretic behavior with high energy dissipation and self-centering with minimal residual/permanent deformation. The analytical model showed satisfactory accuracy and reliability when compared to the experimental results.

Wang et al. (2008) performed quasi-static cyclic testing of four large-scale precast hollow PT concrete bridge columns. One specimen used only PT bars, and the other used mild steel reinforcement through the segments, which acted as internal energy dissipators; test results showed ductile behavior and satisfactory hysteretic energy dissipation capacity.

Ou et al. (2009) investigated the seismic behavior of precast hollow segmental unbonded post-tensioned concrete bridge columns with bonded mild steel bars as energy dissipators with certain unbonded lengths at the critical surface. Test specimens with no or varying amount of external dissipators were tested and analyzed. Specimens with no energy dissipator (ED) bars showed no damage, no residual drift, with good self-centering and little energy dissipation. Increasing the ED bar ratio increased the ductility of the system, with more damage and increased residual displacement.

Marriott et al. (2009) designed, tested, and developed a numerical model at a 1:3 scale for an unbonded PT cantilever bridge pier subjected to quasi-static and pseudo-dynamic loading protocols, and compared the results with an equivalently reinforced monolithic benchmark specimen. Four specimens; a monolithic, a post-tensioned only (PT); a hybrid pier with four unbonded PT and four external replaceable dissipators (HBD3); and a hybrid pier with four unbonded PT and eight external replaceable dissipators (HBD4), were designed and tested at the University of Canterbury. The use of external replaceable dissipators ensures the reinstatement of the structural integrity of the system after the seismic event with minimal downtime. The monolithic specimen dissipated considerable energy with large static residual displacement. Significant pinching and stiffness degradation of mild steel reinforcement were observed. The unbonded PT-only specimen was characterized by a stable force-displacement response with no energy dissipation, no damage, and self-centering. Pier HBD3 displayed a stable hysteretic response with little stiffness degradation, minor cracks, and negligible static residual deformation. Pier HBD4 displayed similar characteristics but had more energy dissipation. In these two piers, static inelastic deformation was concentrated at the external dissipators. The replaceable energy dissipators, which add stability and energy dissipation to the system, allow easy inspection and replacement after the seismic event facilitating quick erection time. The authors developed a numerical model to accurately simulate the performance of the piers under similar loading protocols. Marriott et al. (2011), compared and tested the monolithic pier and

HBD4 (PT pier with eight external energy dissipators under biaxial cyclic loading) and found that the structural performance of both specimens was significantly reduced as compared to uniaxial loading. However, the PT pier maintained structural integrity after the earthquake due to the easy replacement ability of external dissipators.

Use of energy dissipation (ED) bars significantly increases energy dissipation; however, when the columns are subjected to high lateral displacement, a significant joint opening occurs, which may lead to premature failure of the ED bars (Ou et al. 2010). To delay fracture of bars, either debonding or high performance (HP) steel with superior ductility capacity is used. Ou et al. (2010) tested three large-scale precast segmental concrete columns under lateral cyclic load. Precast segments were connected by using unbonded PT bars and internal energy dissipators in the form of bonded mild steel, unbonded mild steel, and bonded HP bars. All three columns showed good self-centering, energy dissipation capacity, and small residual drift of less than 0.4%. ED bars contributed 23-28% of the total lateral strength of the three columns. Columns with HP ED bars reached a higher drift capacity, greater energy dissipation, and higher lateral strength. A numerical model was developed, which was able to satisfactorily predict the envelope response of the columns in terms of lateral force, joint opening, ED bar strain, and tendon forces.

Four 1:4 scale precast segmental concrete-filled fiber tubes (PPT-CFFT) bridge bents were tested and compared with a monolithic RC frame to study cyclic behavior (ElGawady and Sha'lan 2010). Each column was made by stacking three segments on top of each other, except one, which had a single long segment, and then connecting the assembly with unbonded PT bars. Among them, one column used a neoprene pad placed at the beam-column and column-footing interface, and another had an external energy dissipator in the form of a seat angle. The PT frame showed significant lateral drift without damage and low residual displacement; the use of external energy dissipators increased the equivalent viscous damping by 75%.

Yamashita and Sanders (2010) carried out a shake table test and numerical modeling of a one-quarter scale hollow precast segmental column with unbonded prestressed bars. The specimen displayed good ductility with essentially no residual displacement and only limited spalling at the base.

Palermo and Mashal (2012) provided the brief review of the international trends of the seismic accelerated bridge construction around the world. They highlighted the advantages of ABC and pointed out that the proper selection of durable materials with enhanced mechanical properties and appropriate detailing will support the safe design and use of PT precast systems.

Mashal et al. (2014) developed and tested two scaled bridge bents, one being an emulative high damage bent with socket connection and another being a low damage bent incorporating dissipative controlled rocking or hybrid connection. Steel shells 10 mm thick were used in the plastic hinge regions of the columns welded via welded studs inside the concrete column core. The rocking interface on the footing and under the cap beam was armored with steel plates. Internal shear keys were used at the rocking interface to prevent sliding. Steel brackets welded

to the column shell were used to hold the replaceable steel dissipators. The length of the dissipators was encased inside a steel tube to provide buckling restraint. The top end of the dissipators was anchored by nuts against slotted cleats welded to the steel casing, and the bottom ends were anchored to the sockets cast into the footing. No damage was observed in the column, beam, and footing with effective re-centering of the bent. The high self-centering ratio of (1.2- 1.5) ensured no residual displacement.

Davoudi et al. (2014) used seat angles attached to a circular PT rocking pier as the replaceable external energy dissipator and obtained a stable cyclic response and reliable energy dissipation with self-centering behavior.

Sideris et al. (2014a) performed an experimental study on the cyclic response of a large-scale concrete segmental bridge bent with internal unbonded PT and slide dominant joints. All the joints were assumed to be slide dominant except the bottom joint, which was rocking dominant. These are commonly referred to as hybrid sliding-rocking (HSR) columns. HSR columns performed well, reaching a 14.9% drift ratio with minimal damage in the base and the joints. The system did not exhibit good recentering, but the PT tendons behaved elastically. The proposed design equation achieved the design goals.

Two dual-shell cantilever bridge columns were built at a 1:2.4 scale and tested under cyclic loads (Guerrini et al. 2014). The column was a precast PT composite steel-concrete hollow-core with internal and external energy dissipation. High-performance concrete was cast in-between two steel, cylindrical shells with corrugated metal ducts embedded in one of the columns for installing six internal dowels. In the other column, six external dissipators were welded to anchors in the footing and the column outer-shell brackets. A mortar bed was laid in the footing-column interface. The system displayed excellent energy dissipation, but the residual drift ratio was greater than 1.5%, and self-centering ability was compromised. Additionally, the use of polypropylene fibers in the mortar bed with internal dowels delayed concrete crushing and displayed excellent performance beyond a 5% drift ratio.

The same concept by Mashal et al. (2014) was used in the *Wingram-Magdala Link Bridge* in New Zealand. Steel casing was used over the entire height of the circular column, and the replaceable dissipator bolts, hidden inside the footing, connected the stiffened column endplates to the footing and the headstock (Routledge et al. 2016).

Viscoelastic dampers, when used as the external energy dissipator in a bridge pier with PT columns, increased the strength and damping of the pier significantly and enhanced its seismic performance (Guo and Gao 2016).

White and Palermo (2016) performed half-scale testing of non-emulative coupled-bar column-footing connections with unbonded rocking piers under biaxial lateral loading. Replaceable dissipators with grout were used, which displayed excellent seismic performance until premature failure with good re-centering, and negligible residual drift. Research on Multi-performance Dissipative Controlled Rocking (MDCR) with eight dissipators, was performed by

Liu and Palermo (2017). The concept is to delay the onset of collapse so the dissipating devices are activated with a hierarchical order, depending on the level of seismic activity. Different test specimens with only PT with varying amounts of initial PT force, PT with external dissipators termed as Damaged Controlled Rocking (DCR), and MDCR were tested, and results were compared. The increase in the amount of initial PT had vlittle effect on increasing the transverse stiffness of the bridge system. Additionally, activation of a hierarchical activation system in MDCR increased stiffness and damping of the entire bridge system compared to the DCR system with only four dissipators.

Mashal and Palermo (2019) proposed a low-damage seismic design for ABC, which uses DCR, combined with unbonded PT and external dissipaters, connections between the precast elements in bridges. A half-scale precast bent was tested under a quasistatic cyclic loading condition and compared with an equivalent bent with emulative cast-in-place connections. The results showed no damage, low residual displacements and performed better than the conventional one.

Han et al. (2019) studied seismic behavior and post-earthquake performance of three 1:3 scale bent specimens with unbonded PT and energy dissipation devices and developed an analytical model to simulate the seismic response. The bridge bent used two types of energy dissipators, i.e., replaceable mild steel bars and buckling restrained plates. Good self-centering with a residual drift of less than 1% was observed in the specimens with and without external energy dissipators; the use of dissipators increased the system's ductility. The analytical finite element model developed helped predict the behavior accurately.

3. DESIGN AND CONSTRUCTION OF BRIDGE BENT

3.1 Specimen Design and Description

In this research, the system shown in Figure. 3.1 is adopted. Similar to the hybrid system defined by Stanton et al. (1997), the present *tension-only hybrid system* uses unbonded PT bars for bilinear elastic self-centering; however, the present system differs in that the hysteretic system uses SLAs, which are intentionally stressed in tension only. Therefore, the system can be described as "tension-only hysteretic," as shown in Figure. 3.1 (b). The resulting hybrid system of Figure. 3.1(c) has the same general shape as conventional hybrid systems with the difference that the SLAs do not need to be protected against buckling, since they cannot experience compression. It should be noted that an individual hysteresis loop is effective only for the first excursion to that drift ratio until a higher drift is reached. Moreover, it is assumed that SLAs are arranged in a circular pattern so under cyclic loads, a number of anchors are always stressed in tension. In addition, the SLAs do not impede re-centering because hysteretic energy dissipation occurs under tensile stress.

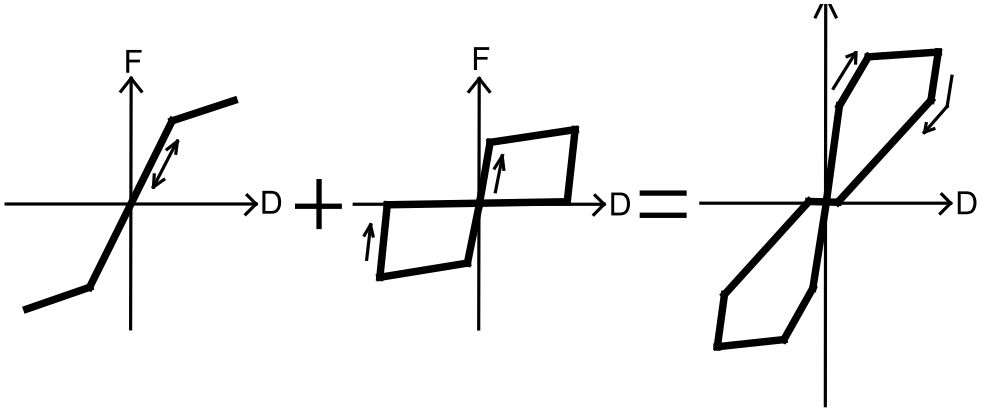

Figure 3.1 Proposed idealized load-deflection curves for (a) bilinear elastic self-centering, (b) tension-only hysteretic energy dissipation, and (c) hybrid systems

SLAs were introduced at the footing and cap-beam interface and were constructed so they would be stressed only in tension. Bent anchors and hexagonal couplers were embedded in the concrete with SLAs protruding at the exterior of the column, which are replaceable. The two footings and the cap-beam were designed as capacity protected elements, whereas, the stretch length anchor served as the ductile elements of the system. The bridge bent was designed according to AASTHO LRFD seismic design specifications (AASHTO 2011) for the maximum credible earthquake (MCE) level seismic hazard for Salt Lake City, Utah. The main objective of the research was to design and test a self-centering bridge bent, as a structural system that can re-center with low residual drift after the maximum credible earthquake. In addition, the research aims to design a system with minimal damage to the structural components, such as the footings, columns, and cap beam. Another objective was to determine whether SLAs can easily be replaced after yielding occurs. Use of replaceable stretch length anchors, which have the properties of self-centering by themselves, and the PT bars makes this research unique.

3.1.1 Columns

3.1.1.1 Existing Columns

The original existing column is a 16 ft (4.90 m) high octagonal in shape, 42 in. (1.10 m) in diameter with 12 No. 6 (19M) longitudinal steel rebar. No. 4 (13M) spiral hoops with 38 in. (965 mm) diameter and 6 in. (152 mm) spacing is used as transverse reinforcement to confine the longitudinal bars. A 1½ in. (38 mm) clear cover was used to protect the rebar against corrosion and other environmental effects. The concrete strength of all precast elements was specified as 5,000 psi, and the reinforcement used was Grade 60 steel rebar. Six 1 3/8 in. (35 mm) Post-tensioned (PT) bars Grade 150 ksi (1034 MPa) conforming to ASTM A-722 were used in each of the two columns to ensure self-centering of the bridge bent. The PT bars were held inside 2 1/8 in. (54 mm) (outside diameter) 36 gauge galvanized corrugated steel ducts. The longitudinal bar reinforcement ratio (ρ_{COL}) in the original column was 0.36%. Similarly, the PT bar reinforcement ratio (ρ_{PT}, col) in the same column was also 0.36%. The dimension and reinforcing details are shown in Figure 3.2 (a).

3.1.1.2 Column Specimen

The scaled columns for the bridge are 7 ft. (2.10 m) high, with an octagonal cross-section with 12 No. 5 (16M) longitudinal bars confined with No. 5 (16M) spiral hoops 15 in. (381 mm) in diameter with a 3 in. (76 mm) pitch. The longitudinal reinforcement ratio (ρ'_{col}) in the new scaled columns is 1.37 %. Likewise, only two No. 8 (25M) 150 ksi (1034 MPa) threaded PT bars, placed 3 in. (76 mm) apart from the centerline of the column on either side, are used in each of the columns with the PT bar reinforcement ratio ($\rho'_{PT, col}$) equal to 0.58%. The two PT bars are encased in two 2 7/8 in. (83 mm) (outer diameter) schedule 80 PVC pipe with 1/5 in. (5 mm) wall thickness. PVC pipes are used to encase the PT bars to ensure that they remain unbonded. Unbonded PT bars ensure distribution of strain along the entire length of the PT bars and behave elastically until high drift ratios, thus ensuring self-centering of the bridge bent. Another purpose of using schedule 80 PVC pipes is to prevent buckling or sagging of the pipes during concrete casting. The 28-day compressive strength of concrete (f'_c) in all precast components was 10,000 psi (69 MPa). Similarly, the concrete strength on the day of testing was 12,500 psi (86 MPa), and tensile yield strength (f_y) of the mild steel reinforcement was 68,000 psi (469 MPa). The clear cover of the reinforcement in the scaled specimen is 1.5 in. (38 mm). The design drawings and construction details of the column specimen are shown in Figure 3.3 and Figure 3.4.

3.1.2 Beams

3.1.2.1 Existing Beams

The original cap beam length center-to-center spacing between the two columns constructed at the Riverdale Bridge is 24 ft (7.30 m) with an extra 8 ft (2.40 m) overhang outward from the centerline of the west column. The beam is 48 in. (1.20 m) wide and 52 in. (1.30 m) high. The heavily reinforced cap beam cross-section consists of 24 No. 10 (32M) longitudinal bars and six No. 7 (22M) longitudinal bars, respectively. The layers of longitudinal reinforcement were confined with No. 4 (13M) rectangular hoops. Transverse reinforcements were placed at 6 in. (152 mm) spacing in the mid-section and the overhang portion of the beam. Stirrups were spaced on a 5 in. (127 mm) interval for a length of 1 ft 6 in. (457 mm) inwards from the column face at the beam-column interface. The clear cover of the beam is 2 in. (51 mm) on all sides. The longitudinal bars were bent on either side to satisfy anchorage and development length criteria. The longitudinal reinforcement ratio (ρ_{beam}) of the beam is 1.36%. Extra confinement is provided in the section where the column meets the cap beam to provide more confinement at the joint to avoid concrete crushing through the application of prestressing force in the PT bars. Extra confinement is provided in the form of 6 No. 6 (19M) bars with a 90^0 hook on one end and 135^0 hook on the other end, spaced equally and tied together by the No. 5 (16M) spiral with a pitch of 3 in. (76 mm). The dimension and reinforcement details are shown in Figure 3.2 (b).

3.1.2.2 Beam Specimen

The scaled cap beam is 14 ft 3 1/2 in. (4.30 m) long, which is connected to two precast octagonal columns spaced 10 ft. (3.0 m) on center. The constructed cap beam is 22 in. (560 mm) wide and 19 in. (482 mm) high with 1 ½ in. (38 mm) clear cover for the reinforcement. A total of 36 No. 5 (16M) longitudinal bars are spanning across the beam without splicing. Bars were bent at both ends to fulfill anchorage and development length criteria. Longitudinal bars spanning across the bars were kept in place and tied with stirrups, as shown in plan, elevation, and cross-section in Figure 3.3. The reinforcement ratio (ρ'_{beam}) of the scaled beam is 2.5%. The longitudinal reinforcement along the corner and edge of the beam cross-section is confined with rectangular stirrups and the inner reinforcement layers along the width and height of the beam cross-section, as shown in Figure 3.3(b). Shear stirrups had 90^0-hooks on one end and 135^0 hook on the other as shown in Figure 3.3(b); these 90^0 hooks of two successive crossties engaging the same longitudinal bars are altered end to end. All stirrups used in the beams are No. 3 (10M) bars spaced at 6 in. (152 mm) on center. A standard hook extension of 3 in. (76 mm) was used to satisfy the seismic hook provision of the ACI code (ACI 318-14 R18.6.4). Two 2 7/8 in. (83 mm) schedule 80 polyvinyl chloride (PVC) pipes were embedded at the beam-column joint to facilitate passing of the unbonded post-tensioned bars through them. Additional confinement was provided along the beam depth where the precast column meets the cap beam, as shown in Figure 3.4, resembling the original cap-beam. This additional confinement was achieved with 12 No. 5 (16M) vertical bent bars (135^0 hooks at one end and 90^0 hooks at the other) wrapped with No. 3 (10M) spirals at a pitch of 2½ in. (64 mm). The design drawings and construction details of the cap-beam specimen are shown in Figure 3.5 and Figure 3.6.

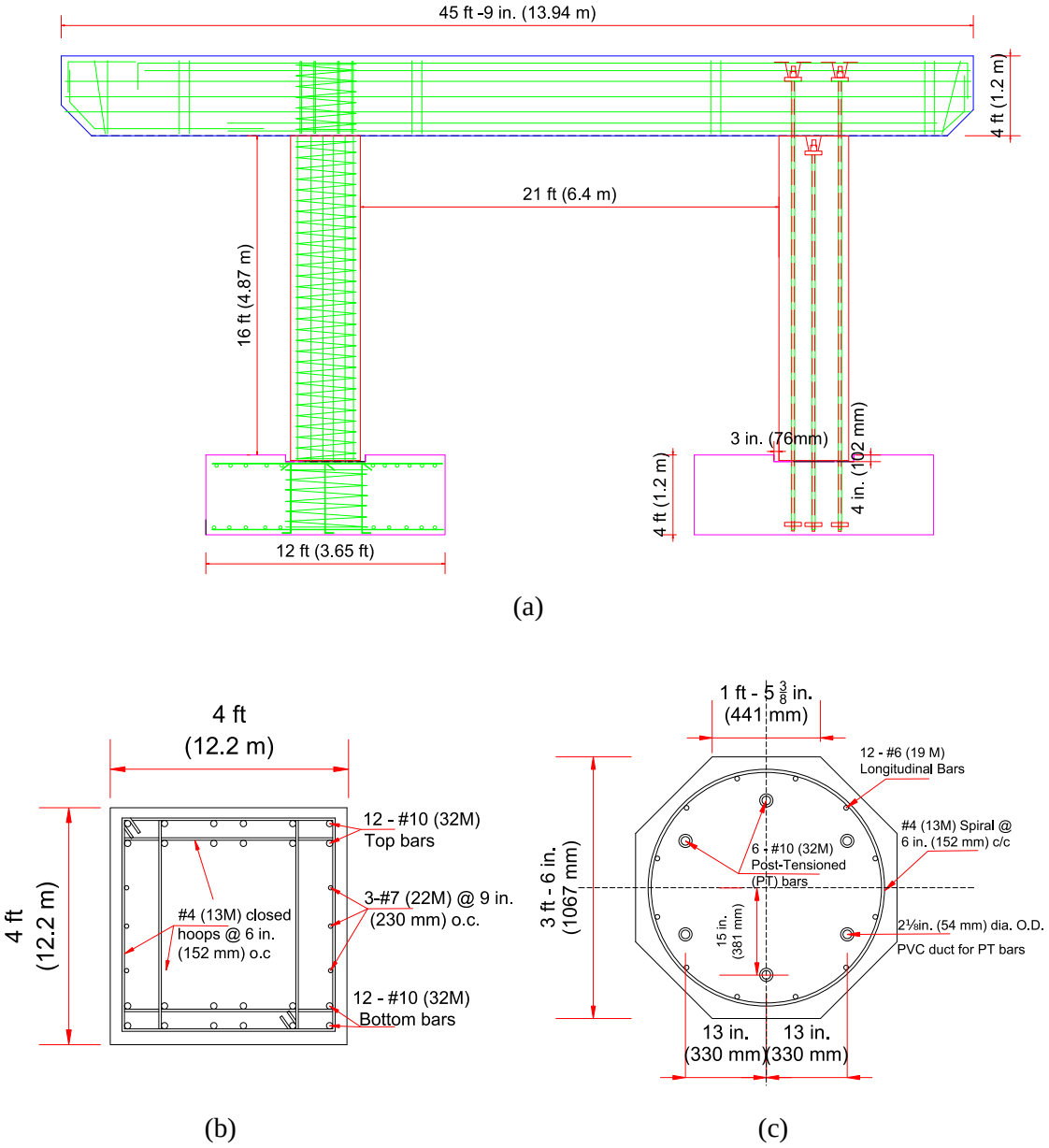

Figure 3.2 Size and reinforcement details; (a) Bridge bent, (b)beam cross-section, (c) column cross section and, (d) footing cross section

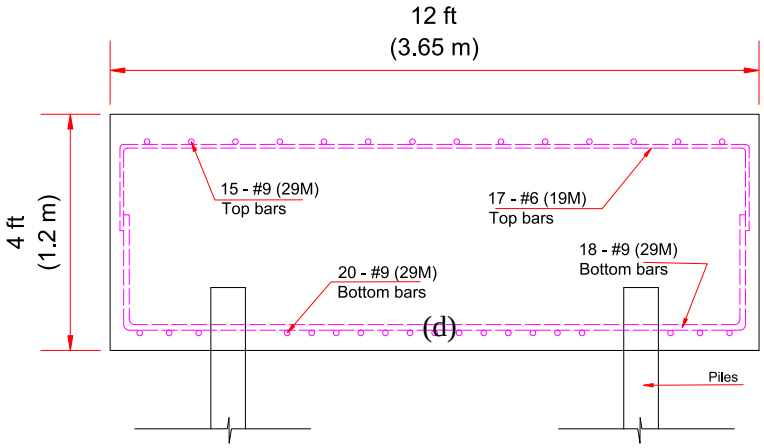

Figure 3.3 Size and reinforcement details; (a) Bridge bent, (b)beam cross-section, (c) column cross section and, (d) footing cross section

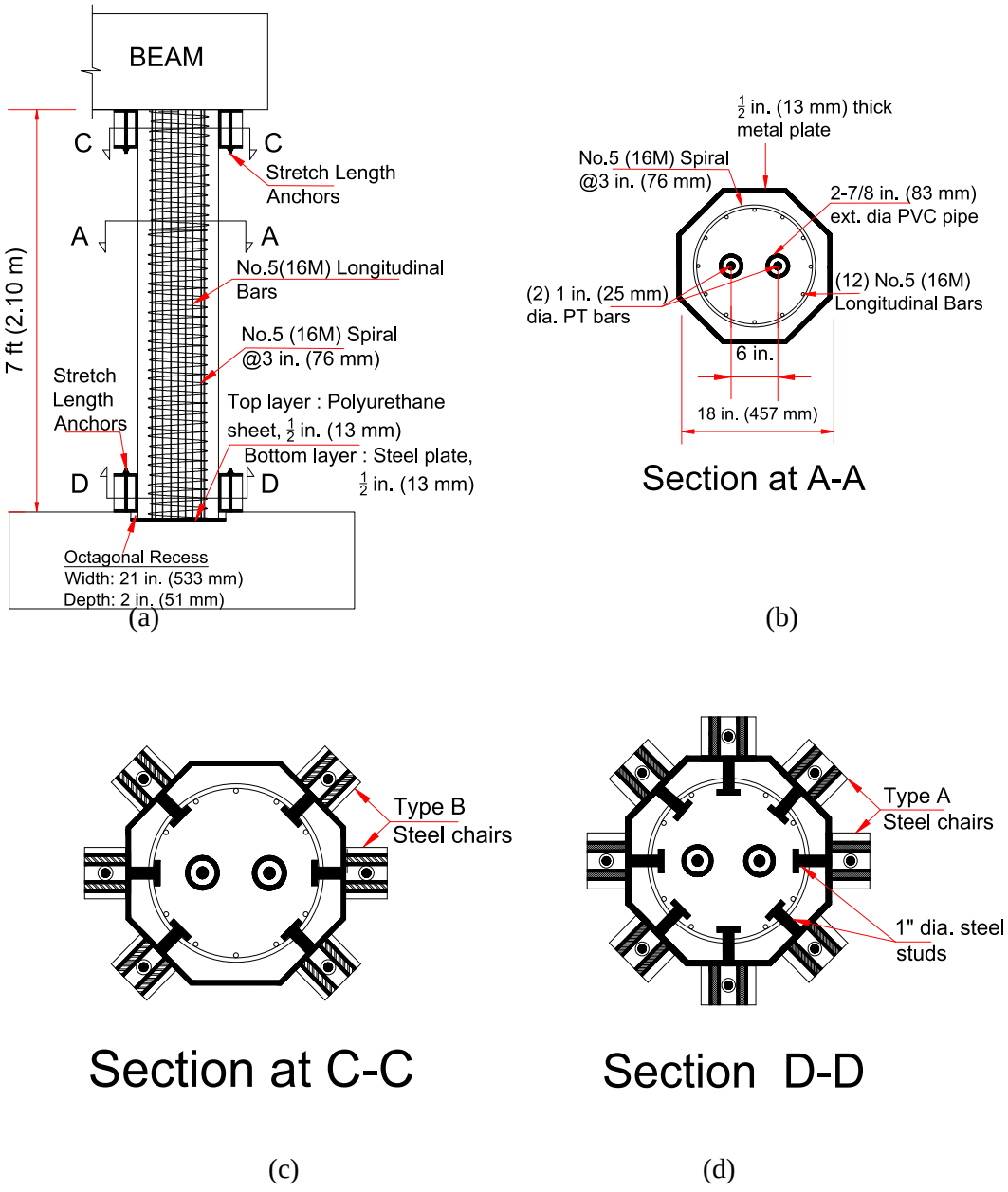

Figure 3.4 Column details (a) elevation, section at (b) middle of column, (c) section C-C at top of the column, and (d) section D-D at the bottom of column

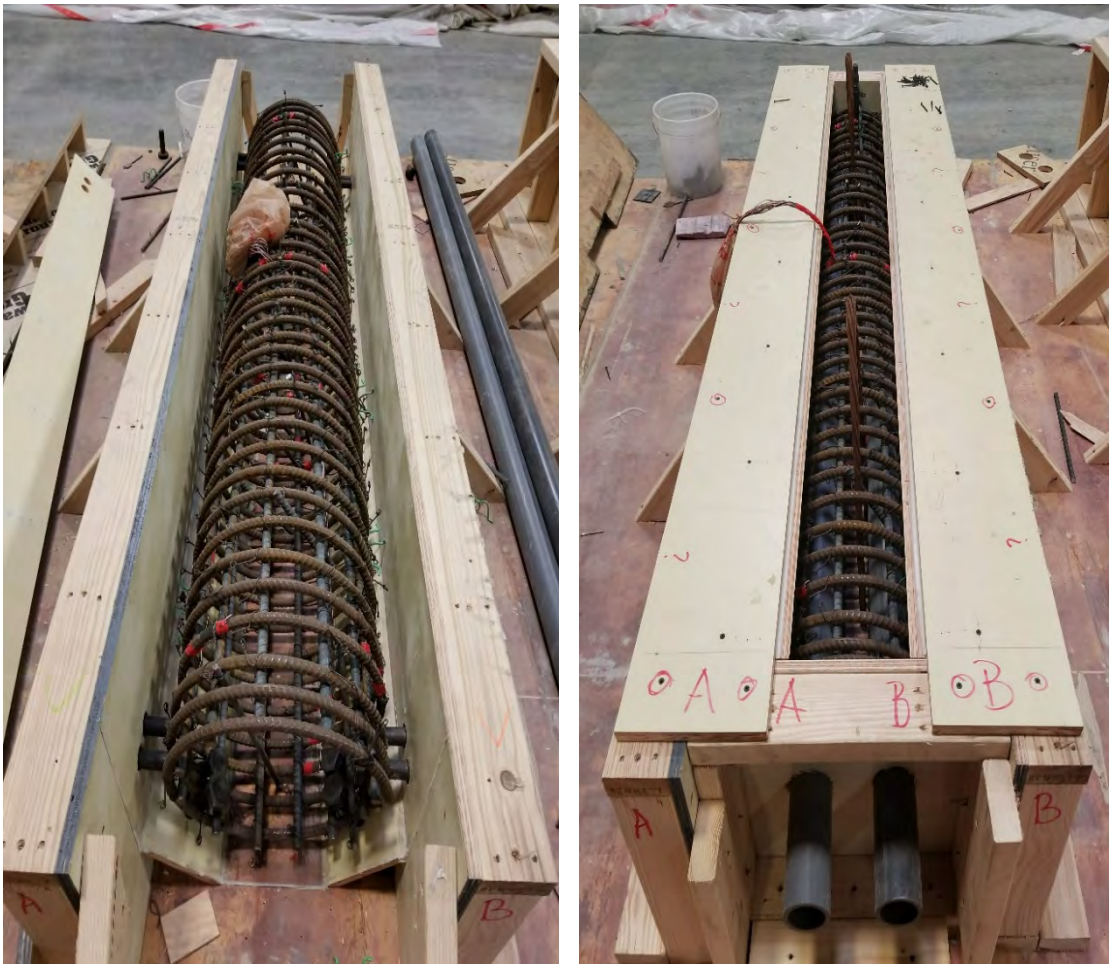

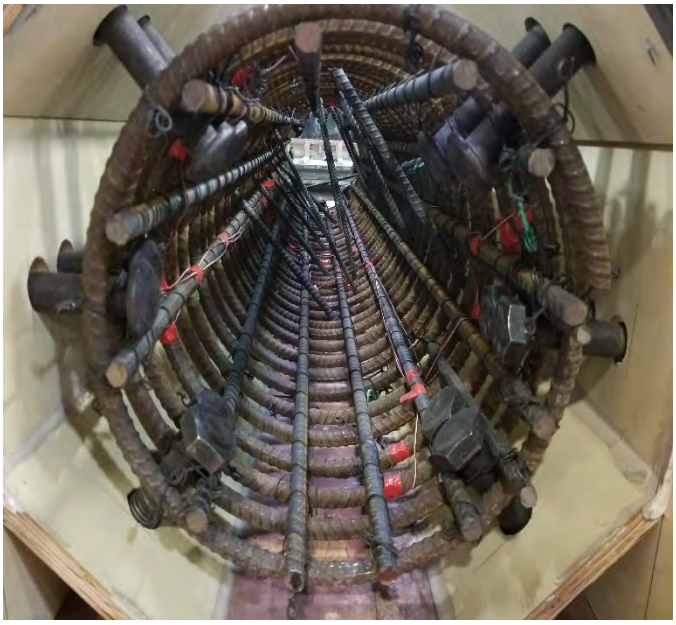

Figure 3.5 Construction details of the columns

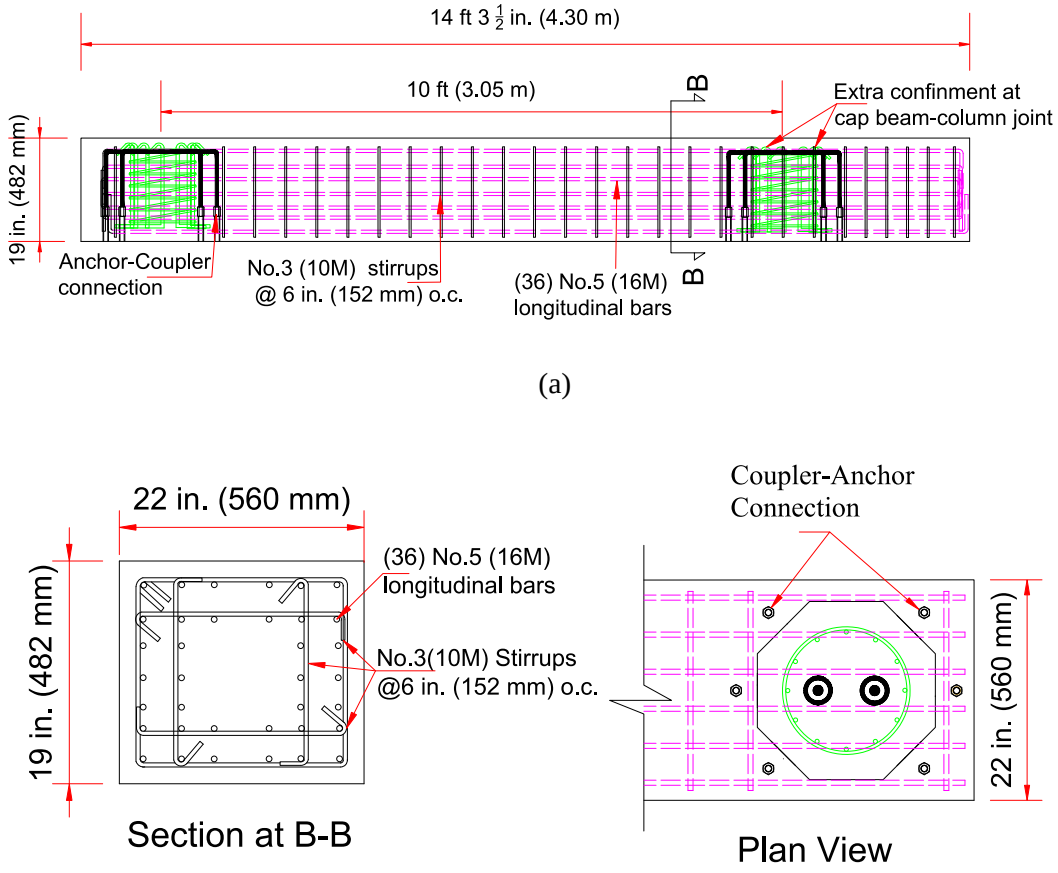

Figure 3.6 Reinforcement details of beam: (a) along the longitudinal axis, (b) cross section of beam at B-B, (c) top view at one end of beam

Figure 3.7 Construction details of the cap-beam

3.1.3 Anchor Bolts

Anchor bolts were embedded in the footings and the cap-beam to connect the precast elements of the bridge bent system. Anchor bolts are installed at all cap beam-column and column-footing interfaces. There are eight ¾ in. (19 mm) ASTM F1554 Grade 36 bolts embedded in the footing and only six bolts embedded in the cap beam at each location. Each bolt has two parts connected with a hexagonal coupler threaded inside, as shown in Figure 3.7 and Figure 3.9. The bottom part of the bolt is an L-shaped bolt (Figure 3.7(b)) with standard 90° bents. This bolt has threads over a 1.5 in. (38 mm) length at its top over which a standard ¾ in. hexagonal coupler (Figure 3.7 (c)) is tightened. This whole assembly is embedded inside the concrete, and later, the threads of the replaceable straight bolt termed as "stretch length anchors" (Figure 3.7(a)) go in the coupler. The L-shaped bolt has a minimum bent diameter of $6d_b$ (4.5 in.), which satisfies the ACI Code provision for minimum inside bent diameter (ACI 318-14 25.3.1). Similarly, the development length of the bolt is $16d_b$ (15 in.).

3.1.4 Stretch Length Anchors (SLAs)

The stretch length anchor, ¾ in. (19 mm) in diameter, is a straight 16.5 in. (419 mm) long bolt threaded on either side with 1.5 in. (38 mm) thread on the bottom and 3 in. (76mm) on the top. The lower threaded portion of the bolt is tightened into the hexagonal coupler, as discussed in the previous section. The hexagonal coupler and bolt assemblies are embedded such that the top face of the coupler is 5 in. (127 mm) below the concrete surface. The top hexagonal surface of the coupler is welded to a 1 in. (25 mm) inside diameter steel pipe to prevent the concrete from getting inside the coupler. This facilitates installation of the SLAs after concrete is cast. This is done to ensure the debonding of the bolts and to serve the primary purpose of being easily replaceable if the bolts are damaged through tensile yielding during successive seismic events. The SLAs are passed through a box-like structure made of steel plates called "steel chairs" that are attached to the face of the column, as shown in Figure 3.8 and Figure 3.9.

More details on steel chairs are provided later in this chapter. The top threaded portion of the SLAs is fastened over the top surface of the top plate of the steel chairs to ensure that the SLAs act only in tension. Had another nut been fastened to the bolt at the top and bottom surface of the top steel plate of the chair, bolts would experience a tensile and a compressive force — the latter is not desirable, as it could buckle the bolt in compression. The total unbonded length of the stretch length bolt is 12 ½ in. (317mm), 5 in. (127mm) below the surface and 7 ½ in. (190 mm) above the top surface of the footing. The total stretch length of the bolt is equivalent to $17d_b$, which exceeds the ACI 314-18 criteria of the minimum length of $8d_b$. The hexagonal coupler used to connect the two-pieces of threaded bolts is A563 Grade A bolt conforming to ASTM A563 Specifications. The A563 Grade A coupler has a maximum of 0.55% carbon, 0.12% of phosphorous, 0.23% of sulfur, and other metals such as manganese, silicon, copper, nickel, and chromium. ASTM A563 Grade A bolts have a proof load stress of 90 ksi. Proof load refers to the amount of force that a fastener must be able to withstand without undergoing permanent deformation. The layout and details of the bolts embedded in the cap beam and footings is shown in Figure 3.9. The stress-strain curve of the bolt is shown in Figure 3.10.

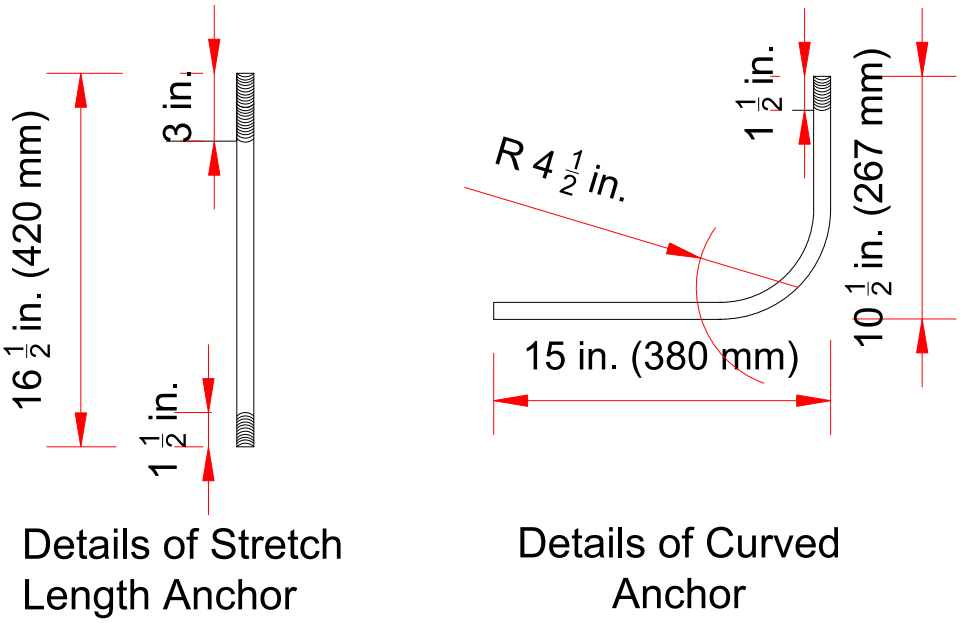

(a) (b)

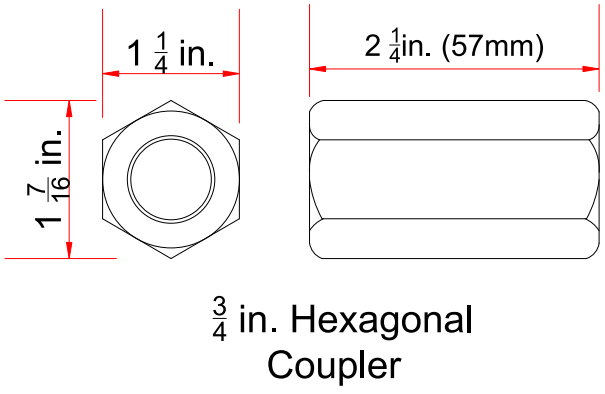

(c)

Figure 3.8 Stretch length bolt details: (a) ¾" dia. bolt, (b) ¾" dia. bent bolt that is completely embedded in the concrete, bolt, and (c) coupler connecting (a) and (b)

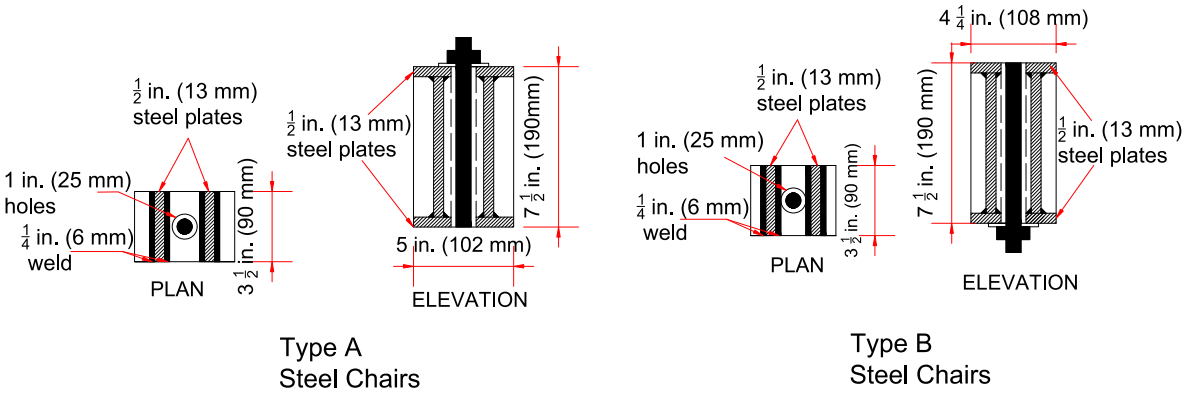

(a)

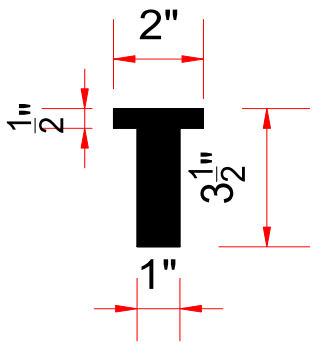

(b)

Figure 3.9 Steel chair details: (a) at bottom (Type A), and top (Type B) of the column, and (b) steel stud

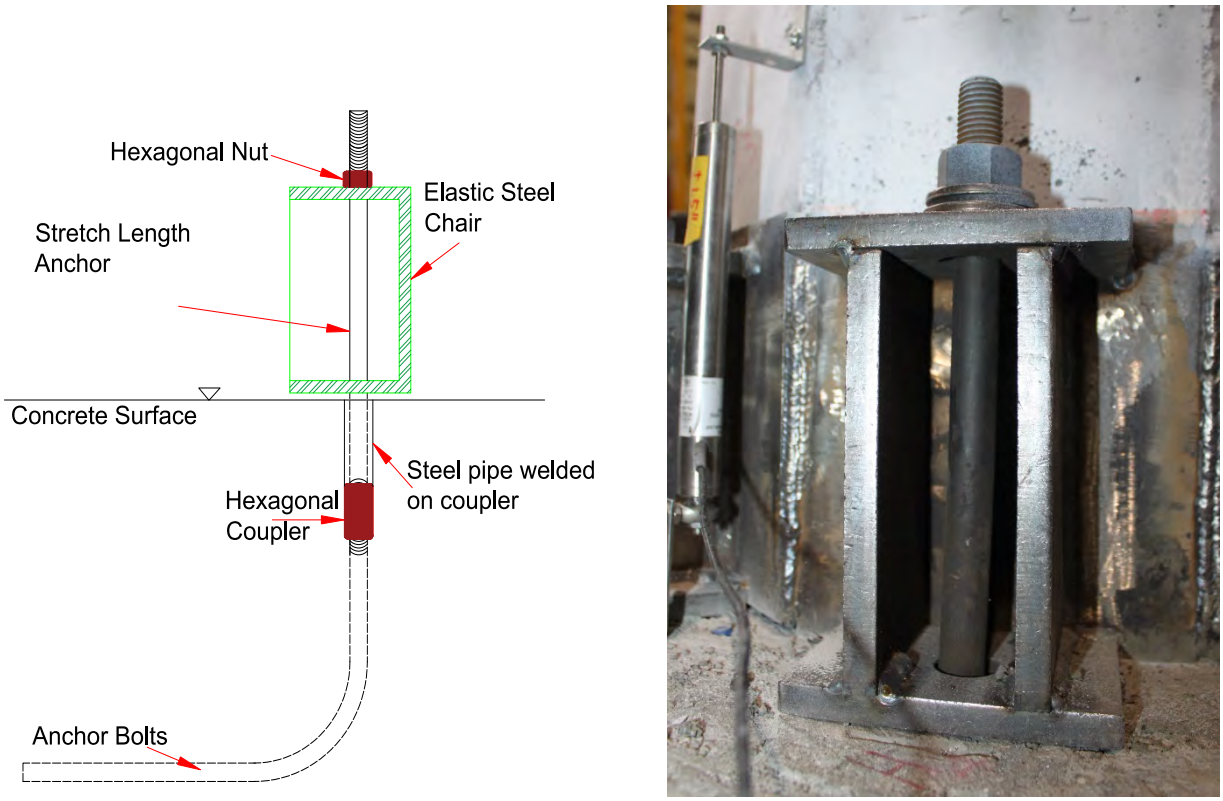

Figure 3.10 Schematic and photograph of stretch length bolt installation with elastic chairs

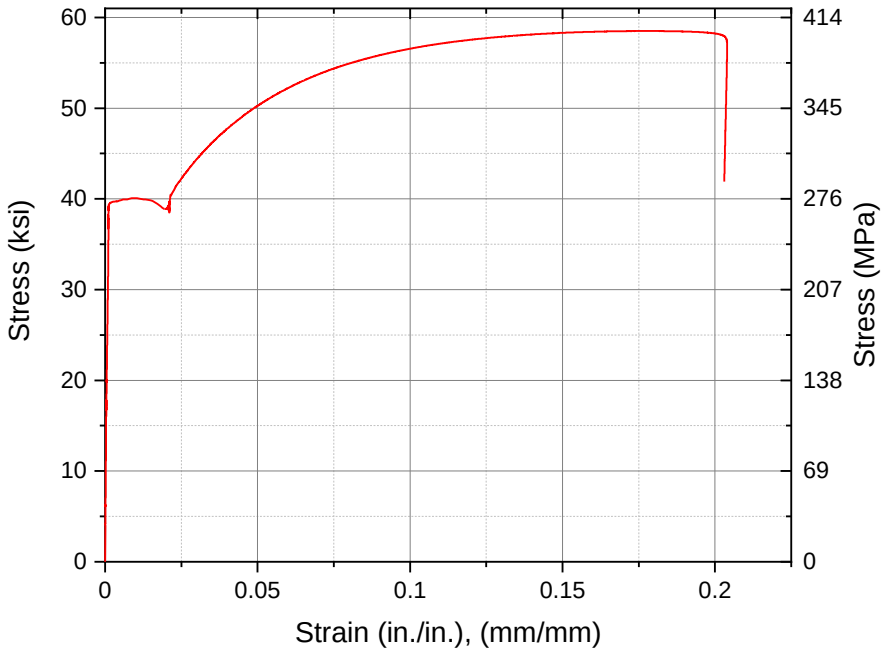

Figure 3.11 Stress-strain curve of stretch length bolt (Parks et al. 2019)

3.1.5 Post-tension (PT) Bar

The post-tensioned bars used in the experiment are Williams 150 ksi all-threaded bars, which are smooth, hot rolled, high strength prestressing steel bars. These bars are manufactured according to ASTM A722 and AASHTO M275 highway specifications. PT bars behave elastically up to 80% of their ultimate tensile strength and are very effective for self-centering systems. The load-displacement curve of a typical PT bar is shown in Figure 3.11. Three 1 in. (25 mm) diameter PT bar, 20 (0.50 m) in length, were tested in the laboratory. Four PT bars with 1 in. (25 mm) nominal diameter, 0.85 in.^{2} (548 mm^2), and 136 in. (3.45 m) long were used in the experiment.

3.1.6 Polyurethane Pads

Polyurethane (PU) is an amorphous thermosetting polyether polyol-based polymer. PU pads of ½ in. (13 mm) thickness were installed in the octagonal recess in the footing, as shown in Figure 3.10. PU pads were used because of their high deformation and damage resistant properties. PU exhibits large elastic deformation capacity and its viscoelastic properties permit large deformation without damage (Nikoukalam and Sideris 2017).

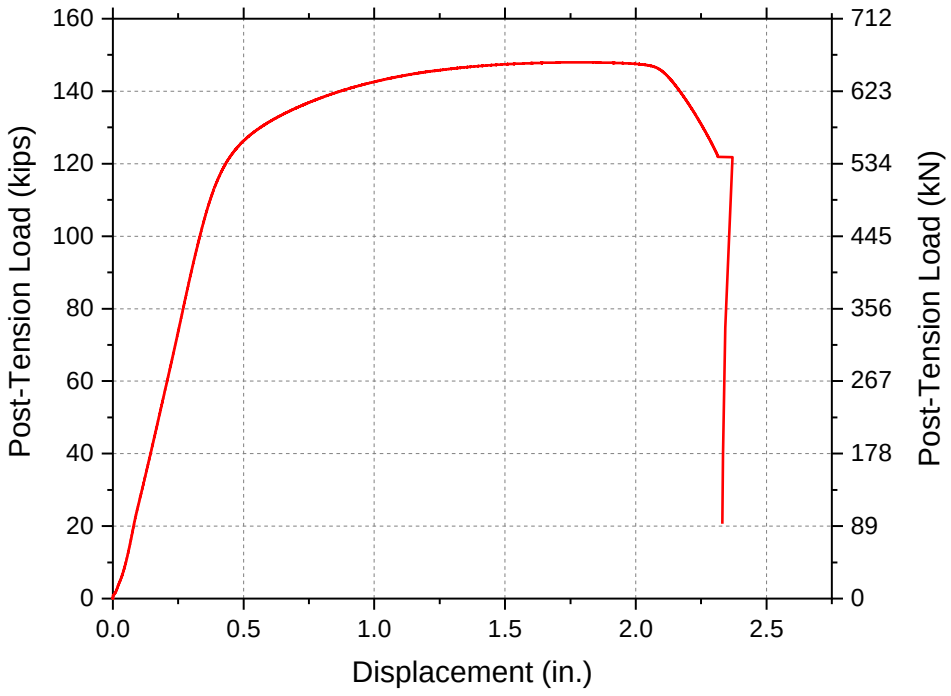

Figure 3.12 Load-displacement curve of the PT bar

Figure 3.13 ½” (12.7 mm) thick steel plate and ½” (12.7 mm) polyurethane plate on the footing recess

3.1.7 Footing Specimen

The two footings are not scaled to the ones from the original Riverdale Bridge. The footings were designed to resist the bending moment and shear force expected during the test and to fit the dimensions of the laboratory. Each footing is 6 ft long, 3 ft wide, and 19 in. high (1.80 x 0.90 x 0.48 m). It has eight No. 8 (25M) bars on top and six No.8 (25M) bars on the bottom. The shear key was designed in the original bridge to transfer the shear force expected from the bridge bent to the foundation. The shear key designed for the original bent was in the form of an octagonal 48 in. (1.2 m) diameter recess and 4 in. (102 mm) deep. An octagonal shear key in the form of an octagonal 21 in. (533 mm) diameter recess and 2 in. (51 mm) deep was used in the footing specimens. All longitudinal bars were bent 90º towards the footing depth to satisfy anchorage and development length criteria. All the top and bottom longitudinal bars were enclosed by No. 4 (13M) double hoops spaced 4 in. (102 mm) on center, as shown in Figure 3.11(c). Additional confinement was provided just below the octagonal recess. Twelve No. 5 (16M) straight vertical bars with 90^0 hooks on one end and 135^0 hooks on the other end were tied with No. 3 (10M) spirals hoops at a 2.5 in. (64 mm) pitch. Two 2 7/8 in. (73 mm) schedule 80 PVC pipes were installed in the middle of the footing to pass the 1 in. (25 mm) diameter unbonded post-tensioned bars. Eight anchor bolts were embedded in the footing with the same procedure as described for the cap-beam to connect to the SLAs using couplers. Design drawings and construction details of the footing specimen are shown in Figure 3.13 and Figure 3.14.

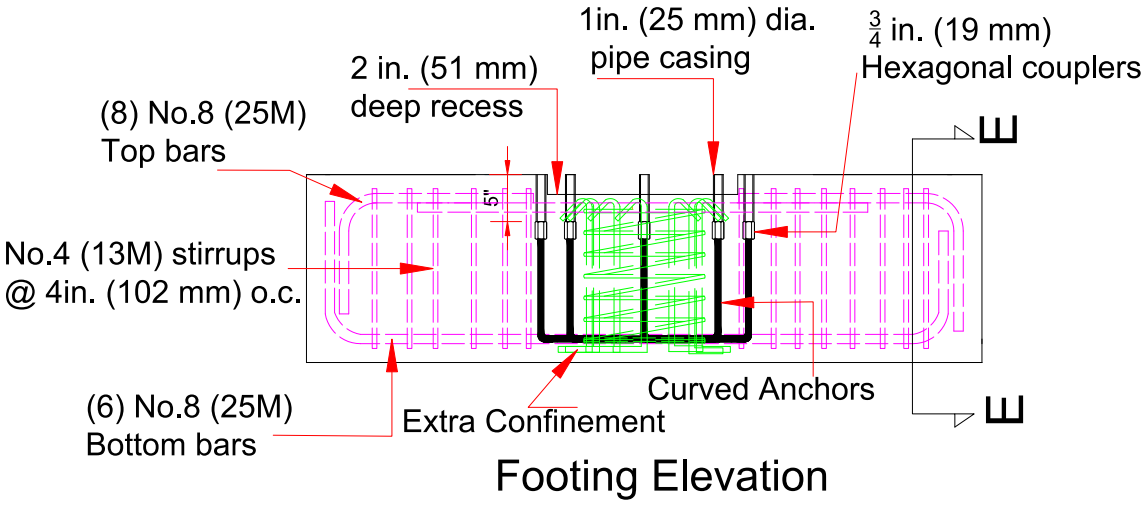

(a)

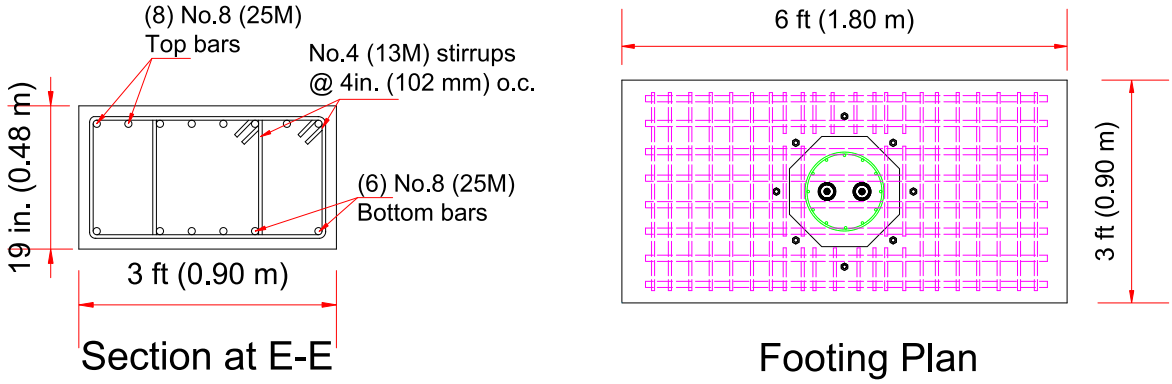

(b) (c)

Figure 3.14 Reinforcement details of typical footing: (a) along the longitudinal axis, (b) top view of the footing, and (c) cross section along E-E

Figure 3.15 Construction details of the footing

3.2 Self Centering and Energy Dissipation

There should be a balance between the self-centering forces provided by the gravity and the PT forces and the energy dissipating forces to obtain proper self-centering and achieve good energy dissipation. Gravity and PT forces should be large enough to close the gap and overcome the overstrength of the energy dissipating force (Restrepo and Rahman 2007). The upper bound for re-centering has been proposed by Guerrini et al. (2015) as:

$$\Lambda_c = \frac{F_{ED}}{P_u + F_{PT}} \leq 0.6 \qquad (3.1)$$

where P_U is the design gravity force, F_{PT} is the total effective PT force (after time-dependent losses), and F_{ED} is the total ultimate strength of all energy dissipators. A limit of 0.6 was recommended for Λ_C to account for uncertainties on post-tensioning losses and for the formation of debris in the gap.

In addition, enough energy dissipation should be provided to the system to avoid large scatter on lateral displacement demands observed of a purely rocking system (Makris and Roussos 1998). Therefore, the second condition for energy dissipation coefficient should be satisfied, as proposed by (Guerrini et al. 2015):

$$\Lambda_D = \frac{F_{ED}}{P_u + F_{PT} + F_{ED}} \geq 0.1 \qquad (3.2)$$

where F_{ED} is the ultimate energy dissipating force (assuming 6 bolts gets yielded, F_{ED} = 106 kips (471.5 kN)), P_U is the gravity load (P_U = 70 kips (311. 4kN)), and F_{PT} is the effective PT force (F_{PT} = 110 kips (489.3 kN), with 65 ksi (620.5 MPa) initial prestress). From this calculation we get, Λ_C = 0.58, Λ_D = 0.37, both of which satisfy the conditions in Eq. (3.1) and Eq. (3.2).

Equations (3.1) and (3.2) can be combined into a single equation as follows:

$$0.11 \leq \Lambda_c \leq 0.6$$

The self-centering capability of the bridge bent was computed using the relative self-centering efficiency (RSE) (Sideris et al. 2014b), which expresses the portion of the peak deformation that is recoverable, defined as:

$$RSE = 1 - \frac{u_{res}^{+} - u_{res}^{-}}{u_m^{+} - u_m^{-}} \qquad (3.3)$$

where u_{res}^{+} and u_{res}^{-} is the positive and negative residual displacement, respectively, and u_m^{+} and u_m^{-} is the maximum positive and negative displacement, respectively. The higher the relative self-centering efficiency of the column, the better it is regarding the minimum residual displacement, which means the residual drift ratio is very small.

Equivalent viscous damping is another quantity that is used to evaluate the relative energy dissipation capacity under cyclic loads. The equivalent viscous damping considers both the hysteretic and strain energy of the system and therefore conveys information on the hysteretic response. The equivalent

viscous damping ratio (ζ_{eq}) was obtained as the ratio of the hysteretic energy to the energy of the equivalent viscous system (Chopra 2007) and is defined as:

$$\zeta_{\text{eq}} = \frac{E_D}{4\pi E_{so}} \tag{3.4}$$

where E_D = hysteretic energy (the area inside hysteresis loop); $E_{so} = \frac{1}{2}Ku_0^2$ = strain energy; and $u_0 = \frac{u_m^+ - u_m^-}{2}$.

A full re-centering condition for a hybrid system can be achieved by ensuring that the ratio of the self-centering moment contribution, provided by the unbonded tendons and gravity load, (M_{pt}+M_N), to the expected moment contribution from the energy dissipation devices is greater than 1.0 (New Zealand Concrete Society 2010):

$$\lambda = \frac{M_{pt}+M_N}{\alpha_0 M_S} \geq 1.0 \tag{3.5}$$

where M_{pt} is the moment contribution of the unbonded tendons, and M_N is the moment contribution of the gravity load, M_S is the dissipation moment contributed by the stretch length anchors, and α_0 is the factor material overstrength factor associated with the stretch length anchors. A value of λ equal to 1.5 is suggested for building applications in the PRESSS Handbook (New Zealand Concrete Society 2010).

4. FABRICATION, TEST SET-UP AND INSTRUMENTATION

4.1 Fabrication of Bridge Bent Specimen

Two octagonal concrete columns, two footings, and a cap beam were connected with unbonded PT bars and partially embedded SLAs in concrete. In the first step of the construction phase, twelve No. 5 (16M) longitudinal column bars were spaced evenly and encased inside No. 5 (16M) spiral hoops. Two wooden templates with 12 holes equally spaced along the circumference were prepared and kept on both ends to ensure equal spacing. The inside spiral hoops were then stretched and tied together, maintaining a pitch of 2 ½ in. (63.5 mm).

After the cages were assembled, wooden formwork was made, and the steel cages were placed inside the form. Holes were drilled around the octagonal formwork at the predefined locations to insert the headed steel studs. Steel studs were inserted such that the headed portion remained inside the reinforcement cage, with a small length protruding outside the forms. The steel studs were then tightened and secured in place using additional support reinforcement and ties. The primary purpose was to hold the 8 x 7½ x ½ in. (203 x 190 x 13 mm) steel plate collar going around the column perimeter both at the top and bottom of each column. A total of 16 studs were embedded on the bottom and 12 studs embedded at the top of each column — two on each face of the octagonal column, as shown in Figure 3.1 and Figure 3.2. Studs were not inserted on the top two opposite faces of the column (North and South) due to space limitations, as shown in Figure 3.1(c). The studs had a 1 in. (25 mm) shank diameter, ½ in. (13 mm) thick head with 2 in. (51 mm) diameter and were 3½ in. (90 mm) long. The headed studs were embedded 3 in. (77 mm) inside the concrete with the head being inside the spiral hoops and the remaining length of ½ in. (13 mm) protruding outside the concrete face. The length of each stud that protruded out of the concrete surface was later welded with steel plates to create the steel collar.

PVC pipes were positioned inside the column cage along its length and secured with support reinforcement. The PVC pipes passed through holes drilled at the top and bottom face of the column formwork. After stripping the formwork, steel plates were welded around the column perimeter at the top and bottom. Two 1¼ in. (32 mm) holes were drilled on each of the steel plates by matching the position of the two protruded studs. These plates were inserted in the protruded portion of the studs and welded together. The vertical edges of the plates were also welded together to form the octagonal steel collar. The connections enabled the steel plates to act as a rigid body with the column. On each face of the steel collar, steel chairs were welded. The top and bottom faces of the chairs were drilled with 1 1/8 in. (28.6 mm) holes through which the SLAs pass to complete the footing-column and column-cap beam connection. The assembly of steel collar, steel chairs, and SLAs is shown in Figure 3.7.

The cap beam was 14 ft 3 ½ in. (4.3 m) long, 22 in. (559 mm) wide and 19 in. (482 mm) deep with 36 No. 5 (16M) longitudinal bars spanning across the beam and encased with No. 3 (10M) stirrups every 6 in. (152 mm). Longitudinal bars were bent 90 degrees inward of the beam height. Longitudinal bars were placed in position, as shown in Figure 3.3(a), and confined with steel hoops. Additional spiral confinement, as described in section 3.1.2.2, was provided. The most critical and detailed work during the construction of the beam and footing was installation of the anchor bolts. For this purpose, a bent bolt-coupler-stretch length bolt subassembly was assembled, as shown in Figure 3.7. Threading consisted of a length of ¾ in. (19 mm) of the bent bolt inside the bottom part of the coupler and the remaining 1½ in.

(38 mm) of the straight bolt inside the top part of the coupler, installed inside the rebar cage but not tightened. A wooden template with the holes drilled in it was used to hold the bolts in their precise locations, as shown in Figure 3.4. Each bolt was then carefully checked for its exact location, leveled vertically along both directions to avoid leaning of the bolts and secured with extra support bars to fix the bolts rigidly. Two holes were also drilled in the same template to hold the PVC pipes to insert the two PT-bars through them.

The bridge bent system was tested at the structures laboratory at the University of Utah and expected to experience high lateral force during the test. The point of application of the lateral load was the mid-point of the cap beam depth. To transfer load effectively in the cap beam, five 30 in. (762 mm) long, and 1 in. (25 mm) diameter threaded high strength bars (150 ksi) were inserted through the cap beam along the transverse direction; this system served the purpose of holding the steel channel sections on either side of the cap beam, which was rigidly connected to the cyclic load application system.

Two footings — 6 ft x 3 ft x 19 in. (1.82 x 0.90 x 0.48 m) — were built with eight No. 8 (25M) longitudinal bars and six No. 8 (25M) bars on the bottom encased using No. 4 (13M) double hoops 4 in. (102 mm) on center, as shown in Figure 3.11. Additional confinement, in the form of spiral hoops at the footing column-footing interface and identical to that described for the cap beam, was provided in the footing. There were eight bolts embedded in the footing. Anchor bolts and PVC pipes were installed in both footings with the same procedure as for the cap beam. Shear keys in the form of an octagon with a 21 in. (533 mm) width and 2 in. (51 mm) depth were maintained with additional formwork to support the shear transfer mechanism from the column to the foundation or cap beam.

After the steel reinforcement cages were completed in the structures laboratory at the University of Utah, they were transported to *Forterra Structural Precast*, located in West Valley, Utah, where concrete was cast. There was one formwork each for the beam, column, and footing. In the first step, one of each beam, column, and footing was cast, and the forms were stripped when the concrete reached sufficient strength. In the second step, the remaining one column and one footing were cast reusing the previous formwork. The forms were stripped again after the concrete had reached sufficient strength. The target compressive strength of concrete was 10,000 psi (69 MPa). Self-consolidating concrete was used for the specimen. Mechanical vibrators were used to ensure proper mixing of all components of concrete. Concrete cylinders 4 x 8 in. (102 x 203 mm) were prepared according to ASTM C31 for self-consolidating concrete. A total of 18 cylinders were cast in the first pour and 15 cylinders during the second pour to obtain the concrete compressive strength at the 7th, 14th, 28th, and test day.

4.2 Test Procedure

4.2.1 Experimental Setup

The five precast components, two footings, two columns, and cap-beam, were connected using SLAs and the unbonded post-tensioning bars. The entire bridge bent system had to be raised 1 ft (305 mm) from the floor level to match the centerline of the cap-beam to the actuator centerline, which would apply the lateral load. Four W12x53 steel beams were bolted down with the existing fixed beams on the strong floor of the laboratory. Two steel beams supported each footing. First, the footings were laid down on the floor at the measured locations. A ½ in. (13 mm) thick octagonal steel plate and a ½ in. (13 mm) thick

octagonal polyurethane sheet were drilled with two 3 in. (76 mm) holes, 6 in. (152 mm) on center and placed to fit exactly on the octagonal recess in the footing, as shown in Figure 3.12. Eight ½ in. (13mm) thick steel plates were welded around the column with the steel studs, and with each other at the top and bottom, as described previously. Columns were then lowered so the PVC pipes in the footings and columns matched. The erected columns were then plumbed on all sides to make them truly vertical. All bolts protruding from the footing on all eight sides were plumbed to make them straight. The combination of two 5 x 3½ x ½ in. (127 x 89 x 13 mm) horizontal steel plates with a centrally drilled 1 1/32 in. (26 mm) diameter hole, and two 6 ½ x 3½ x ½ in. (165 x 89 x 13 mm) vertical steel plates make up the steel chair, as shown in Figure 3.6(a) and Figure 4.2(a). Steel chairs were welded around the steel collar on all sides of the octagon so the bolts fit perfectly. Bolts were tightened with the nut over the top plate of the chair to ensure they act only in tension. The steel chairs were designed thick enough to act elastically during the experiment. The remaining gap between the octagonal column and the recess in the footings was filled using grout to prevent sliding of the column and nsure adequate transfer of base shear from the columns to the footings.

The cap beam was then lowered down precisely so the holes in the PVC pipes in the cap-beam matched exactly the holes in the columns. Steel chairs were then welded around the top face of the columns. In this case, the horizontal steel plates of the chairs were 6½ x 4¼ x ½ in. (165 x 108 x 13 mm) and the chairs were welded only on six sides of the octagon, leaving behind the north and south face of the column, as shown in Figure 3.6(b) and Figure 4.2(b). This was done due to the space constraint on the cap-beam. The PT bars were then lowered down from the top of the cap-beam to pass completely down to the floor of the laboratory. A 1 in. (25 mm) thick steel plate was placed on the top of the cap-beam to pass the PT bars through the plate over which the load cells were installed. High-strength sleeve nuts were tightened over the load cells for tensioning the PT bars, as shown in Figure 4.4. PT bars were also tightened at the bottom of the footing with the steel plate over the sleeve nuts. The system was rigidly supported and tightened with the W14x132 box-beam on top of either side of the footing and tightened to the ground floor to prevent movement of the system during the test, as shown in Figure 4.1. The system was supported on all four sides on the floor to prevent its movement. The system was restrained from out-of-plane movement during the test, as shown in Figure 4.1. The axial load application system was installed, as described in section 4.2.4. On test day, the cyclic loading system was installed, as described in section 4.2.3, and the test specimen was connected to the loading end of the actuator. The strain gauges, LVDTs, string potentiometers, and load cells were calibrated before the test. A pneumatic torque wrench was used to tighten the sleeve nuts, and to provide initial PT to the PT bars. Readings from the load cells were checked to ensure sufficient PT was applied.

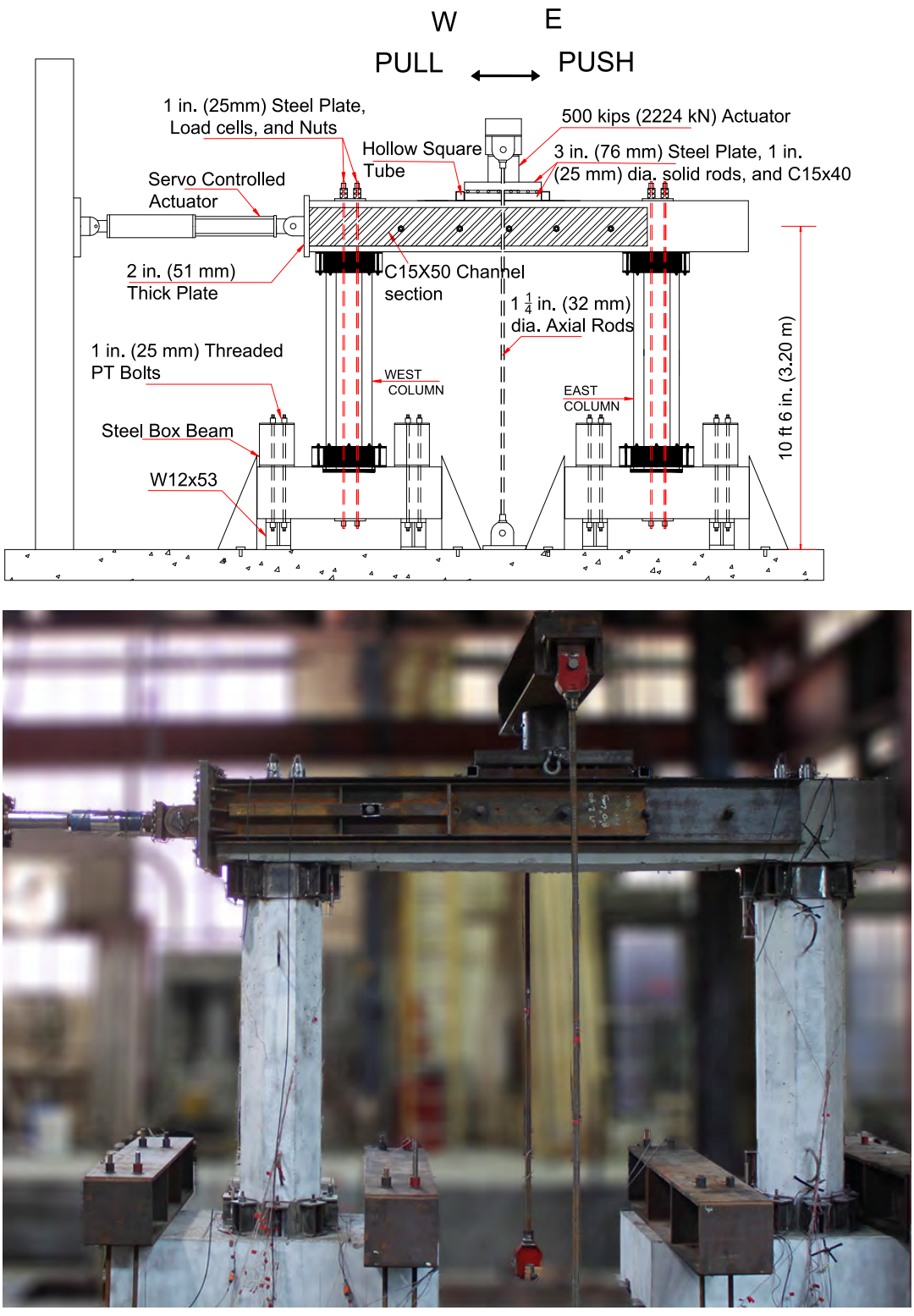

Figure 4.1 Experimental setup of the test

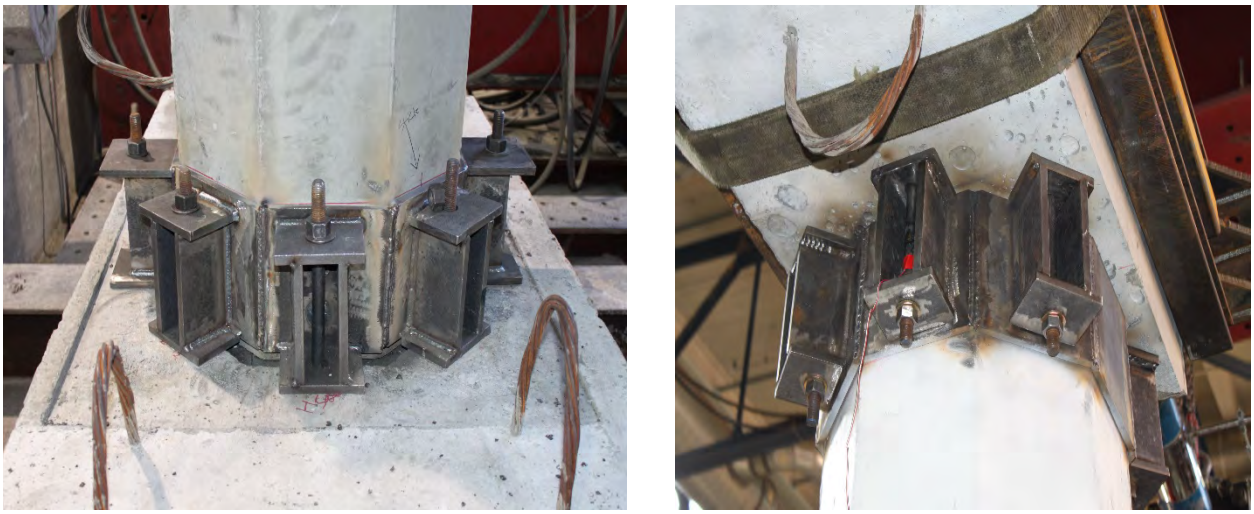

(a) (b)

Figure 4.2 Steel chairs with SLAs at (a) bottom, and (b) top of the column

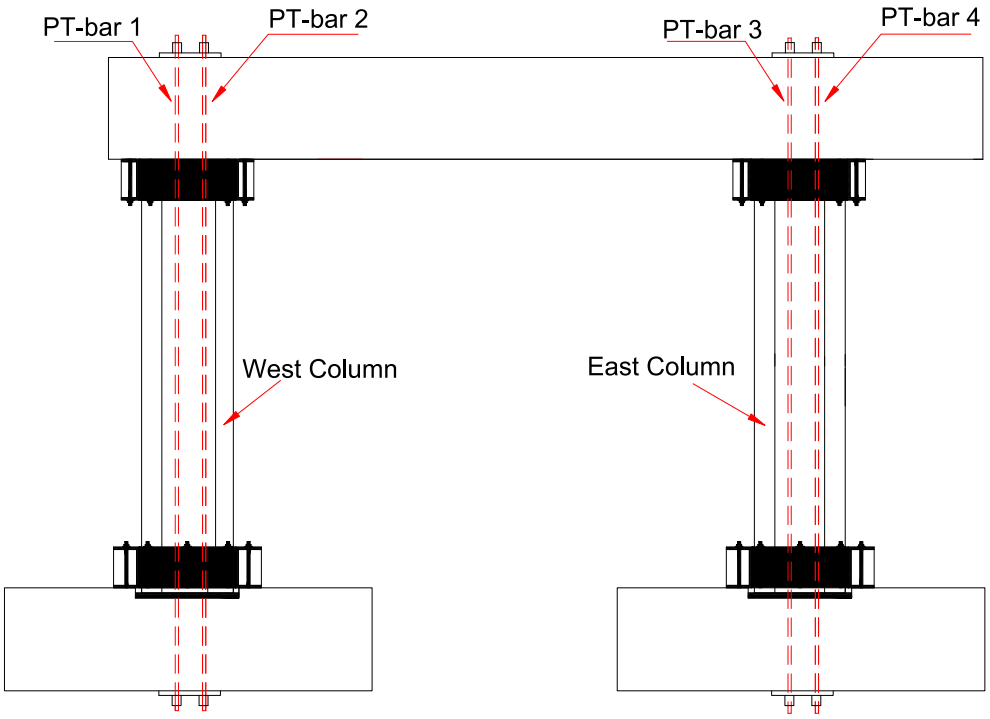

Figure 4.3 Location of PT bars in the specimen

4.2.2 Instrumentation

The precast bridge bent specimen was instrumented with 22 strain gauges. Strain gauges were installed in the plastic hinge region, to a height equivalent to half the column width, attached to longitudinal steel bars, spirals, and stretch length bolts. Four extreme longitudinal bars and the adjacent spiral hoops in the east, west, north, and south direction of the columns, and at the top and bottom of the column were instrumented with strain gauges. A total of 16 strain gauges were installed in each column. Strain measurements in the SLAs are of prime importance in this type of connection, so strain gauges were also installed on the SLAs. Four strain gauges were installed at the bottom of each column; two on the extreme two bolts along the east and west face of the column and two on the opposite two bolts installed adjacent to the column neutral axis along the north-south direction on both the east and west faces. Similarly, two strain gauges along the extreme two bolts were installed at the top of both columns. In total, there were 12 strain gauges installed on the stretch length bolts. Two strain gauges were also installed, one on each of the axial rods to measure the axial load on the system, simulating gravity load.

String potentiometers were used to measure the specimen displacement during the test. They were attached at two locations, one at the start of the beam and the other at the end of the beam. The bent displacement was taken as the average of the two potentiometer readings. Load cells were installed at the top of each PT bar. Four load cells were installed to measure the applied initial PT force and its variance at different drift ratios. Steel plates, 1 in. (25 mm) thick were placed below the load cells and high strength nuts over the load cells. Linear variable differential transducers (LVDTs) were installed to obtain the gap opening, base rotation, and global vertical movement of the specimen. A total of three LVDTs on each column, one at the top east face, and one each at the bottom east and west face of the column were installed.

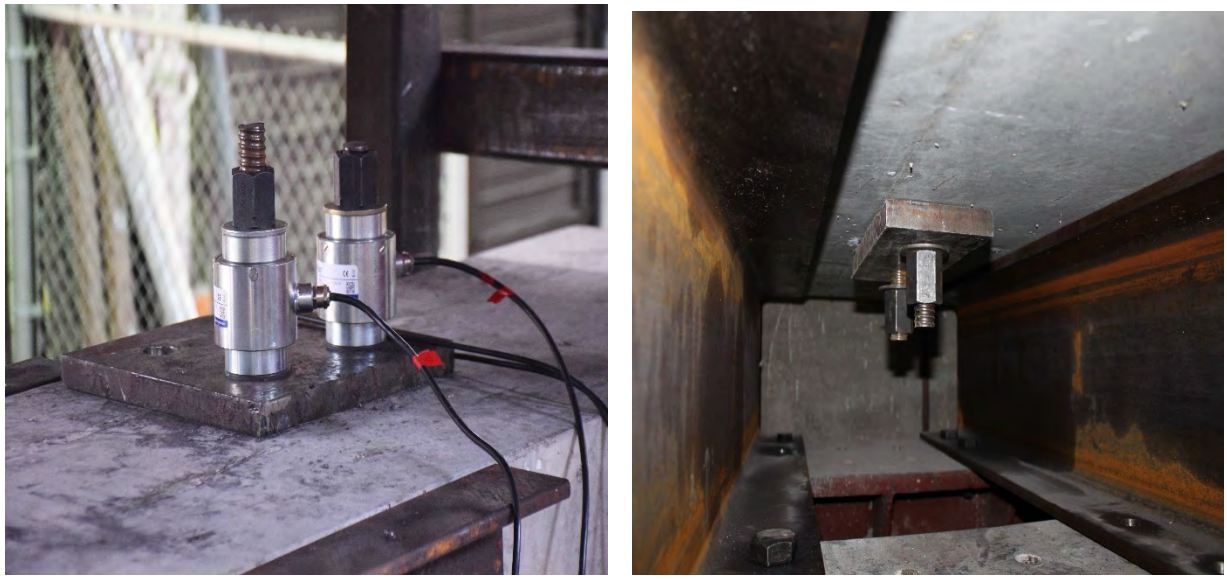

Figure 4.4 Plate and load cells at the top, and plate at the bottom of PT bar

4.2.3 Lateral Load Application System

The lateral load application system consisted of two 11 ft (3.30 m) long channel sections (C15x40), the webs of which were drilled and bolted on each side of the beam along the beam's longitudinal axis with the protruded ends of five high-strength 1 in. (25 mm) diameter threaded rods that were embedded in concrete during casting, as shown in Figure 4.1. At the actuator end of the two channels, two 6 x 6 x ½ in. (152 x 152 x 13 mm) angle sections 10 in. (254 mm) long were welded on each side. The two angle sections were stiffened with a steel plate at both ends at midheight to ensure sufficient strength, as shown in Figure 4.5. An assembly of 24 x 36 x 2 in. (610 x 914 x 51 mm) the steel plate was mounted with a double clevis with four A490 1 in. (25 mm) diameter bolts. The whole plate assembly was bolted against the welded angle section with four A490 1 in. diameter (25 mm) bolts at one end and pinned against the extended end of the actuator at the other end. A 240 kip (1068 kN) servo-controlled hydraulic actuator with an overall stroke of 18 in. (440 mm) was used to apply the lateral displacement-controlled, cyclic quasi-static load.

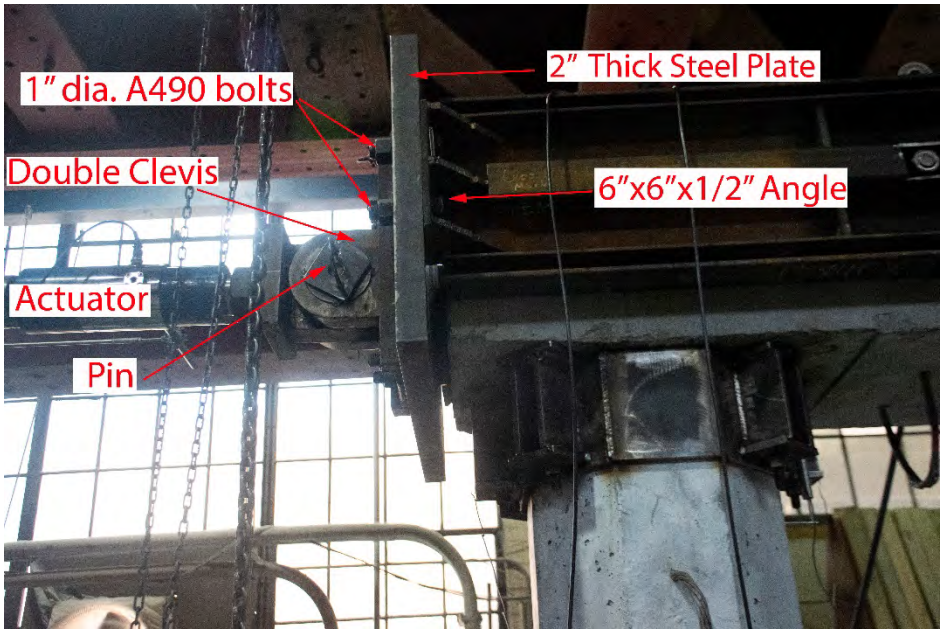

Figure 4.5 Lateral load application system

4.2.4 Axial Load Application System

The axial load application system consists of a 500 kips (2200 kN) hydraulic actuator, and the HP 14x89 stiffened steel spreader beam, eight 1 in. (25 mm) diameter ,12 in. (305 mm) long, hot rolled C1045 steel TGP (turned, ground, polished) bars with a yield stress of 77 ksi (524 MPa), 36 x 18 x 3 in. (914 x 457 x 76 mm) steel plate, 3 ft (914 mm) long C15x40 channel section, two hollow square tubes, and two 1¼ in. (32 mm) diameter 14 ft 6 in. (4.40 m) long high PT bars. The setup of the axial load application system is shown in Figure 4.6. The 3 in. (76 mm) thick steel plate is placed at the center of the beam along the longitudinal axis. Two square tubes were welded with the channel sections bolted on either side of the beam to prevent the system from moving. The eight solid hard steel bars were spaced equally and sandwiched between the steel plate and the channel section. Graphite powder was spread to minimize the

friction in the system. The cylindrical hydraulic actuator, 14 in. (356 mm) tall and 14 in. (356 mm) diameter was placed at the midpoint of the channel section. The HP14X89 stiffened beam was placed at the top of the actuator, along the north-south direction.

The spreader beam was connected to the floor steel plates using the two high strength PT bars. The axial rods were pinned at the top of the spreader beam and at the bottom near the floor to ensure smooth rotation of the bent. The axial load application system stays at its original position when there is lateral movement of the concrete cap-beam due to cyclic lateral load; this is done to minimize elongation of the two high strength PT bars when the whole bridge bent is displaced laterally and thus prevent the 1¼ in. (32 mm) bars from yielding; in addition, this ensures that the axial load remains constant throughout the test. A total axial compressive load of 136 kips (604 kN), 2.3% of axial load capacity, was applied to simulate actual gravity loads on the bridge bent. Figure 4.1 shows a schematic and a picture of the scaled bridge bent test specimen.

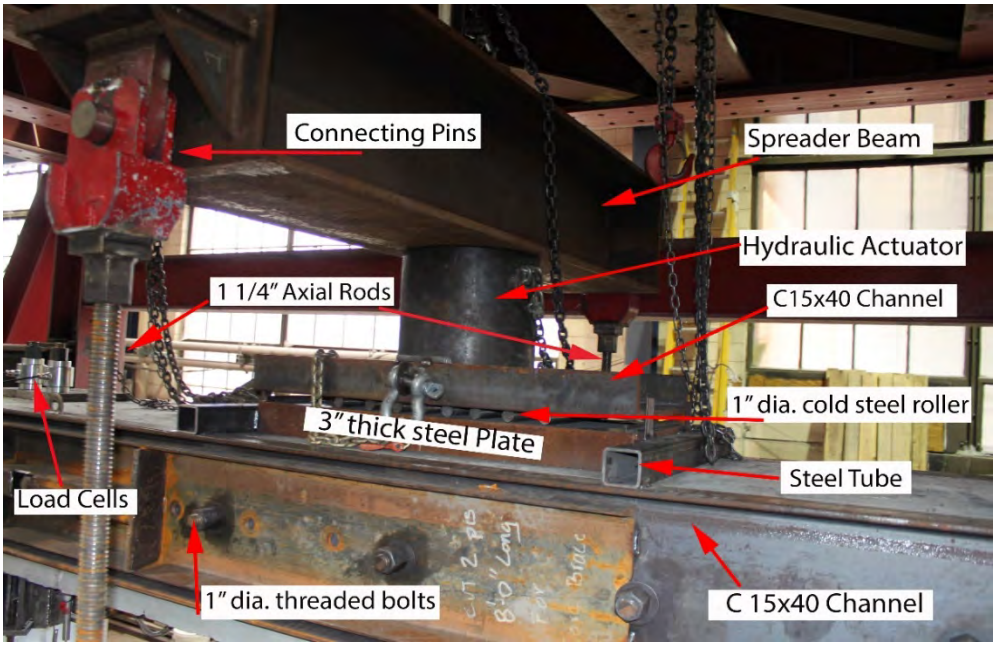

Figure 4.6 Axial load application system

4.2.5 Loading Protocol

The axial load and the lateral load were applied simultaneously to the test specimen. A total of 136 kips (604 kN) axial load was applied on the beam at the beginning of the test, which later increased to 184.5 kips (821 kN) at the end of the test due to slight elongation of the axial rods. The reversed cyclic quasi-static displacement-controlled load was applied at the midpoint of the beam section, at 94 in. (2.40 m) from the top surface of the footing. The loading protocol used in the experiment is shown in Figure 4.7. The displacement rate was set to 1.2 in./min (30.5 mm/min) throughout the entire test; the test was terminated when the displacement reached a 6% drift ratio. The variation of the axial load on one of the axial load rod is shown in Figure 4.8.

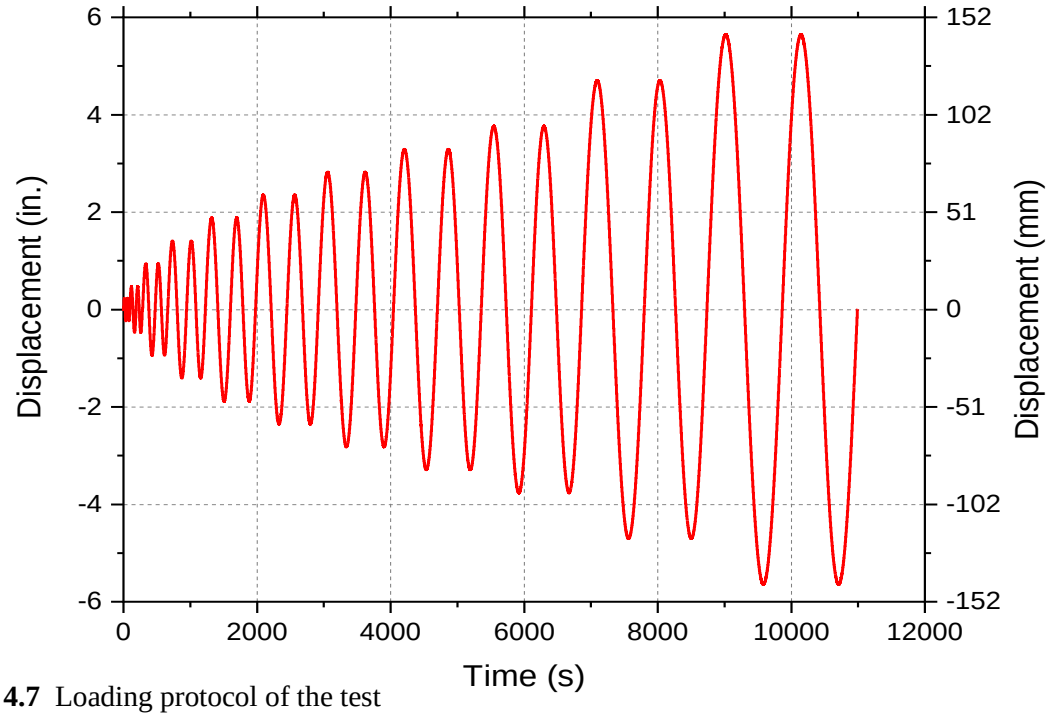

Figure 4.7 Loading protocol of the test

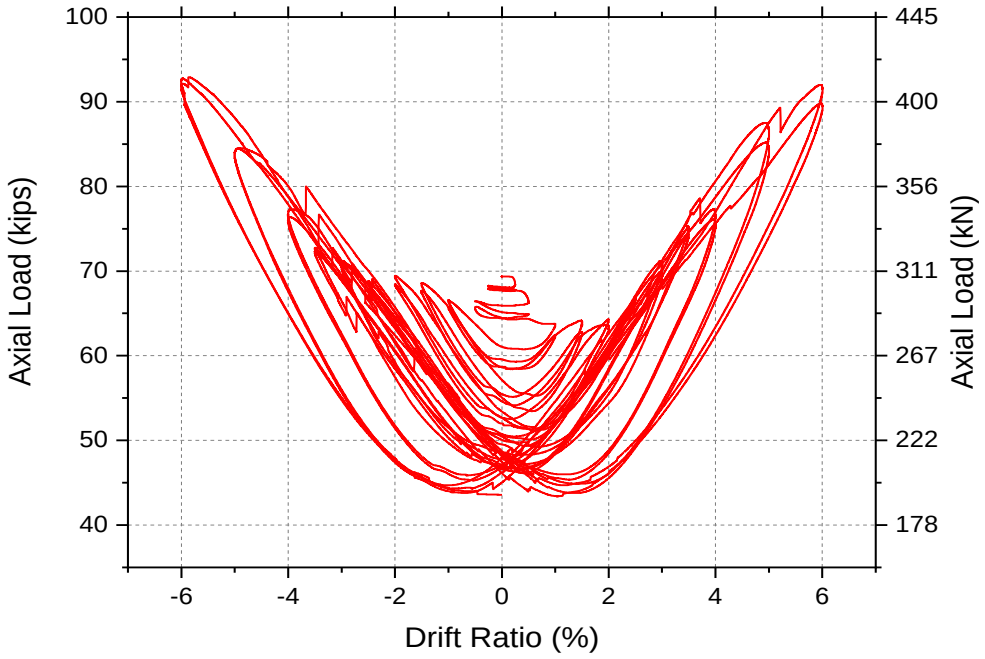

Figure 4.8 Axial load vs. drift ratio in one of the axial rod of the bridge bent

5. PERFORMANCE OF HYBRID BRIDGE BENT

5.1 Test Results

The specimen was tested under reversed cyclic, quasi-static lateral load with constant axial load. The test was conducted up to a 6% drift ratio and was terminated after the high tensioned PT bars had yielded inside the two columns. The axial load application system with the rollers performed well, and the maximum axial load was 35% greater than the initial load. The axial load increased after the 4% drift ratio, as presented in Figure 4.8, which shows the axial rod in one of the rods. Although there was an increase in the axial load applied to the system, the overall response of the specimen was stable. The increase in the load is attributed to elongation of the axial rods. In the following sections, experimental results and visual observations, the hysteretic response of the specimen, the force in the PT bars inside the columns, the response of the stretch length bolts, energy dissipation, stiffness degradation, and the residual drift are discussed in detail.

5.2 Hysteretic Response

Figure 5.1 shows the hysteresis curves of the bridge bent. Four damage states are identified: mild steel column bar yielding, concrete cracking and spalling, yielding of stretch length bolts, and yielding of the PT bars inside the columns. The first mild steel longitudinal column bar yielding, concrete spalling, first bolt yielding, and first PT bar yielding were observed at 2.0%, 2.0%, 1.1%, and 5.4% drift ratios, respectively. The backbone curve of the bridge bent is shown in Figure 5.2. The peak lateral strength of the specimen was 162.9 kips (725 kN) during the first positive cycle at a drift ratio of 5.0% (push) and -153.1 kips (-681 kN) during the first negative cycle at a drift ratio of 6.0% (pull). No significant loss in lateral strength was observed. However, the specimen started to lose strength during the second cycle of the 6.0% drift by 9.6 kips (43 kN). The lateral force vs. drift ratio curve shows symmetric and stable curves with good energy dissipation. The hysteresis indicates that overall force-displacement performance was controlled by yielding of the SLAs at the top and bottom of the columns. The specimen was not tested to failure because of safety precautions. The residual drift ratio was 1.0% in the positive and 1.1% negative cycles; therefore, the specimen had good recentering capacity.

5.3 Experimental Observations

Very little concrete cracking and spalling was observed during the test. The opening of the joint between the precast components, i.e., foundation and column, and cap-beam and column, increased as the lateral force increased. As can be seen in Figure 5.3, the columns rotated very well during the pull and push cycles, with a maximum rotation of 0.059 radians, which demonstrates that the columns rocked like a rigid body. Minor cracking of concrete started at the 2.0% drift ratio on the east face of the east column at its bottom; however, the crack opening was small and did not grow bigger as the drift increased. Similarly, at the 2.0% drift ratio, slight spalling of concrete just above the octagonal steel collar was observed on the east face of both columns, but the damage increased after the 5.0% drift ratio, as shown in Figure 5.6. There was slight concrete spalling and crack developing just below the steel collar on the west face of the east column at the top at a 5.0% drift ratio, as shown in Figure 5.6. There was no significant damage in terms of spalling, crushing, and cracking of concrete in the cap-beam, columns and footings. Figure 5.6 shows the maximum damage the structure has seen during the experiment, which is

minimal compared to what one would expect during such a high lateral load and drift ratio. Column damage was concentrated just above the steel collar on the bottom and just below the steel collar on the top of the columns, respectively. The damage extended to a height of 5½ in. (140 mm) above the steel collar at the bottom of the column and 2½ in. (63.5 mm) below the steel collar at the top of the column, as shown in Figure 5.6. The height of the steel collar was 8 in. (203 mm) from the toe of the column. The extent of damage was beyond the theoretical plastic hinge length of 9 in. (228 mm) from the bottom of the column. The toe of the concrete both at the top and bottom was not crushed or even damaged slightly. The embedded studs and steel collar assembly protected the concrete from crushing. In addition, the polyurethane pads placed at the footing to column interface contributed in avoiding crushing of the concrete at the column toes.

PT bars played a significant role in self-centering of the specimen and reduced the residual drift. PT bar 1 at the west side of the west column was stressed with the lowest initial PT force and did not yield during the experiment. However, the other three PT bars were stressed higher than PT bar 1, and they yielded at the 5.4% drift ratio, as shown in Figure 5.7. Among the three PT bars with high initial post-tensioning, PT bar 2 reached 104.8 kips (466 kN) during the 6% drift pull cycle, which just passes the yield load of 102 kips (454 kN) obtained from the tensile test of the PT bar shown in Figure 3.9. The PT bars reached 80% of the ultimate tensile strength; thus, they behaved elastically overall. During the 22 cycles of quasi-static cyclic loading, PT bars lost an average of 64% of initial PT load. Table 5.1 summarizes details of the PT forces on all four PT bars. Compressive stress in the PT bars and flexure of the columns due to lateral loading, friction loss, and relaxation of the PT bars were the main reason accounting for the post-tensioning loss encountered during the test. Slight buckling of the PT bar was observed at the end of the experiment, as shown in Figure 5.8.

Fourteen SLAs were engaged with good axial tensile elongation and energy dissipation in each of the columns during the experiment, six on the top of the column and eight on the bottom. They performed well and displayed good hysteretic energy dissipation. The SLAs were designed to experience only tensile load; therefore, they were tightened with a nut only at the top of the steel chair. The outermost bolts on the longitudinal axis of the columns at the top and bottom experienced the highest strain. In Figure 5.9(c) bolt B12 on top east corner of the east column yielded early at about 1.2% drift ratio. Bolts on the extreme edges along the longitudinal axis at the top of the column yielded at similar times. Similarly, SLAs located next to the extreme anchors on both column faces experienced similar strains as shown for bolts B7 and B9 in Figure 5.9(a), and for bolt B10 in Figure 5.9(b), whereas the anchors along the transverse axis experienced low strains. The yield strain of the bolt (1360 με) was determined based on the yield strength, which was 39.5 ksi (272 MPa) with a Young's modulus of 29,000 ksi (200 GPa), as given in Figure 3.10. A sudden drop in strain was observed at the 5% drift ratio in most of the bolts, which implies that the bolts reached the yield strength plateau at that drift, and the PT bars started to dominate resistance of the lateral load. The maximum stress experienced by the extreme bolts was 47 ksi (324 MPa). All the top bolts elongated ½ in. (13 mm), the bolts of the west column at the bottom elongated ¾ in. (19 mm), and the west and east bolts at the bottom of the east column elongated 3/8 in. (9.5 mm) and 3/16 in. (4.8 mm), respectively. Elongation of the bolts is shown in Figure 5.10. Several bolts had little damage on the threads at the top of the bolt. Moreover, many SLAs experienced slight bending and flexural stress in addition to tensile elongation and axial stress.

The strains in the longitudinal bars and mild spiral steel inside the column at different drift ratios are shown in Figure 5.11. Strain gauges were installed at the outermost longitudinal bars and adjacent spirals on the north, south, east, and west direction inside the columns, approximately 7.5 in. (190 mm) to 9 in. (229 mm) from the toe of the column. Some of the strain gauges were damaged during concrete casting; therefore, some strain data is not available. The strains in the outermost bars along the east and west direction of both columns is presented in Figure 5.11(a) through Figure 5.11(d). Longitudinal mild steel bars started yielding at approximately the 2.0% drift ratio. Two longitudinal bars yielded in each column, one adjacent to the east face and the other adjacent to the west face of each column. The tensile strain reached four times the yield strain (2344 με) in one of the longitudinal bars at the bottom of the east column on the east face, as shown in Figure 5.11(b). Strains in the spirals were small, as shown in Figure 5.11(e) and (f). The maximum strain in the longitudinal column bars occurred at the bottom of the column, within 38 mm (1.5 in.) from the top face of the steel collar. The reason for yielding at these locations can be attributed to pinching of the mild steel longitudinal bars just above the steel chairs where the maximum bending moment was expected. Observation of concrete damage at these locations also proves that pinching of the bars occurred at these locations. This was due to the insufficient height of the steel jacket provided around the column perimeter. As shown in Figure 5.12, almost all bars experienced very low compression strain compared to tensile strain. The remaining longitudinal column steel bars experienced low strains in tension and compression. Similarly, hoop strains exceeded the yield strain at a single location of the east column, as shown in Figure 5.13.

As presented in Figure 5.11(a) and 5.11(b), tensile strain was large in the west bar during push and in the east bar during pull cycles. Figures 5.4 and Figure 5.5 show the behavior of the bridge bent in the maximum push and pull cycle at the 6.0% drift ratio. When the bridge bent is in the push cycle, the top west face of the column is in compression due to axial load and increasing post-tensioning force; the bottom toe lifts up and tensile force increases at the bottom, as is evidenced in Figure 5.11(a) and Figure 5.11(b). Similarly, the same phenomenon occurs when the specimen is in the pull cycle, causing the east bar to sustain maximum strain. The column has seen maximum damage on the bottom east face of each column, so the maximum compressive strain is experienced on that end of the column. The east column was damaged the most, and therefore, the strains in the longitudinal bars of that column are the maximum strains recorded. Longitudinal bars at the top of the column witnessed smaller strains compared to the bottom of the bars, which is supported by the extent of concrete spalling at those locations. The strains on the spiral bars at the bottom and top ends of the columns, presented in Figure 5.11(e) and Figure 5.11(f), demonstrate the same concept of the column being damaged the most at the bottom. Strains were normalized by dividing the strain value by the yield strain. Normalized strains plotted against column height for different drift ratios, presented in Figure 5.14, show variation of strain with the height of the column. Longitudinal bar strains are maximum at the bottom of the column as expected. It can be seen that most of the bars reach the maximum strain at 4% and 5% drift ratio, which supports the idea that after the 5% drift ratio, PT bars start yielding and dominate in resisting the lateral load.

Table 5.1 Post-tensioned forces and loses on PT bars

PT bar no.	Initial PT load	Maximum PT load	Final PT load	Post-tensioning loss	% of Ultimate tensile load
	(kips)	(kips)	(kips)	(%)	(%)
1	43.5	97.3	12.8	70.6	76
2	53.5	104.8	20.72	61.3	81.9
3	50.2	101.9	17.7	64.7	79.6
4	58.8	103.4	22.5	61.7	80.78

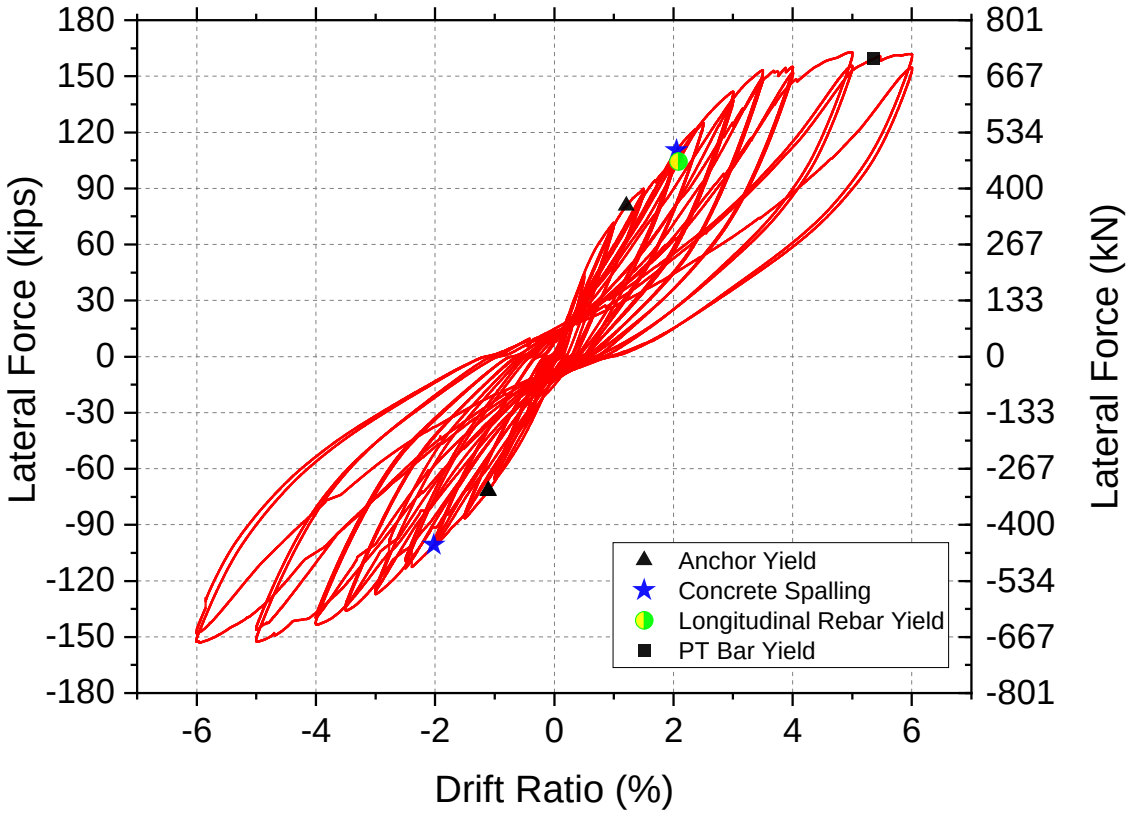

Figure 5.1 Hysteresis of the test result of the bridge bent

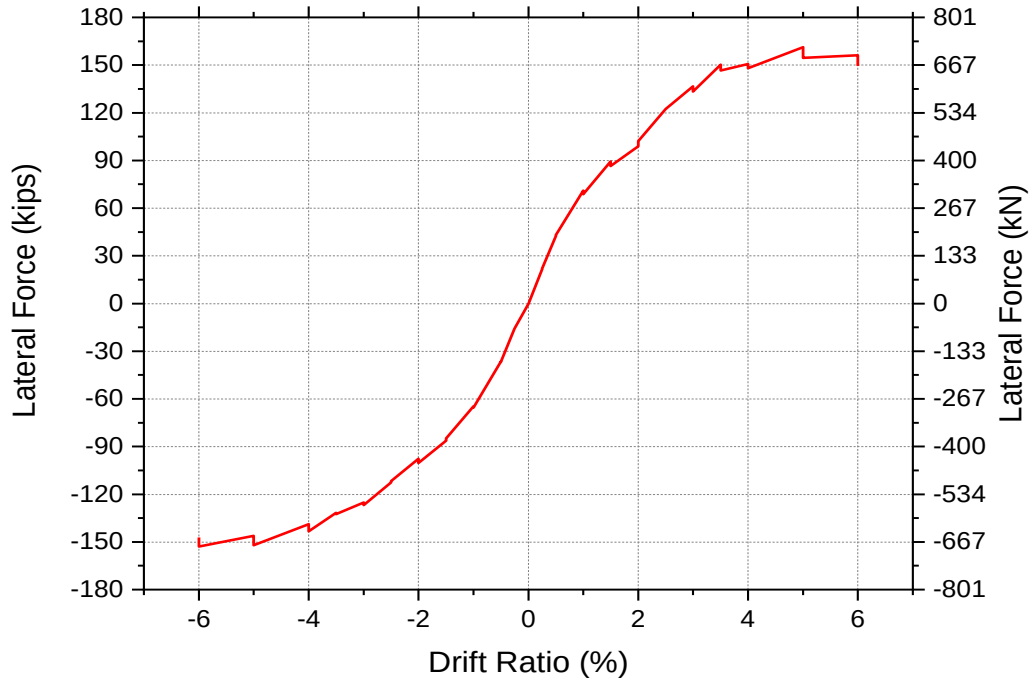

Figure 5.2 Hysteresis envelope of the test result of the bridge bent

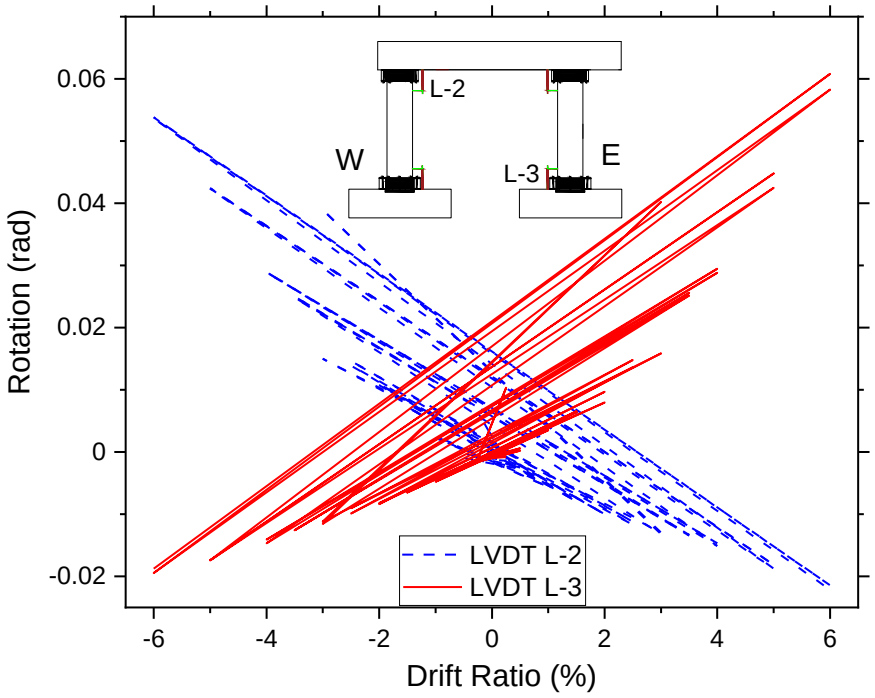

(a)

Figure 5.3 Column rotation vs drift ratio at the top and bottom of the columns

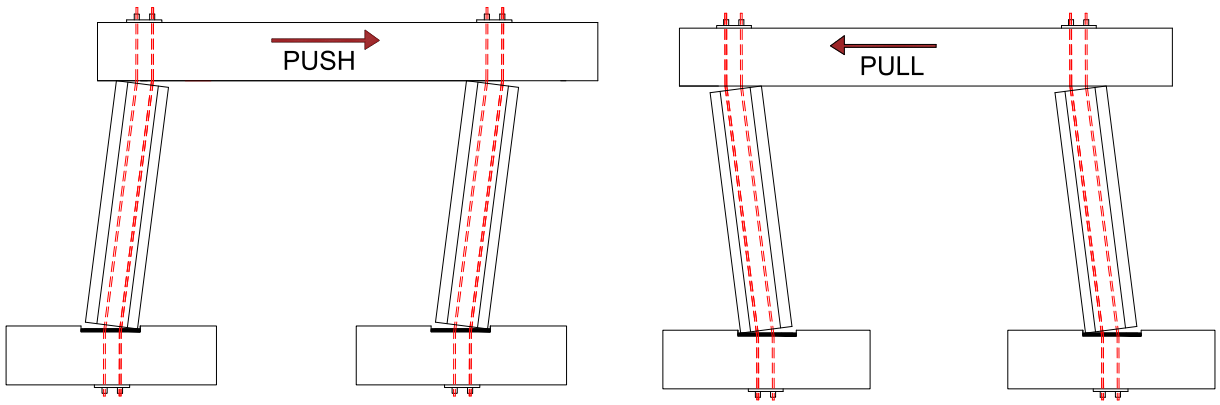

Figure 5.4 Schematic of the behavior of bridge bent during push and pull

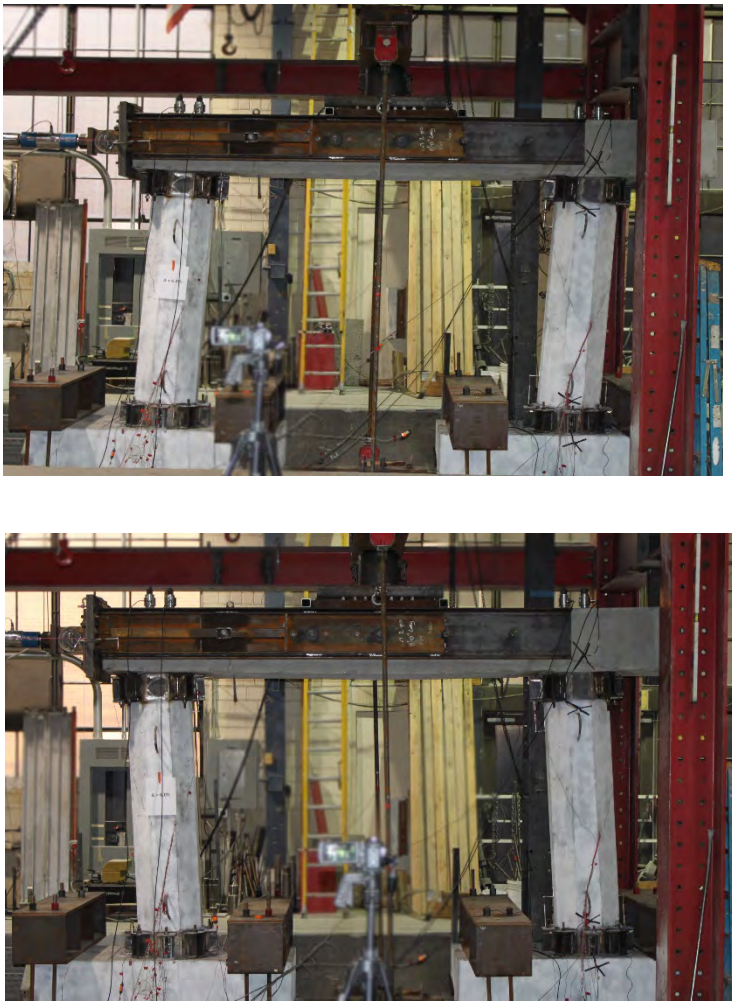

Figure 5.5 Maximum displacement at 6% drift on the push and pull of the bridge bent

Figure 5.6 Damage in the concrete at the end of the experiment

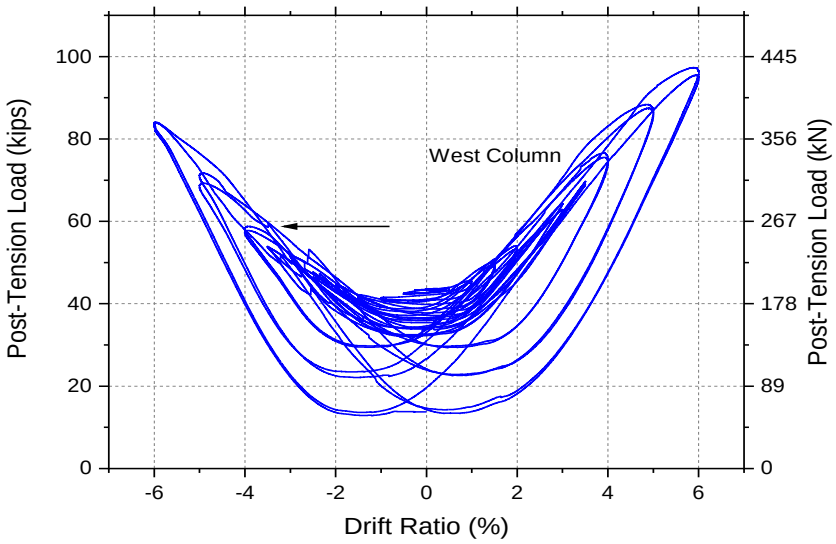
West Column
Post-Tension Load (kips)
Post-Tension Load (kN)
Drift Ratio (%)
100
80
60
40
20
0
445
356
267
178
89
0
-6
-4
-2
0
2
4
6

(a)

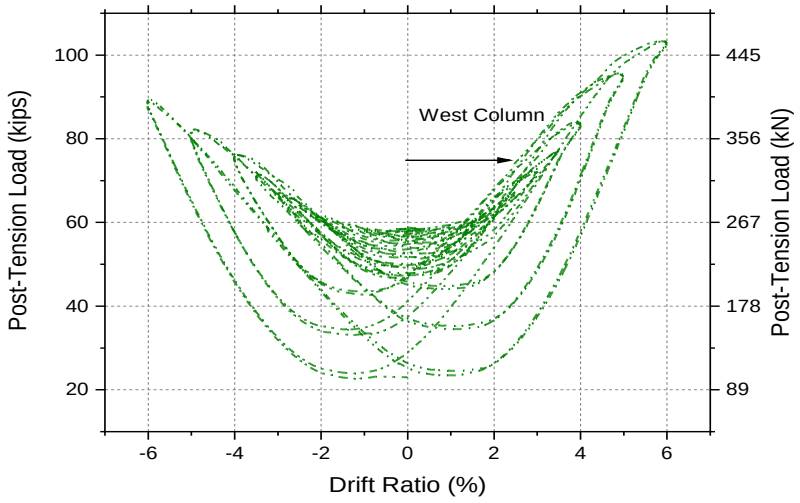
West Column
Post-Tension Load (kips)
Post-Tension Load (kN)
Drift Ratio (%)
100
80
60
40
20
445
356
267
178
89
-6
-4
-2
0
2
4
6

(b)

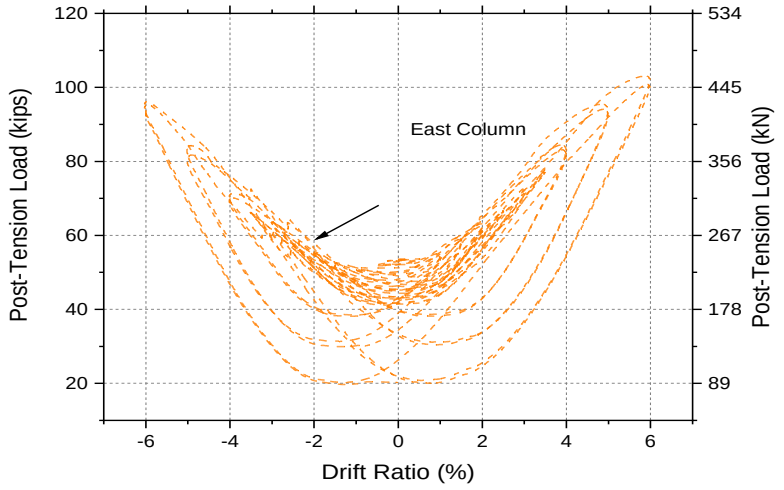

(c)

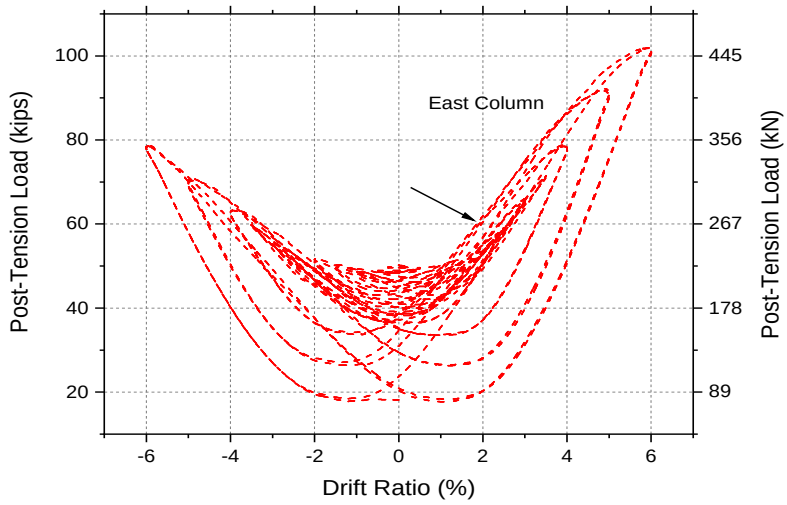

(d)

Figure 5.7 Post-tensioned load vs drift ratio on (a) PT bar 1, (b) PT bar 2, (c) PT bar 3, and (d) PT bar 4

Figure 5.8 PT bar buckling

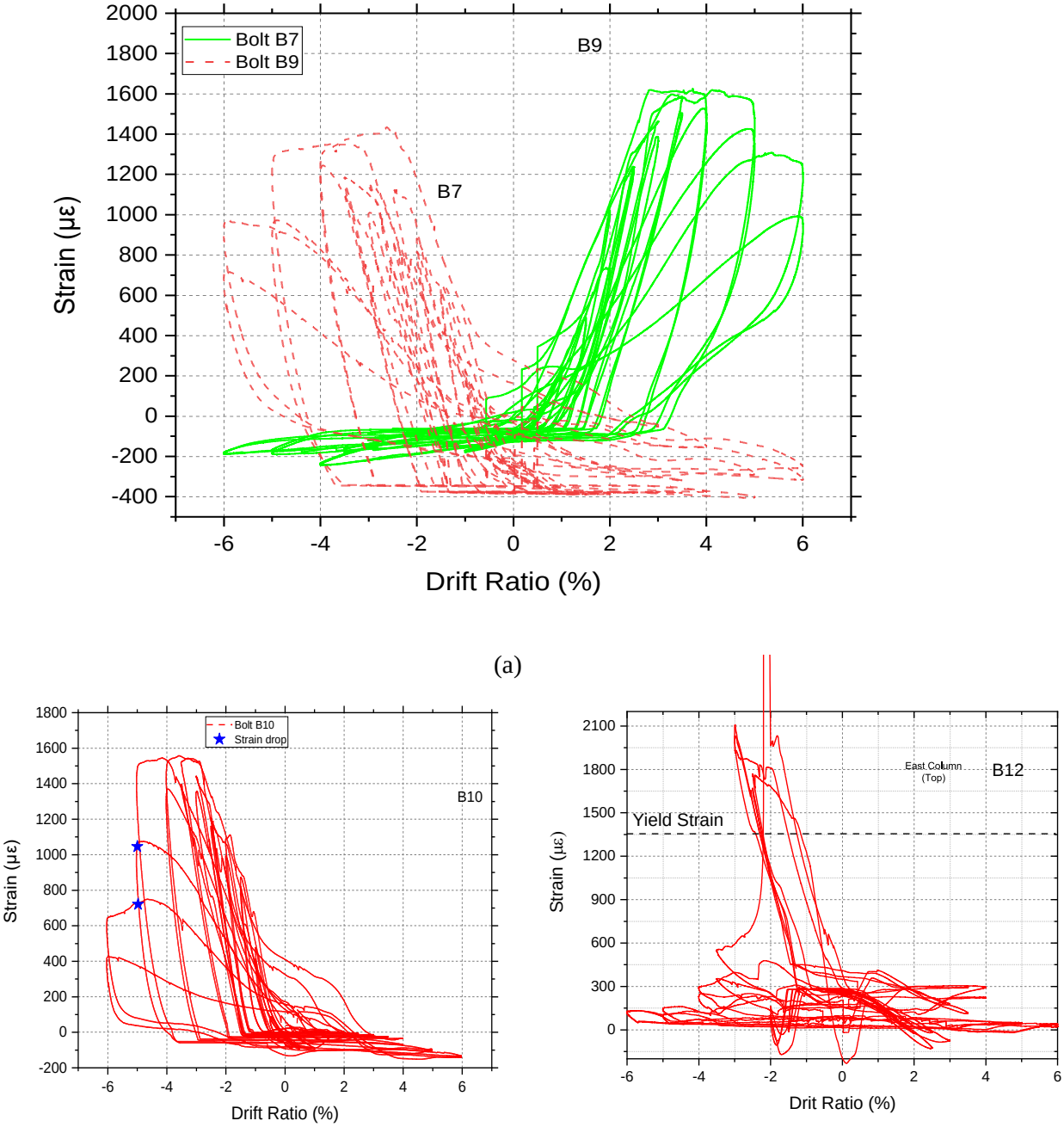

Figure 5.9 Strain in bolts vs the drift ratio at (a) bolts B7 and B9 at the bottom of east column, (b) bolt B10 at the bottom of east column, and (c) bolt B12 at the bottom of east column

Figure 5.10 Elongation and damage in SLAs

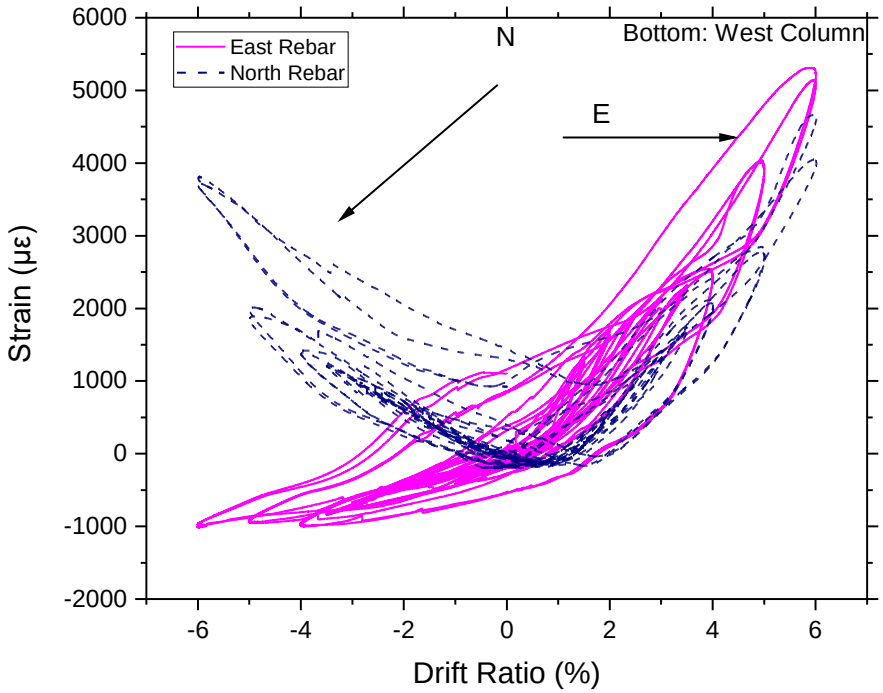
Bottom: West Column
East Rebar
North Rebar
N
E
Strain (με)
Drift Ratio (%)
6000
5000
4000
3000
2000
1000
0
-1000
-2000
-6
-4
-2
0
2
4
6

(a)

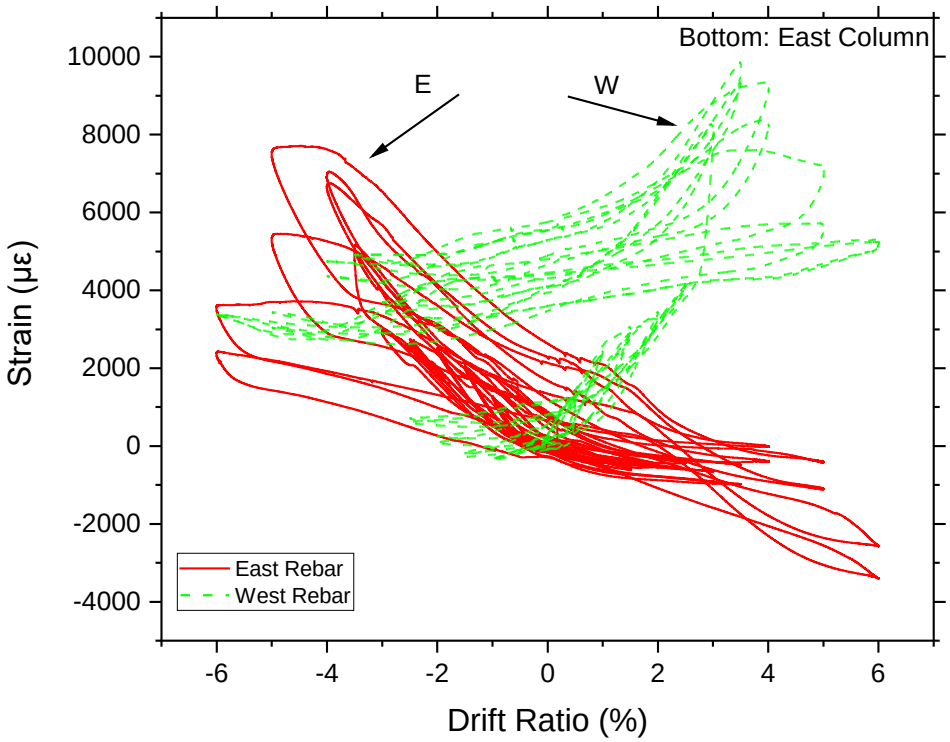
Bottom: East Column
E
W
East Rebar
West Rebar
Strain (με)
Drift Ratio (%)
10000
8000
6000
4000
2000
0
-2000
-4000
-6
-4
-2
0
2
4
6

(b)

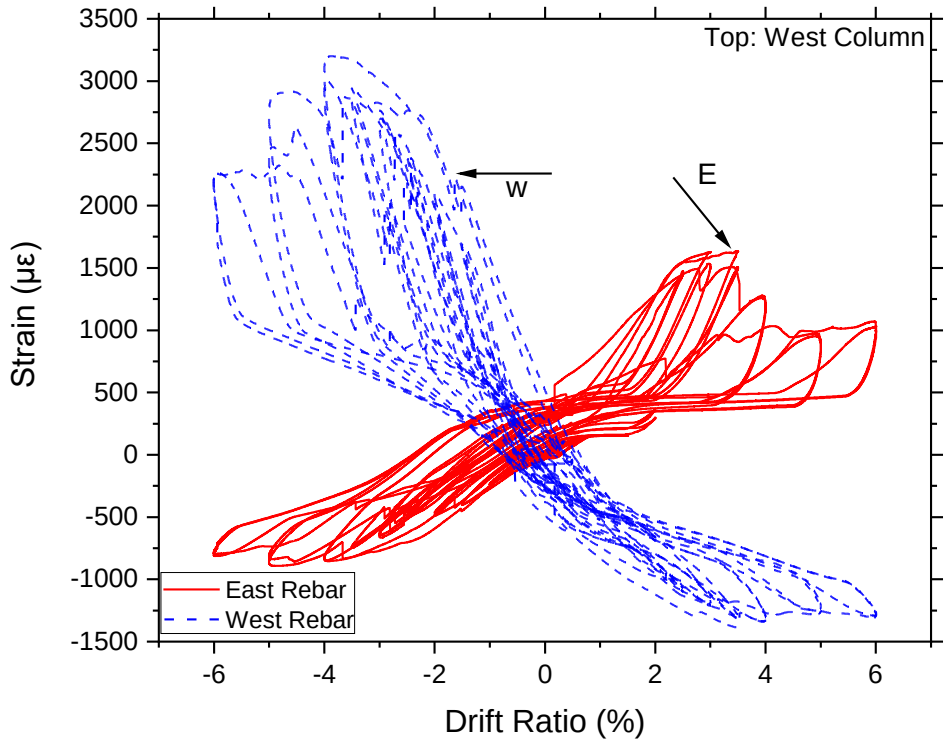
Top: West Column
W
E
East Rebar
West Rebar
Strain (με)
Drift Ratio (%)
3500
3000
2500
2000
1500
1000
500
0
-500
-1000
-1500
-6
-4
-2
0
2
4
6

(c)

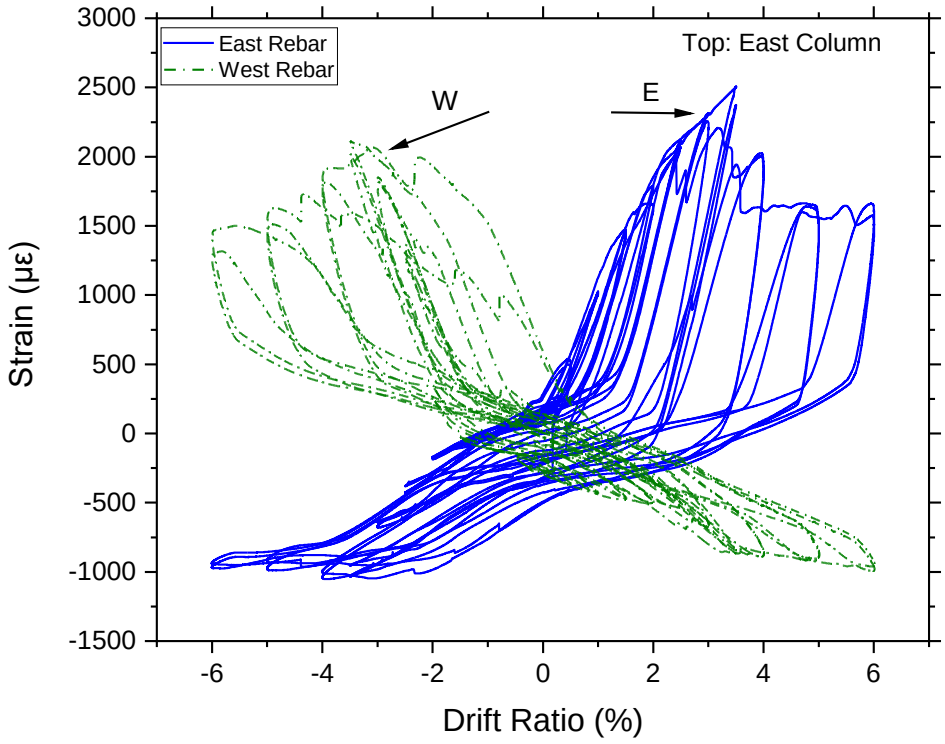
East Rebar
West Rebar
Top: East Column
W
E
Strain (με)
Drift Ratio (%)
3000
2500
2000
1500
1000
500
0
-500
-1000
-1500
-6
-4
-2
0
2
4
6

(d)

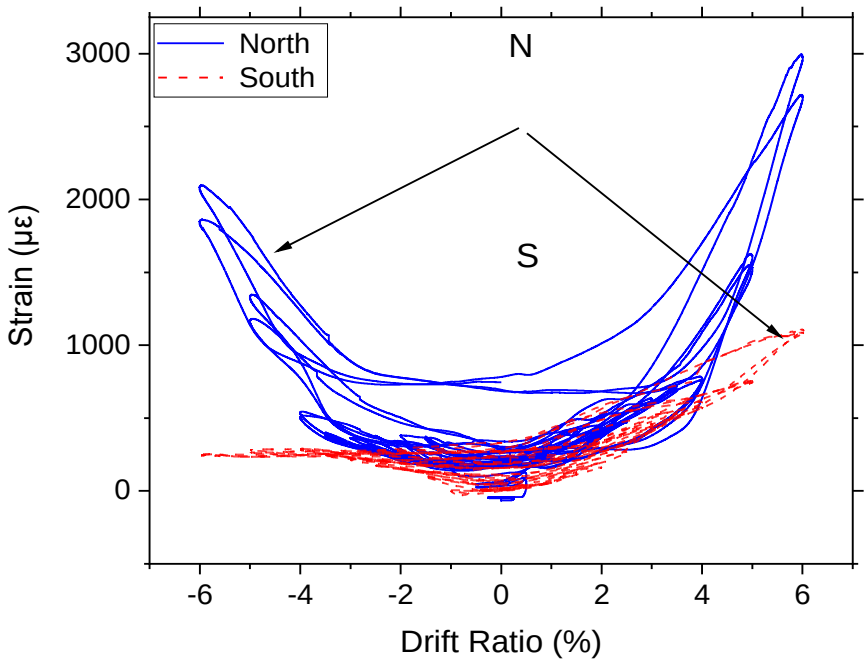

(e)

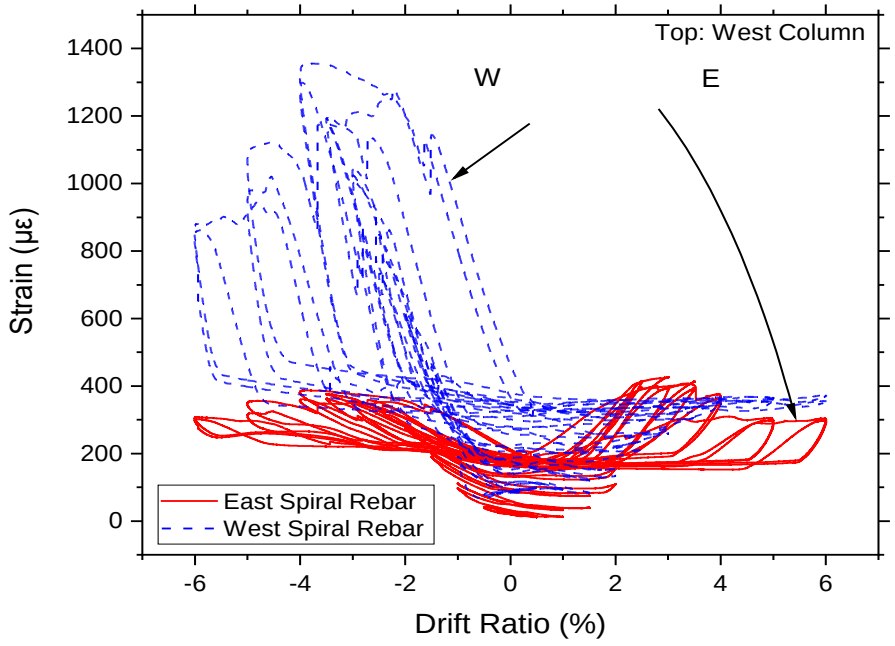

(f)

Figure 5.11 Strain vs drift ratio at (a) N/W bottom longitudinal bar of west column, (b)E/W bottom longitudinal bar in east column, (c) E/W top longitudinal bar of west column, (d) E/W top longitudinal bar of east column, (e) N/S bottom spirals of east column, and (f) E/W top spirals of west column

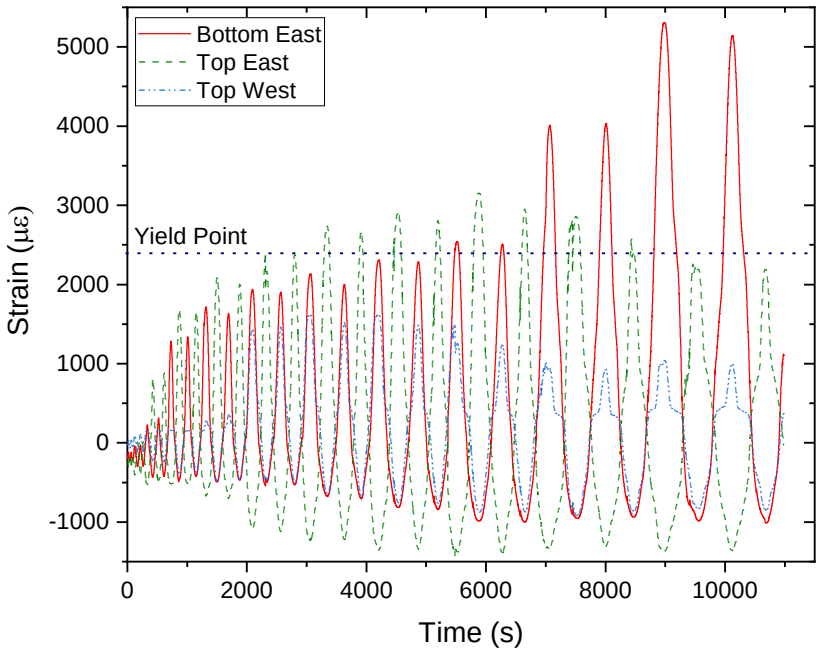

(a)

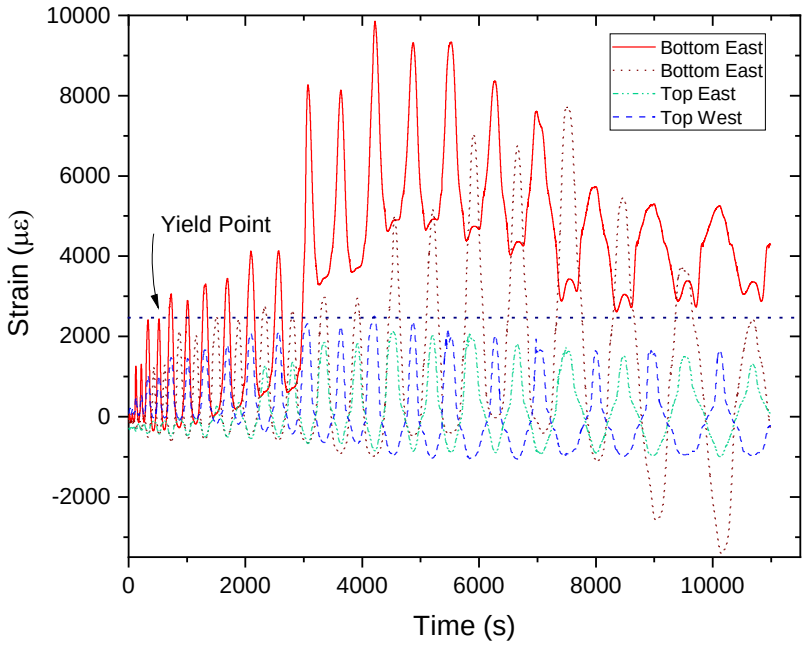

(b)

Figure 5.12 Column Longitudinal steel bar strains at end of steel collar; (a) west column; (b) east column

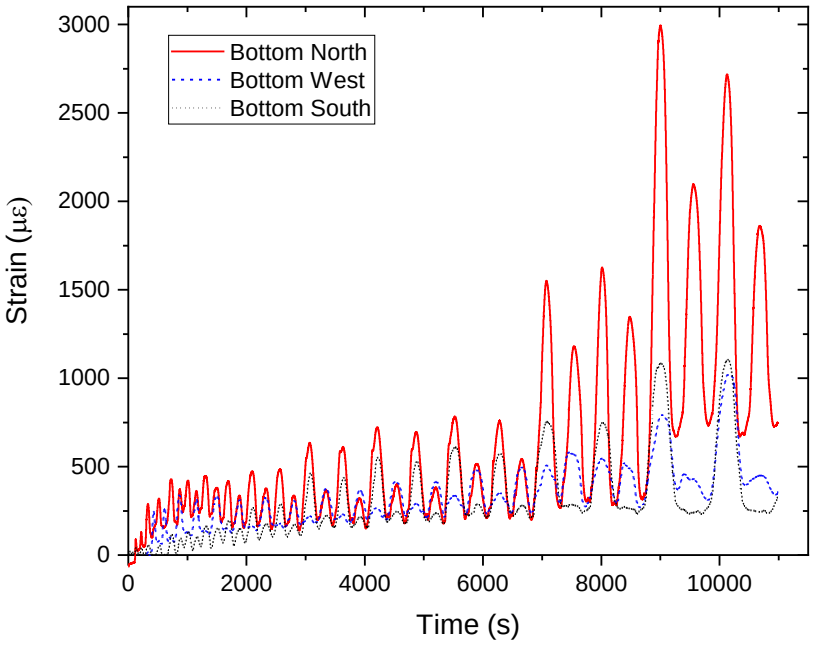

(a)

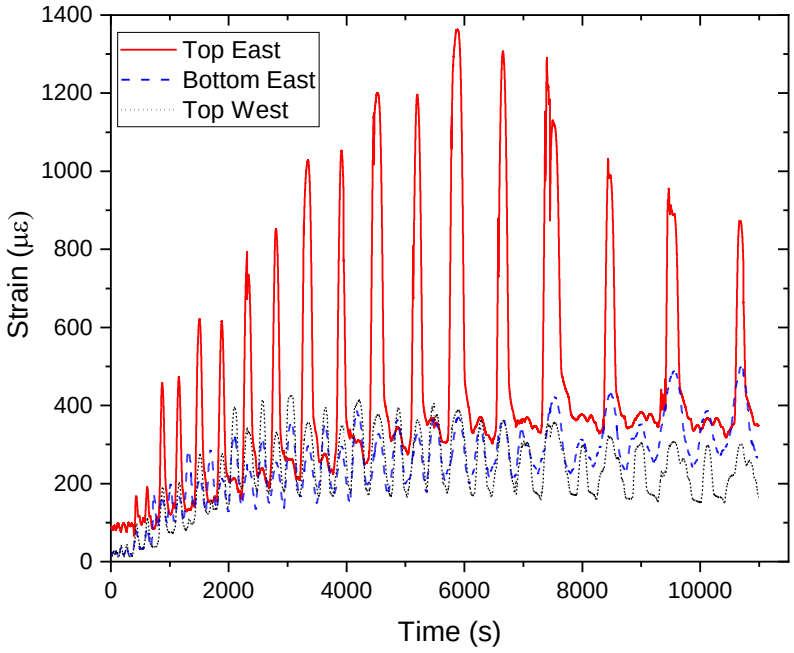

(b)

Figure 5.13 Column steel spiral hoop strain at end of steel collar; (a) west column; (b) east column

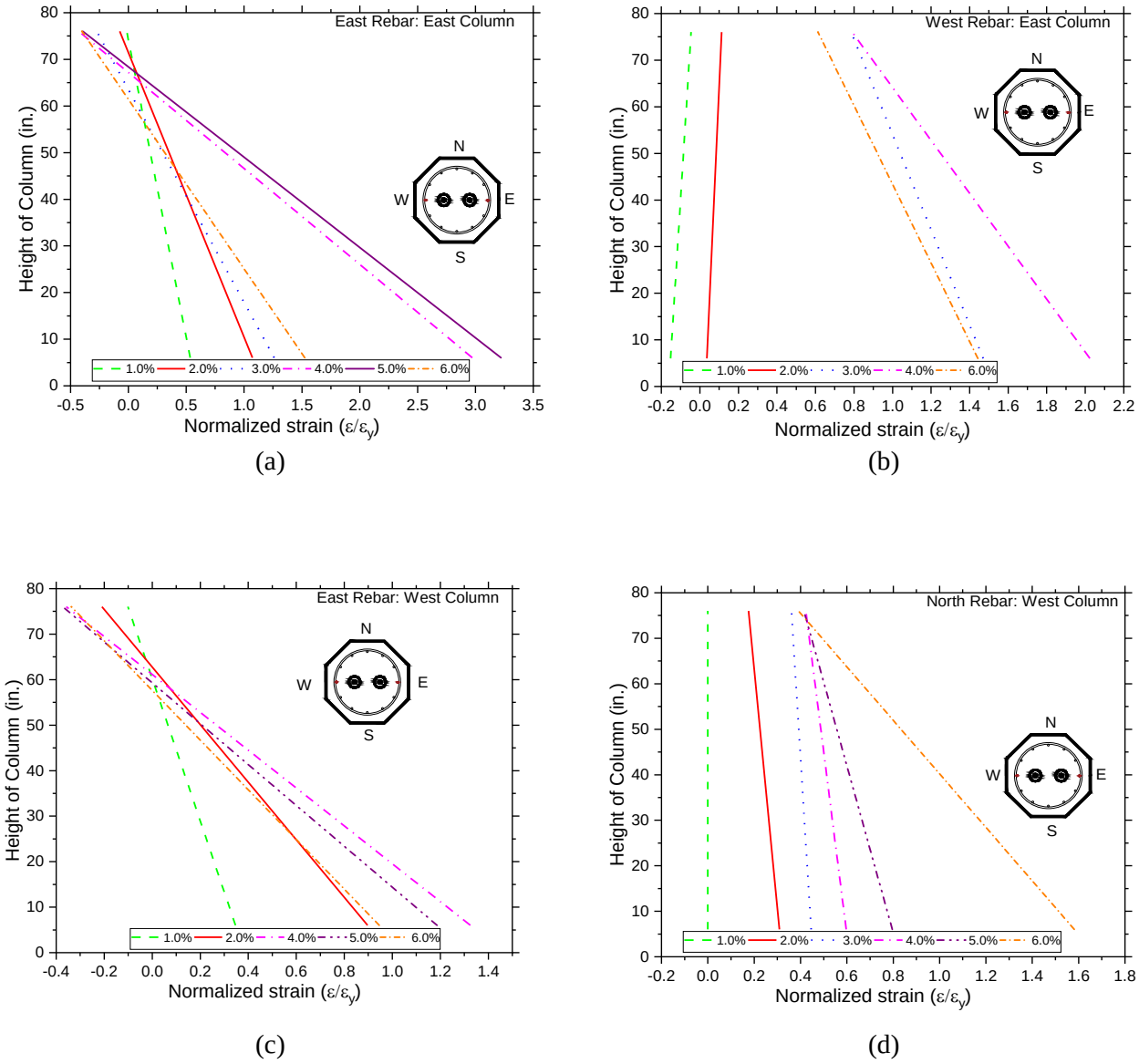

Figure 5.14 Normalized strain vs the height of the column in (a) East rebar of east column, (b) west rebar of east column, (c) east rebar of west column, and (d) north rebar of north column

5.4 Damage States

New damage states are defined for precast post-tensioned bridge bents with SLAs based on the experimental results. The definition of damage states was adopted from Dutta and Mander (1999). The damage states for this type of bridge bent are summarized in Table 5.2 with the resulting limits given on a theoretical pushover curve in Figure 5.15. Four damage states have been defined in this study: DS1, DS2, DS3, and DS4. The first damage state (DS1) is "Minor," which refers to yielding of longitudinal mild steel bars in the columns. The second damage state (DS2) is "Moderate," which refers to yielding and elongation of the stretch length bolts. Similarly, the third damage state (DS3) is "Serviceability," which refers to spalling of cover concrete in the columns. Finally, the fourth damage state (DS4) is "Life

Safety," which refers to yielding and buckling of the PT bars. The related repair needs and drift ratios for these damage states are also given in Table 5.2.

Table 5.2 Definition of damage states

Damage State		**Failure Mechanism**	**Repair Needs**	**Drift Ratio (%)**
DS1	Moderate	SLAs Yielding & Elongation	Replace Stretch Length Bolts	1.1
DS2	Minor	Longitudinal Rebar Yielding	No Repair	2.0
DS3	Serviceability	Concrete Spalling	Patching	5.0
DS4	Life Safety	PT bar yielding/bucking	Replace PT bars	5.5

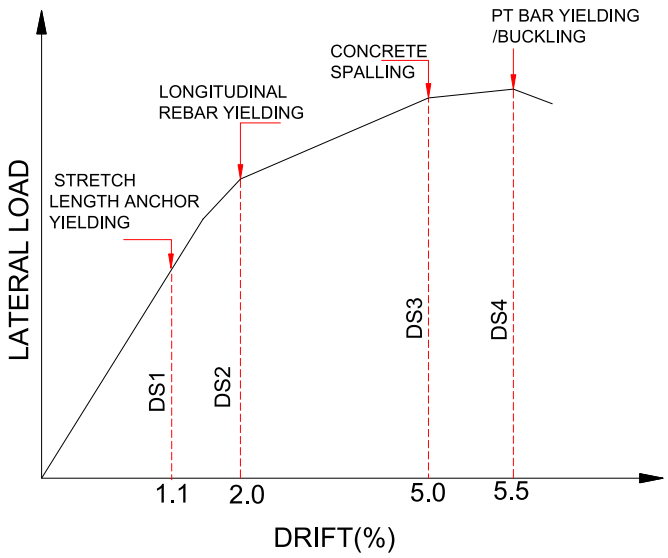

Figure 5.15 Damage states defined in this study

5.5 Cumulative Hysteretic Energy Dissipation

Hysteretic energy dissipation of hybrid PT systems is typically less than conventional monolithic systems because conventional monolithic systems sustain large inelastic deformations and large permanent damage. A high amount of hysteretic energy is dissipated by concrete cracking, crushing and spalling, and yielding and buckling of longitudinal steel bars and spirals. One of the essential parameters of a ductile system is its energy-dissipating ability, which is the ability of the structure to dissipate energy through a combination of elastic and inelastic deformations. The variation of axial load, PT forces, and the axial tension in the bolts at different drift ratios is shown in Figure 5.16. Figure 5.17 presents the hysteretic energy accumulated at different drift ratios. The area enclosed by one loop of the hysteretic curve gives the energy dissipated in that loop. The final energy dissipated is the sum of the areas obtained from all the hysteresis loops, which is significant. The equivalent viscous damping ratio of the system was fairly

constant throughout the experiment because the system is a precast post-tensioned bridge bent with minimal damage, as shown in Figure 5.18. Eq. (3.2) in section 3.2 requires that the energy dissipation coefficient should be greater than 0.1 for effective energy dissipation of the system. Figure 5.19 presents the energy dissipation coefficient at various drift ratios; there is good energy dissipation of the system above the 1% drift ratio.

5.6 Stiffness Degradation

The stiffness of each cycle is taken as the average of the secant stiffness through the origin to the maximum displacement in both the positive and negative directions. The stiffness degradation curve of the specimen is shown in Figure 5.20. The stiffness of the system was high at the beginning of the test and decreased at higher drift ratios. This degradation of stiffness can be attributed to yielding of SLAs and mild steel reinforcement, prestressing losses, PT bar yielding, and spalling of concrete at higher drift ratios.

5.7 Residual Drift and Self-centering

In this type of hybrid system with both post-tensioning and energy dissipators, the system is designed to return to its original position upon unloading. Provided the energy dissipation devices dissipate energy within a certain threshold, the axial load from the superstructure and the prestressing force brings the structure back to its original position by overcoming the bending moments created by the lateral force. The residual and maximum displacement of the system at each cycle is presented in Figure 5.21. The residual drift of the specimen at the end of the test was 1.1% for the negative cycle and 1.0% for the positive cycle. The maximum and residual displacement at each drift ratio is presented in Table 5.3. The plot of relative self-centering efficiency (RSE) from Eq. (3.3) vs. drift ratio is shown in Figure 5.22. For a perfectly self-centering system, the RSE should equal 100%. The RSE of this system was more than 82%, which is a satisfactory self-centering capability. Furthermore, Eq. (3.1) in section 3.2 requires the system to have a re-centering coefficient less than 0.6 for effective self-centering. Figure 5.23 demonstrates that this ratio is less than 0.6 at all times. Thus, the re-centering of the system is adequate. The permanent residual drift obtained in the experiment has resulted from the residual strains in the SLAs and the concrete spalling. Similarly, for the present case, based on the measured values, the minimum value of λ (Eq. 3.5) was found as 1.74, which implies that the ratio between re-centering and dissipative contribution was 63.5% to 36.5%.

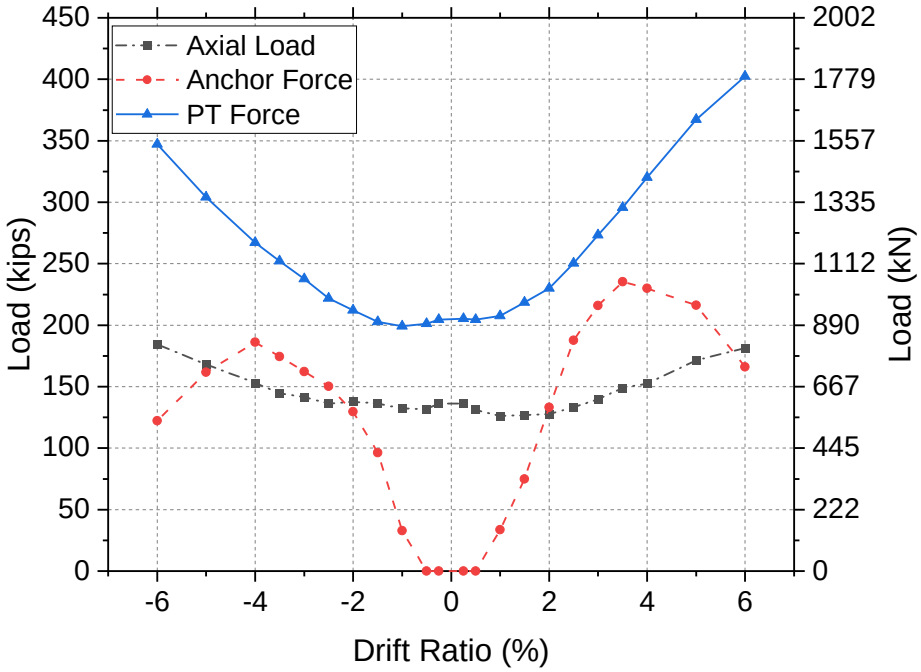

Figure 5.16 Axial load, PT force and tension in bolt at different drift ratios

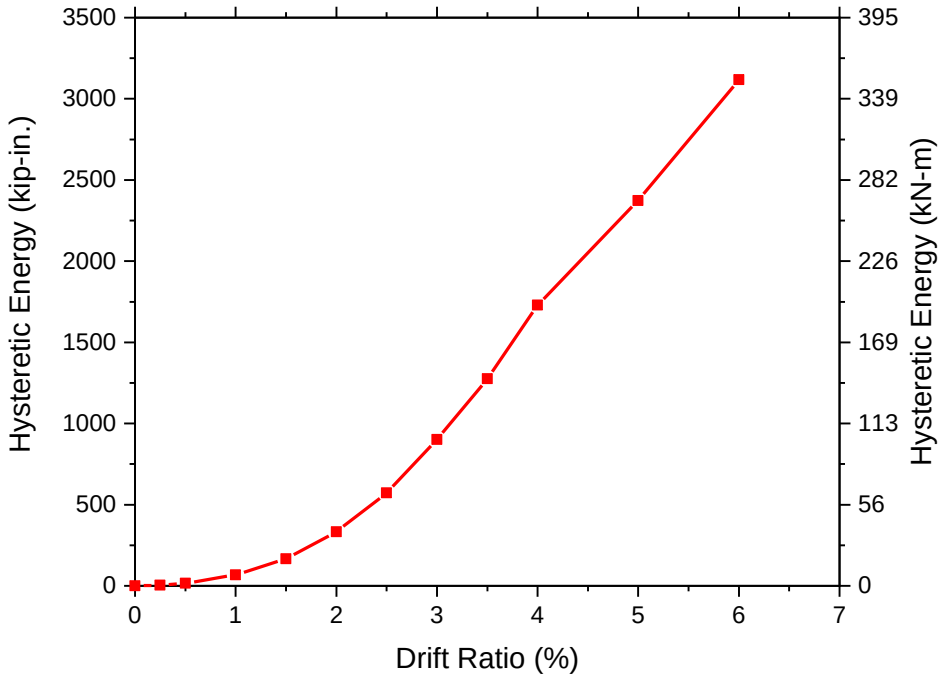

Figure 5.17 Cumulative hysteretic energy

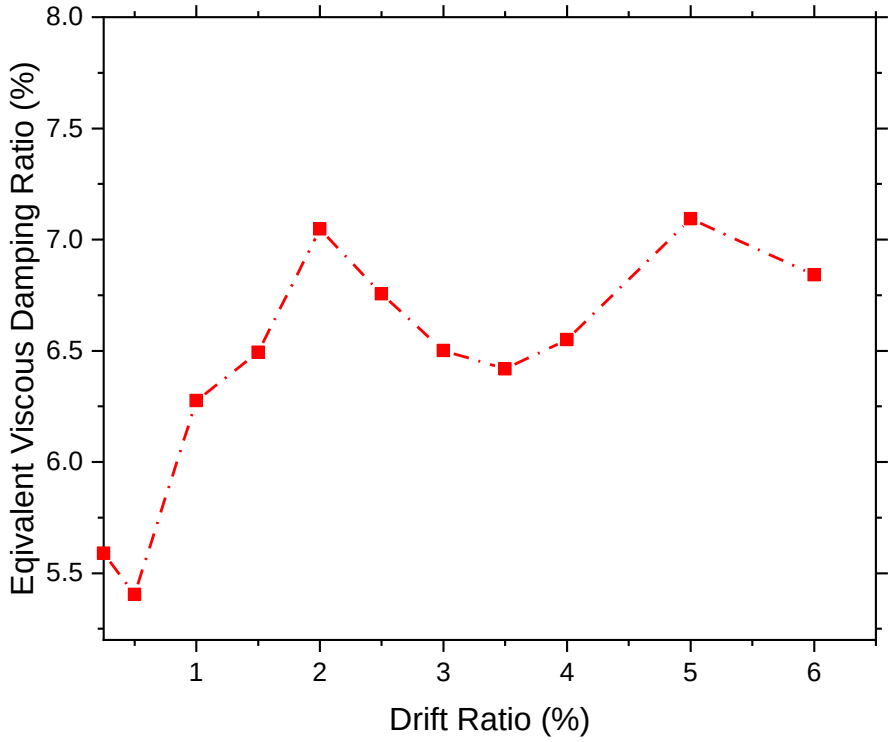

Figure 5.18 Equivalent viscous damping ratio of the bridge bent

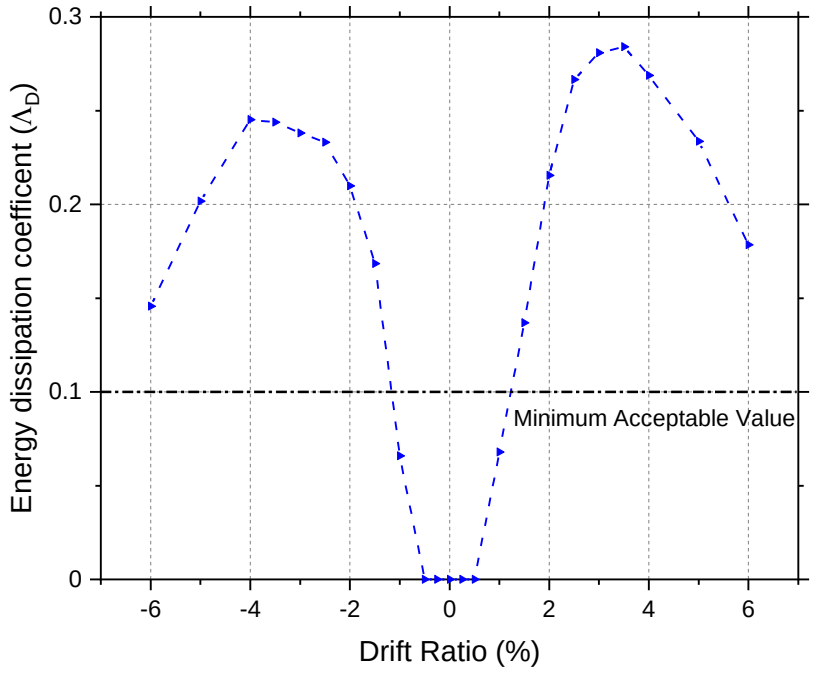

Figure 5.19 Energy dissipation coefficient at different drift ratios

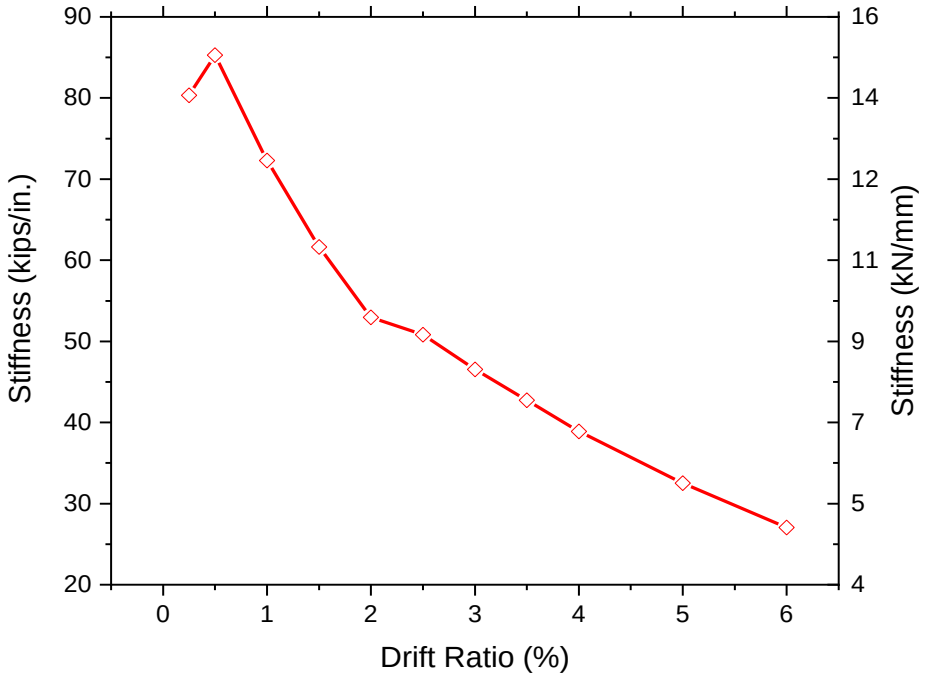

Figure 5.20 Stiffness deterioration of the bridge bent

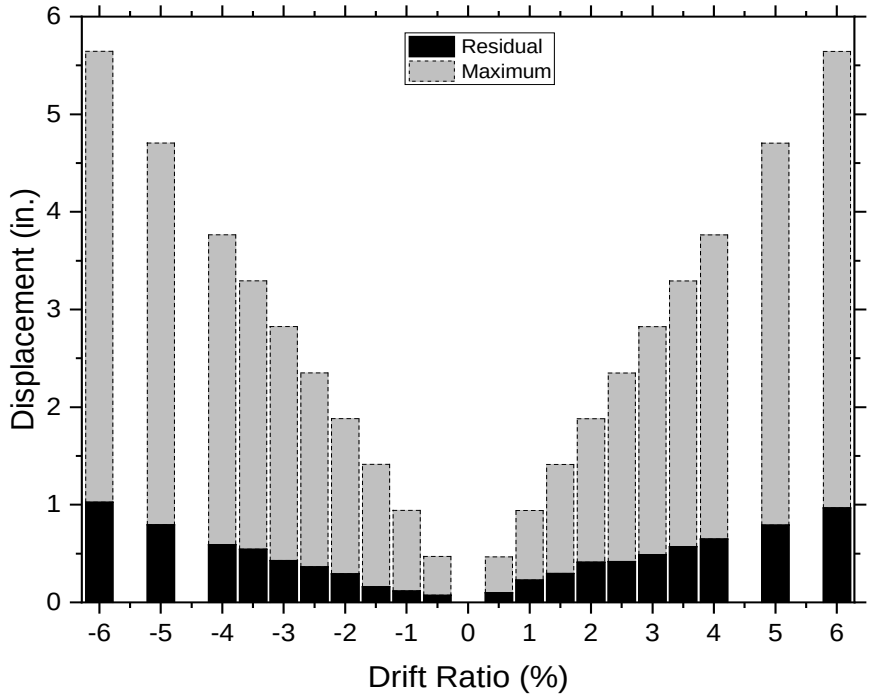

Figure 5.21 Residual and maximum displacements at each drift ratio

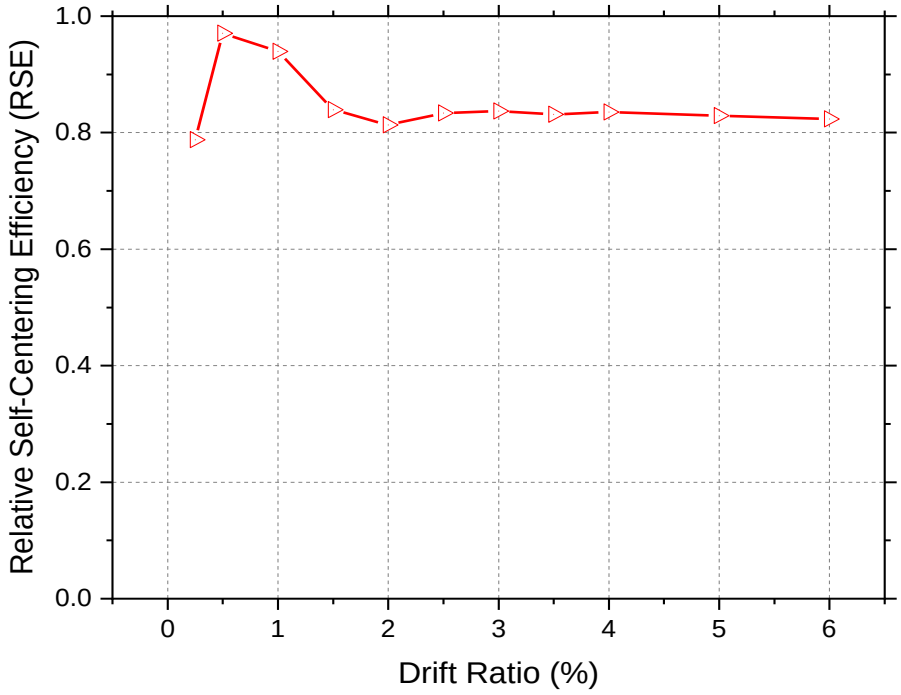

Figure 5.22 Relative self-centering efficiency of the bridge bent

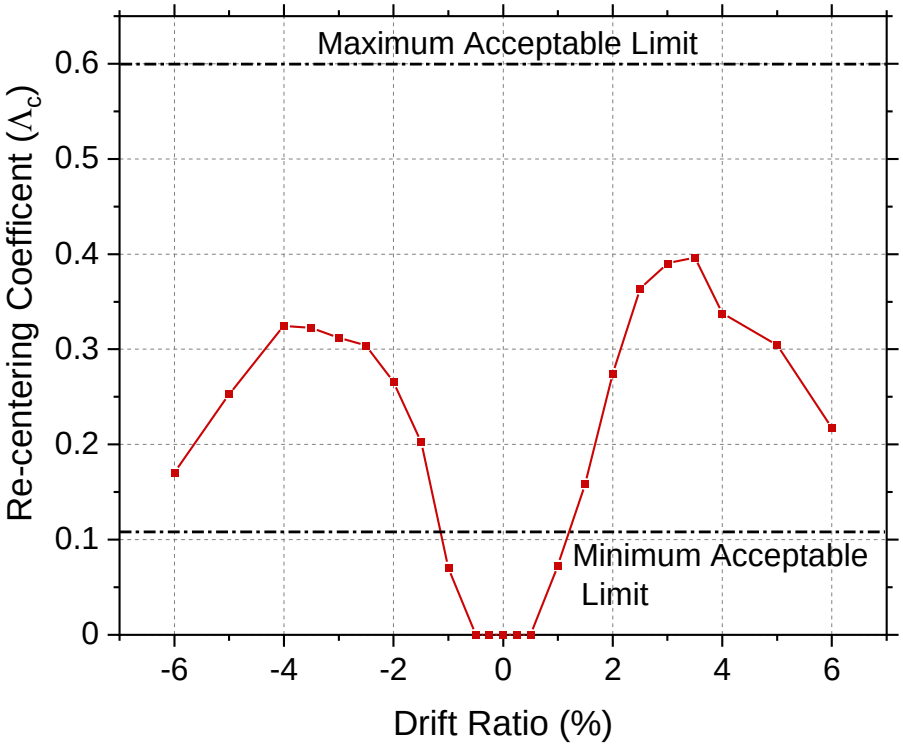

Figure 5.23 Re-centering coefficient of the system at different drift ratio

Table 5.3 Residual and maximum displacement at different drift ratios

Drift Ratio (%)	Displacement (in.)		Drift Ratio (%)	Displacement (in.)	
	Maximum	Residual		Maximum	Residual
0.25	0.23	0.05	-0.25	0.23	0.05
0.50	0.47	0.10	-0.50	0.47	0.07
1.00	0.94	0.23	-1.00	0.94	0.11
1.50	1.41	0.30	-1.50	1.41	0.16
2.00	1.88	0.41	-2.00	1.88	0.29
2.50	2.35	0.42	-2.50	2.35	0.36
3.00	2.82	0.49	-3.00	2.82	0.43
3.50	3.29	0.57	-3.50	3.29	0.54
4.00	3.76	0.65	-4.00	3.76	0.59
5.00	4.70	0.79	-5.00	4.70	0.79
6.00	5.64	0.97	-6.00	5.65	1.03

6. ANALYTICAL MODEL OF THE HYBRID BRIDGE BENT

6.1 Analytical Modeling

An analytical model for the post-tensioned rocking bridge-bent with external dissipators was developed using the open-source finite element software framework OpenSees (McKenna et al. 2010). A 2-D model was created with different modeling techniques to represent the material properties, rocking interface between column-footing and column-cap beam, unbonded post-tensioning, and stretch-length bolts. In this section, the modeling technique used to simulate the rocking-interface is described in brief and the material properties, elements, and analysis objects used to simulate the model.

Unlike modeling of conventional reinforced concrete frames, there are several challenges when modeling precast post-tensioned concrete frames mainly because of the gap opening and rocking behavior. The curvature of the rocking interface is infinite due to its gap opening nature; therefore, it violates Bernoulli's theory that "plane sections remain plane" (Marriot 2009). The contact surface and opening of the gap at the rocking interface, constraining of the PT-tendons inside the ducts, the application of initial post-tensioning, and modeling of the external replaceable bolts are a few of the challenges in modeling the specimen.

6.2 Material Model

6.2.1 Concrete

Concrete is modeled with two different properties for the cover and core concrete. The cover concrete is defined as unconfined concrete and modeled to replicate the cylinder concrete compression tests. Similarly, the core concrete is defined as confined concrete and is modeled, taking into account the confining pressure provided by the hoops. Both confined and unconfined concrete are modeled as *uniaxialMaterial Concrete04 (Popovic Concrete Material). Concrete04* Material is basically defined by four parameters: the 28-day compressive strength of concrete (f_c'), concrete strain at maximum strength (ε_{cc}), concrete strain at crushing strain (ε_{cu}), and initial stiffness of the stress-strain curve (E_c). The parameters are discussed below. The ratio of the volume of spiral reinforcement to the total volume of core confined by the spiral with diameter (*D*) of 15 in. (381 mm) and pitch (*s*) of 2.5 in. (64 mm) expressed as

$$\rho = \frac{\pi D A_{sp}}{\pi D^2 s/4} = \frac{4A_{sp}}{Ds} \tag{6.1}$$

Eq. 6.1 gives ρ=0.033. Young's modulus of elasticity of the concrete is given as:

$$E_c = 57000 * \sqrt{f'_c} \tag{6.2}$$

Hence $Ec = 5700\ ksi$

The stress in the steel, fs is given as:

$$f_s = E_s \left(0.0025 + 0.21 \left(\sqrt[3]{\frac{k_e \rho_s}{f'_c}} \right) \right) \leq f_{yt} \leq 200{,}000 psi \tag{6.3}$$

Using the equation, we obtain that:

$$f_s = 69\ ksi$$

The confining pressure is given as,

$$f_3 = \frac{2f_s A_{sp}}{Ds} = \frac{\rho_s f_s}{2} \quad (6.4)$$

$$f_3 = 1.14\ ksi.$$

Standard cylinder compressive strength is given by:

$$f'_{cc} = Cf'_c + 4.1f_3 \quad (6.5)$$

(Recommended value of C = 0.85)

$$f'_{cc} = 13.174\ ksi$$

The strain at peak stress for confined concrete is given as:

$$\varepsilon_{cc} = \varepsilon_0 \left(1 + 5\left(\frac{f'_{cc}}{Cf'_{cc}} - 1\right)\right) \quad (6.6)$$

(strain at peak stress in unconfined concrete, $\varepsilon_0 = 0.02$)

$$\varepsilon_{cc} = 0.00746\ in./in.$$

The maximum strain capacity of confined concrete is given as:

$$\varepsilon_{cu} = 0.004 + 0.075\frac{\rho_s f_{yt}}{f'_c} \quad (6.7)$$

which gives, $\varepsilon_{cu} = 0.0211\ in./in.$

6.2.2 Mild Steel Rebar

The column longitudinal steel rebar is modeled as a *uniaxialMaterial Steel02 Material -- Giuffré-Menegotto-Pinto Model* with Isotropic Strain Hardening. This material was used to define the stress-strain behavior of the steel rebar. This model is defined by five parameters: Yield Strength (F_y) of steel, Young's modulus (E_s), strain-hardening ratio (ratio between the post-yield tangent and initial elastic tangent) (b), parameters to control the transition from elastic to plastic branches (R), and isotropic hardening parameter (a), y of 69 ksi (476 MPa), E_s of 29000 ksi (200 GPa), b of 0.05, R of 18, a1 of 0.03, a2 of 1.0, a3 of 0.03, and a4 of 1.0 are taken as an input parameter when modeling the steel rebar.

6.2.3 Post-tensioned Bar (PT)

The uniaxialMaterial Steel02 Material is used in conjunction with *Initial Stress Material* to model the unbonded PT bar. The *uniaxialMaterial Steel02 Material* is used to define the tensile stress-strain behavior of the PT bars; the initial PT force applied was modeled by the initial stress material. The *uniaxialMaterial Steel02 Material* used has five major parameters, as discussed in the previous section. Yield stress of PT bar (F_{PT}), which is 120 ksi (827 MPa), and Young's modulus of elasticity (E_{PT}) of the PT-bar, which is 29000 ksi (200 GPa) are the only different parameters and the rest are same as for the steel rebar. Similarly, *uniaxialMaterial InitStressMaterial* has one main parameter that needs to be defined, the initial stress, which was taken to be 40% of the ultimate strength of the PT bar equal to 60 ksi (414 MPa). *Corotational Truss* elements that consider non-linear element geometry were used to represent the PT bars because they would be inclined by an amount approximately equal to the base rotation as the column uplifts (Trono 2014). A total of four PT bars with a diameter of 0.85 in.^{2} (506 mm^2) were used in the experiment. The PT bars were fully restrained at the bottom and rigidly fixed at the top node of the beam using the *elasticBeamColumn* element.

6.2.4 Stretch Length Anchors

SLAs were designed to experience only tension, so the numerical model was also required to capture tension behavior of the bolts. *Elastic perfectly plastic (EPP) gap* material with bilinear curve was used to model bilinear tension behavior of the bolts. The modulus of elasticity (E_{sb}) equal to 29,000 ksi (200 GPa), yield force of bolts (F_{yb}) equal to 36 ksi (248 MPa), a gap equal to 0.0, hardening ratio (eta) equal to 0.005, and area of the bolt (A_b) equal to 0.44 in.^{2} (284 mm^2) are the main parameters used for the EPP gap material. These properties were used from tensile tests of SLAs conducted at the structures laboratory of the University of Utah (Parks et al. 2019). *Truss* element was used to connect the top and bottom nodes of each bolt. The bottom end of the bolts was fully fixed to the footing, whereas the upper end of the columns was connected rigidly using *elasticBeamColumn* element to the center node of the column.

6.3 Beam-column Elements

The reinforced concrete column is modeled using fiber-based elements. Each section of fiber represents a different stress-strain behavior. *Nonlinear-BeamColumn* element, which is based on an iterative force-based formulation, was used to represent the column. The octagonal column shape was represented with an equivalent circular section, and *Section* command was used to create the composite section. The circular section is divided into 20 radial divisions and 20 angular divisions for the core concrete, and four radial divisions and 20 angular divisions for the cover concrete, respectively. The *Patch* command was used to construct the core and cover concrete subdivisions. Twelve longitudinal bars were modeled using the *Layer* command in OpenSees. The *Nonlinear-BeamColumn element* had five integration points. The bottom nodes of the column were connected to the top nodes of each *zero-length* spring rigidly by an *elasticBeamColumn* element and were then connected to the foundation nodes. Similarly, the top node of the column was rigidly connected to the free nodes of the springs representing the rocking surface at the cap beam-column interface whose other end was rigidly connected to the cap-beam. The cap beam is assumed to behave elastically during the loading protocol; therefore, *elasticBeamColumn* element is used to represent the cap beam. The entire schematic of the model is shown in Figure 6.1.

6.4 Coordinate Transformation

The OpenSees geometric transformation object (*geomTransf*) is employed to transform the element's stiffness and resisting force from the local to the global coordinate system (Trono 2014). Linear, PDelta, and Corotational transformation are three options that can be used for coordinate transformation. The *Linear* transformation was used for both the columns and the cap-beam.

6.5 Rocking Surface

The most common modeling technique used for rocking interface simulation is the multi-spring contact surface, which uses multiple elastic, compression-only springs (Marriot 2009). This approach defines the axial stiffness of the contact springs to be a function of the depth/width ratio, concrete properties and cantilever length of the column. Similarly, in the modeling approach used by Trono (2014), multiple compression-only vertical springs represented by zero-length elements were used. This approach enabled the uplift of one side of the column, during rocking motion, while the compression force in the springs resist the other side of the column. The number of springs to be used should be adequate so they can

capture response of the structure with minimal analysis time. Among various approaches for modeling the rocking interface between precast footing-column and cap beam-column, the lumped plasticity model and the multi-spring model are the most common. In the lumped plasticity model, the rocking interface is represented by a set of rotational springs at the rocking bed. In the multi-spring model, multiple non-linear axial compression-only springs are used to capture the rocking characteristics of the post-tensioned system. The multi-spring model has the greatest potential to model a PT system in terms of accuracy and computational effort (Marriot 2009). The multi-spring model is used in the present model. The most crucial part of modeling the contact surface is assigning properties of the contact material. Two different types of springs were used at the rocking interface to account for confined and unconfined concrete. Each spring was connected using two nodes. The lower nodes were fully fixed, while the upper nodes were free to elongate to simulate uplift of the column. Both nodes have the same coordinates; zero-length elements are used to connect the nodes. Since the spring had zero tensile resistance, it offered no resistance to uplift of the rocking plane. The octagonal column area was discretized by subdividing the area segmentally into eighteen divisions, and each division was represented by a spring located at the center of the segment with a unique area. The vertically free node of every spring was connected rigidly with the center point to the single node representing the column base.

The material used to simulate the contact surface was *Elastic perfectly plastic (EPP) gap* material because this material has zero tensile resistance. The parameters used in Concrete01 material *Elastic perfectly plastic (EPP) gap* material is the yield stress of the springs (f_{yc}), and the modulus of elasticity (E_{cs})of the contact spring. The stress values were multiplied by the area of each spring, and the modulus of elasticity was provided to give the force-displacement relationship for each spring.

6.6 Analysis

Gravity and cyclic analysis were performed using static analysis in OpenSees. A cyclic analysis was performed by applying a unidirectional pull until a certain drift ratio and subsequently pulling back to the same drift ratio in the negative direction and finally pushing back to a zero-drift ratio. The static analysis was carried out by the *DisplacementControl* integrator object; this means that analysis was displacement controlled such that each successive analysis step is carried out at each incremental displacement at one degree of freedom. The displacement increment was assigned as one percent of the column height for all static analyses. The N*ewton, Broyden NewtonLineSearch, and KrylovNewton* were employed to solve the non-linear residual equation at each time step because of its robust method for solving non-linear algebraic equations (Bowman 2016).

6.7 Comparison between Experiment and Numerical model

An analytical model was developed in OpenSees to evaluate the performance of the bridge bent specimen under a quasi-static lateral cyclic load combined with axial load. The analytical model was developed, as described in the previous sections. Figure 6.1 presents a schematic of the OpenSees model. The analytical model was able to capture the initial stiffness, lateral strength, and hysteretic energy dissipation capacity of the test successfully and nearly matches the experimental results. Figure 6.2 represents the lateral load vs. drift ratio showing experimental and analytical results. The model predicted the hysteretic behavior of the experiment. As presented in Figure 6.3, the analytical model dissipated a similar amount of total

hysteretic energy as in the actual experiment. Figure 6.4 presents the comparison of energy dissipated in each cycle between the experimental and analytical results. The analytical model was successful in capturing the stiffness degradation of the bridge bent effectively, as shown in Figure 6.5. Comparison of the forces for the PT bars at different drifts with the experiment bolster the validity of the proposed analytical model, as shown in Figure 6.6.

The hysteresis curve of the bridge bent tested with PT bars and SLAs was compared with the analytical models of a similar monolithic bridge bent, and a PT bridge bent without stretch length bolts, as shown in Figure 6.7. The equivalent monolithic bridge bent did not have PT bars but the equivalent mild steel bars representing the area and strength of the PT bars were included in the model. There were only continuous mild steel longitudinal bars from the footing to the column and from the column to the cap beam. Also, there were no SLAs included in the monolithic bridge bent. The monolithic bridge bent had full curves with large energy dissipation and high residual displacement, as shown in Figure 6.7(a). The hysteretic energy dissipation of the monolithic bridge bent is 13883 kip-in. (1569 kN-m), which is four and one-half times the hysteretic energy dissipated by the hybrid bridge bent. Yielding of the mild steel reinforcement and crushing and spalling of concrete contributed to such a high amount of hysteretic energy dissipation and residual drift. The lateral strength of the equivalent monolithic bridge bent is less compared to the tested bridge bent.

The bridge bent incorporating PT bars only, displays excellent self-centering with a residual drift of 0.21%, which is five times less than the residual drift ratio of the tested bridge bent, and with negligible energy dissipation. The lateral strength of the bridge bent with PT bars only was 28 kips (125 kN) less than the tested specimen, i.e., 17% less compared to that of the tested specimen, as shown in Figure 6.7(b).

The comparison of hysteretic energy dissipation of the three bridge bents is shown in Figure 6.8. Similarly, the comparison of the test results of the original bridge bent and the aforementioned analytical models are shown in Table 6.1. The use of PT bars in conjunction with SLAs dissipated a good amount of energy, three times more than the bridge bent with PT-only, with higher lateral strength as compared to the bridge bent with PT bars only, which is desirable during an earthquake. Similarly, the residual displacement of the hybrid system incorporating SLAs and PT bars is minimum compared to the equivalent monolithic bridge bent, which makes the proposed system serviceable after minor repairs following an earthquake.

Table 6.1 Comparison between the tested and the analytical models of the bridge bent

Bridge bent type	Lateral Strength (kips)	Hysteretic Energy Dissipation (kips-in.)	Residual Drift (%)
Original (Tested)	162.9	3117	1.10
Original (OpenSees)	154.5	3244	0.53
PT without SLAs(OpenSees)	135	976	0.21
Equivalent Monolithic (OpenSees)	140	13883	5.15

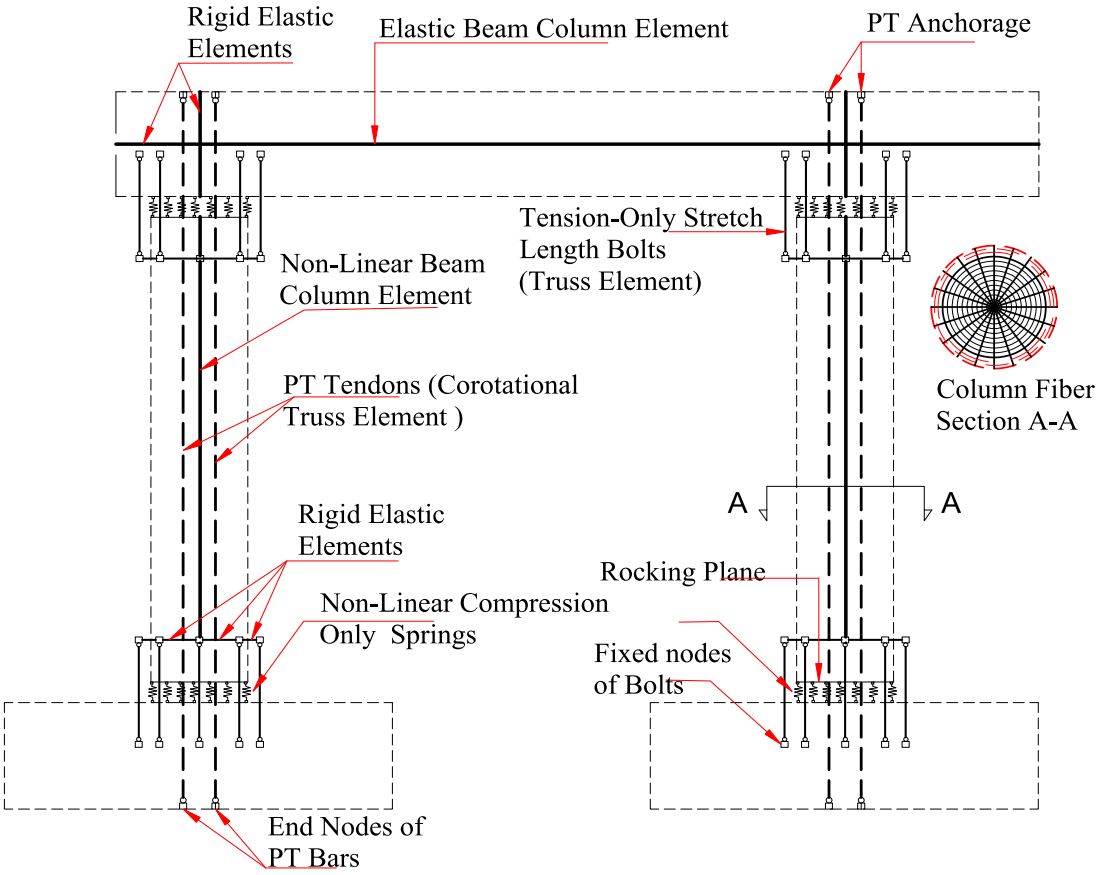

Figure 6.1 OpenSees model for precast post-tensioned bridge bent

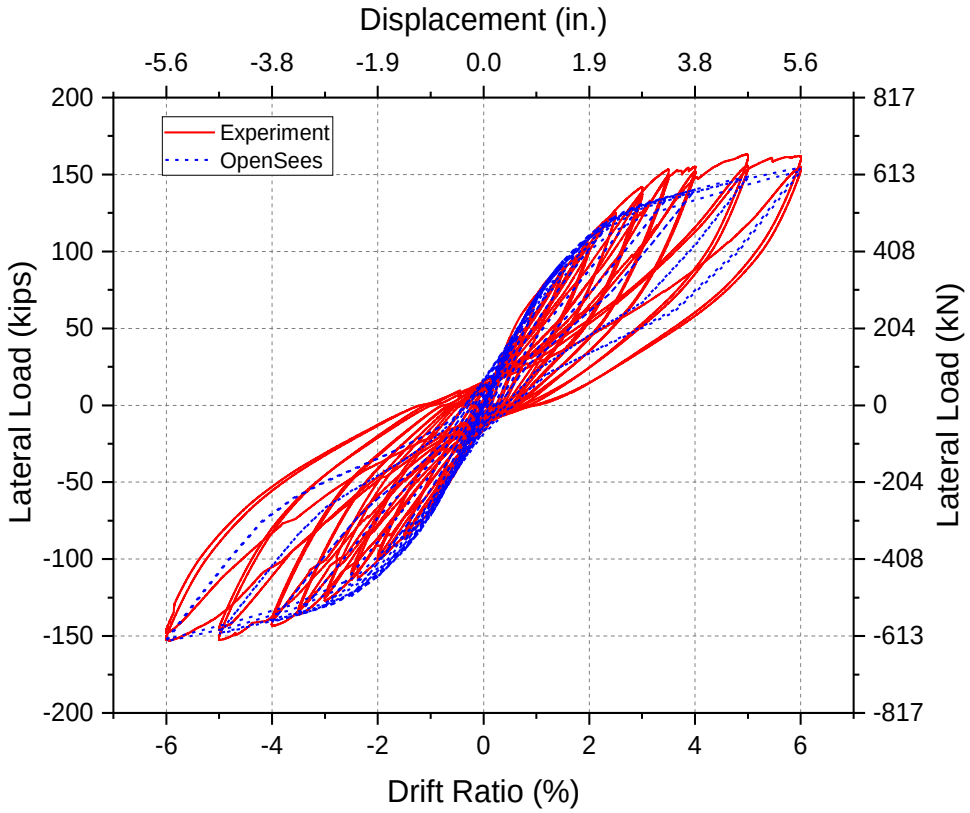

Figure 6.2 Hysteresis comparison between experiment and numerical model

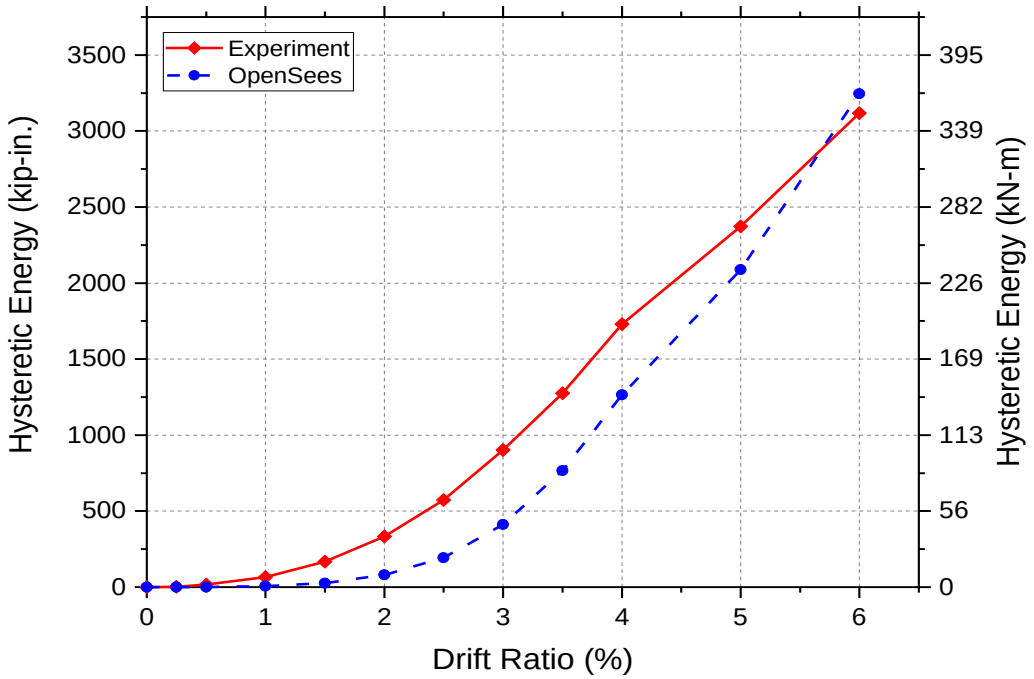

Figure 6.3 Comparison of cumulative energy dissipation

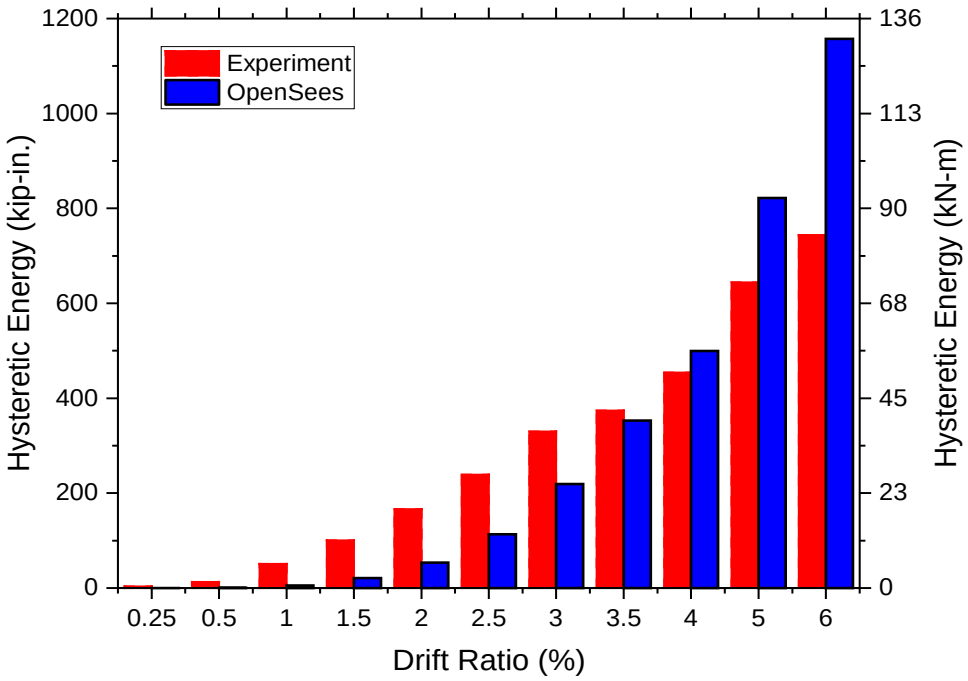

Figure 6.4 Comparison of hysteretic energy at each drift ratios between experimental and analytical model

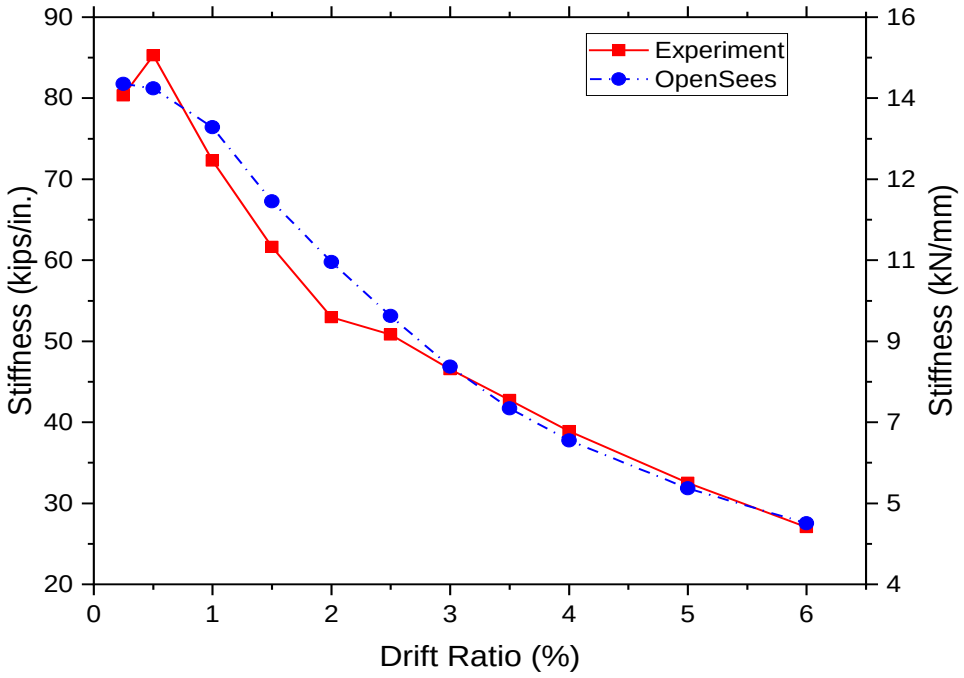

Figure 6.5 Comparison of stiffness degradation

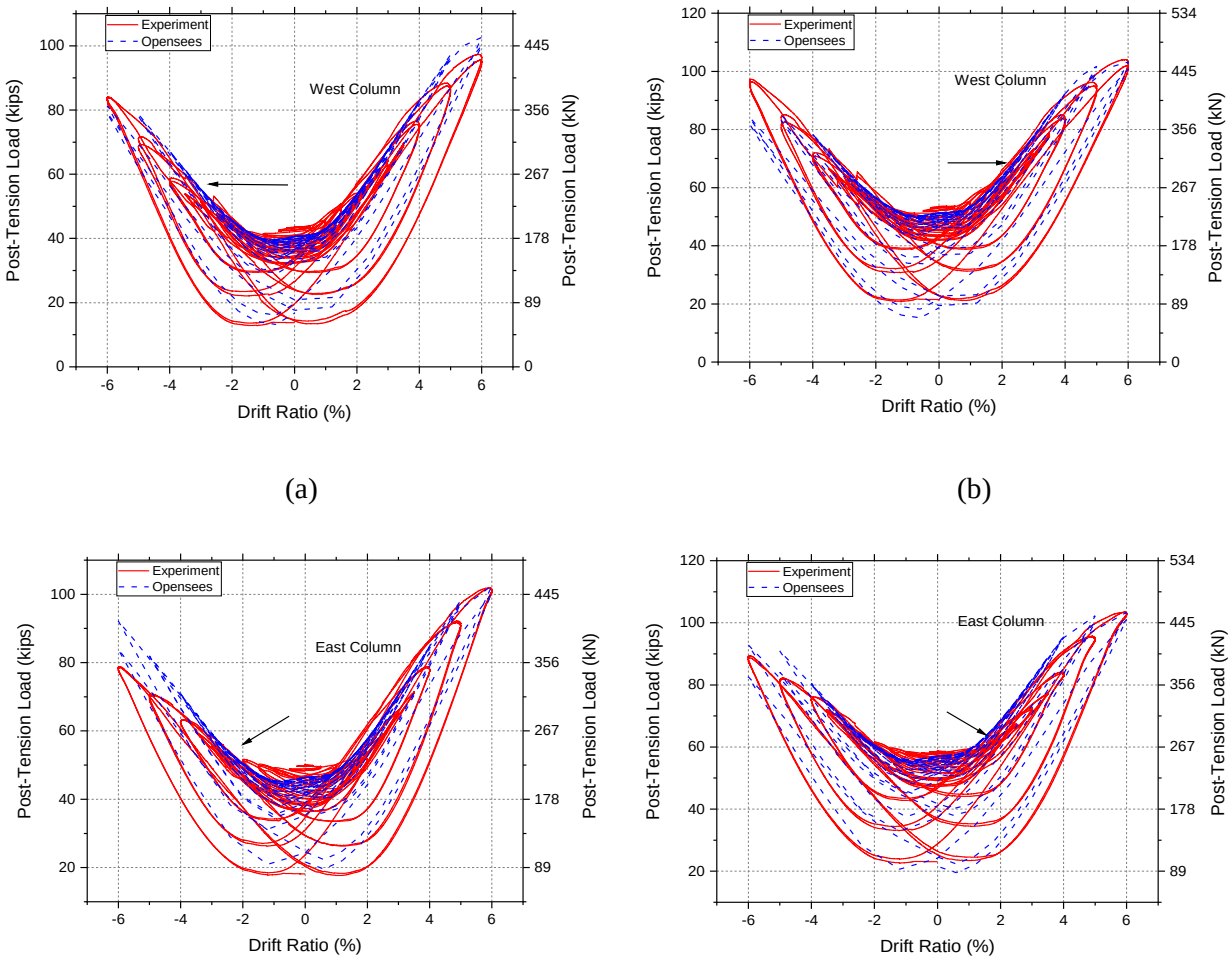

Figure 6.6 Comparison of PT forces at different drift ratio

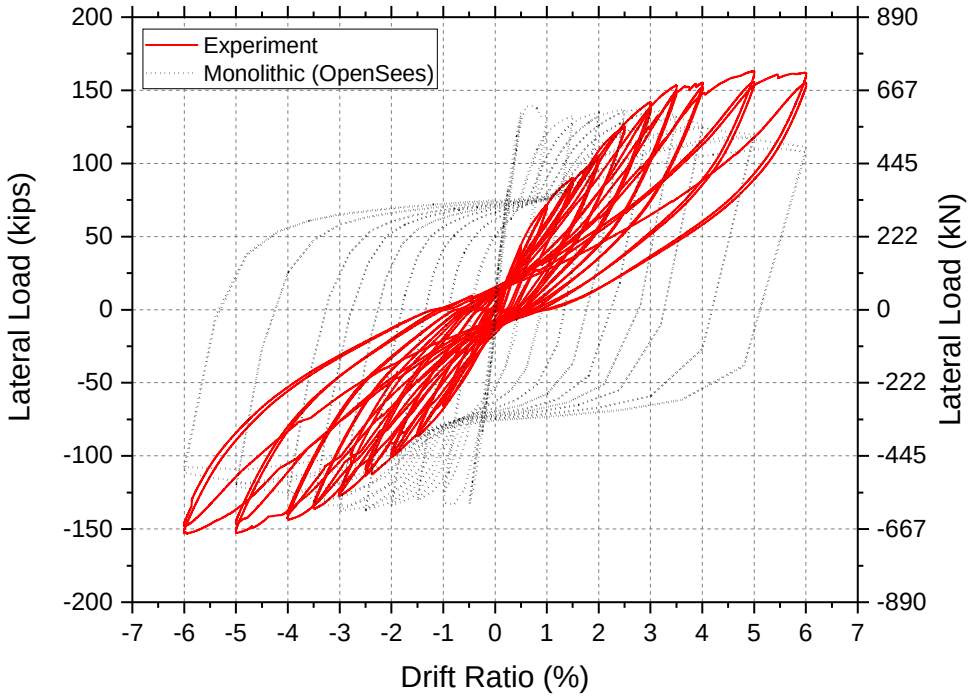

(a)

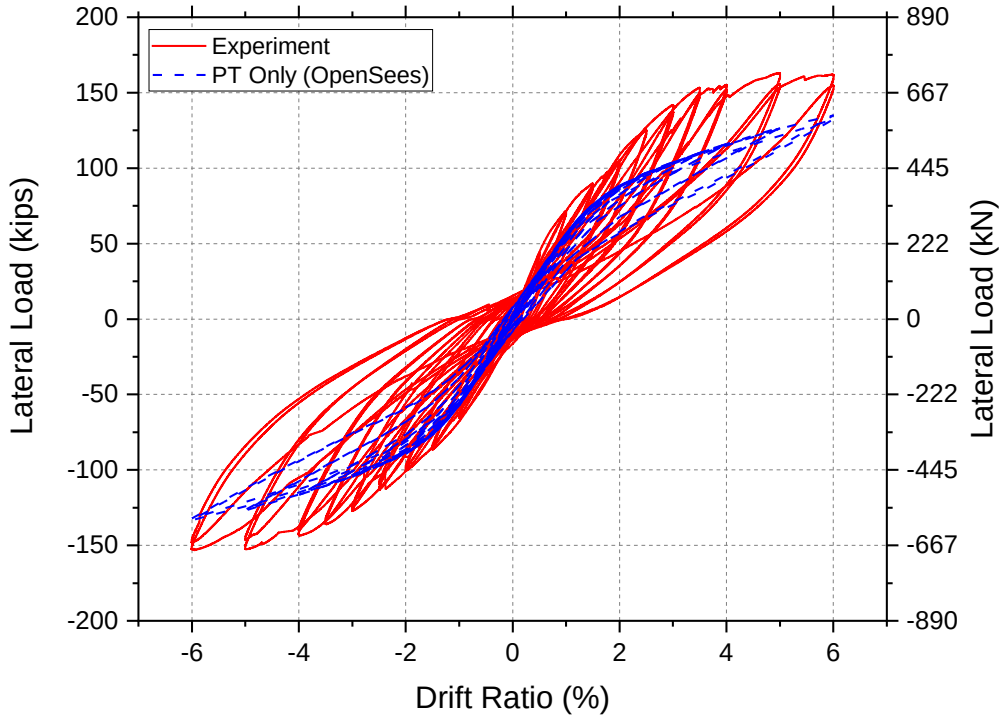

(b)

Figure 6.7 Hysteresis curve comparison between PT bars with SLAs(experimental) with (a) Monolithic (OpenSees) and, (b) PT-only (OpenSees), bridge bent

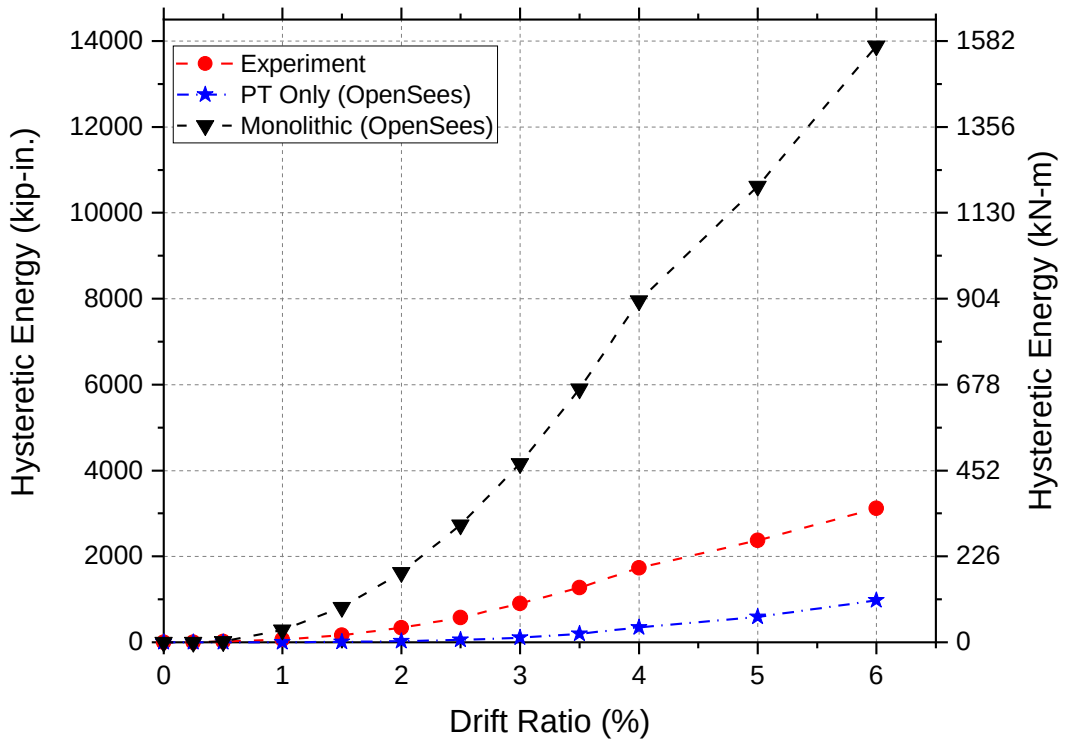

Figure 6.8 Hysteretic energy comparison between PT with SLAs(experimental), PT-only (OpenSees), and Monolithic (OpenSees) bridge bent

7. SUMMARY AND CONCLUSIONS

7.1 Summary

This research investigated a precast post-tensioned concrete bridge bent in seismic regions. Unbonded PT bars are used to encourage distributed straining of the PT bars in seismic events, re-centering of the system, and minimizing residual displacements. Energy dissipating devices in terms of stretch length bolts, and unbonded post-tensioning bars, are used to increase the hysteretic energy dissipation capacity of the whole system. Past research has suggested that hybrid systems are effective in seismic zones in terms of ductility, and minimal residual drift and therefore, can be used in ABC bridges. The precast PT bridge bent is a 42% scaled prototype of an actual bridge bent in Utah. The original bridge bent consists only of bonded PT bars without energy dissipating devices. However, the scaled bridge bent used in the experiment used unbonded PT bars with external energy dissipators in the form of stretch length bolts, which are easily replaceable after earthquakes.

The tested specimen consists of two precast footings, two columns, and a cap-beam. All the precast components are connected by four PT bars, two per column. In addition, the SLAs connect the two footings with the columns and the two columns with the cap-beam. The SLAs are very effective in dissipating energy and are replaceable. Mainly the size and shape of the bridge-bent was scaled down to 42% of the actual bridge bent, and the reinforcement and PT bar ratios were designed specifically for this project. The columns, footings, and cap-beam were heavily reinforced, and concrete compressive strength was equal to 12,500 psi (86 MPa) using self-consolidating concrete. The footings had a 2 in. (51 mm) deep octagonal recess, which acted as a shear-key to transfer loads from the columns to the footings. A ½ in. (13 mm) thick steel plate, and ½ in. (13 mm) thick polyurethane pad were used in the recess to prevent concrete from crushing. Steel chairs were welded around the faces of the octagonal columns both at the top and bottom through which SLAs were secured and tightened against the coupler-bent bar assembly embedded in the footings and the cap-beam. The PT bars were pre-tensioned with 52 kips (231 kN) on average per column before starting the test. A combined axial load of 150 kips (667 kN) was applied to simulate gravity load. A displacement-based lateral quasi-static load was applied to the specimen. The specimen was tested up to a 6% drift ratio, when the PT bars had yielded. The use of replaceable components such as stretch length anchors, which act as an energy dissipation tension-only element, combined with PT bars as the re-centering element was investigated. The performance of the specimen was evaluated under different seismic parameters such as hysteretic energy dissipation, lateral load capacity, stiffness degradation, gap opening, and damage to the structure. An analytical model was developed in OpenSees to evaluate the behavior of the system numerically.

7.2 Conclusions

An experiment for a precast, unbonded PT bridge bent specimen, with external energy dissipators has been conducted to evaluate the seismic performance and rocking behavior of such hybrid systems and their future use in real bridges in seismic zones. The experimental test data provided qualitative and quantitative measures to study the performance of the bridge bent under quasi-static cyclic loads. A summary and conclusions of the experimental study are presented as follows:

- This research is unique because limited research has been done on precast PT concrete bridge bents with large scale specimens. Much research on PT systems is focused on single columns. This is the first time PT bars were combined with SLAs in a hybrid system. PT bars were combined with SLAs in a tension-only hybrid bridge bent for the first time. The bridge bent can recover after an earthquake and be functional by replacing the SLAs in the hexagonal couplers embedded in the footings and cap beam.
- The structural system displayed adequate lateral strength with stable and symmetric hysteresis. Rocking of the precast concrete columns was controlled without stability or twisting issues and a smooth stiffness degradation was observed — a maximum rotation of 0.059 radians was measured.
- Steel chairs performed elastically without any damage. The SLAs acted in tension and bending, and the bolts yielded and elongated, as can be observed in the strain profiles. The bolts started yielding at a 1.2% drift ratio and dissipated a substantial amount of hysteretic energy. All bolts at the top of the two columns elongated ½ in. (13 mm). The east and west bolts of the west column at the bottom elongated ¾ in. (19 mm). The west and east bolts at the bottom of the east column elongated 3/8 in. (9.5 mm) and 3/16 in. (4.8 mm) respectively. The elongation of the bolts is approximately 4% on average of the original stretch length of 12½ in. (318 mm). The strains in the bolts started to drop at a 5% drift ratio when the PT bars started to dominate in sharing the lateral load.
- The total cumulative hysteretic energy dissipated throughout the test was 3117 kips-in. (352 kN-m). The energy dissipation coefficient was well above 0.1, which is the minimum required value to avoid a large scatter in displacement demands of a purely rocking system. The bolts served their purpose of being easily replaceable after an earthquake, as evidenced by the fact that the damaged bolts were taken out easily from the specimen after the end of the test.
- The combination of axial load and PT force from the two columns re-centered the bridge bent near its original position. The residual drift of the specimen after the test was 1.0% for the positive (push) direction and 1.1% for the negative (pull) direction. The re-centering coefficient was significantly lower than the maximum value of 0.6 for most of the tests. The relative self-centering efficiency (RSE) was above 82%. The PT bars behaved elastically for the majority of the test and reached 80% of their ultimate tensile capacity on average. Three of the PT bars yielded during the last drift ratio of 6.0% imposed in the experiment. The losses on the PT bars were attributed to compressive stresses from the axil load and PT, friction loss, anchorage slip, relaxation of the PT bars, and yielding of the mild steel and concrete crushing.
- The bridge system experienced little damage, and no significant damage to the structure was observed throughout the experiment. Concrete spalling over the bottom east face of both columns was observed; however, spalling was not significant and did not compromise the strength of the specimen. The east column sustained most of the damage with concrete spalling over its bottom

east face, and cracks and spalling developed over its top west face. Minor spalling with a maximum depth of 1 in. (25 mm) was observed at 12 in. (305 mm) above the footing and 11 in. (280 mm) below the cap-beam, which is just above the theoretical plastic hinge length; the plastic hinge length is assumed as half the column width or 9 in. (229 mm) for the column. The steel collar prevented the column toe from experiencing damage. Polyurethane pads placed at the bottom of the column prevented the column toe from crushing and helped to re-center the column. All the damage observed was just above the steel collar at the bottom and just below the steel collar at the top, respectively.

- By comparing the experimental results with the analytical model developed in OpenSees, it was evident that the analytical model was capable of capturing initial stiffness, lateral strength, drift ratio, total energy dissipation of the system, forces in the PT bars, and PT losses with good accuracy. The assumed bed of distributed compression-only elastic springs captured the rocking behavior of the columns. A similar analytical model could be used to predict the behavior of actual bridge structures and analyze their seismic behavior.
- Comparison of the experimental test results with the analytical model of an equivalent monolithic bridge bent and a bridge bent with PT bars only excluding the SLAs demonstrates the benefits and advantages of the hybrid system for use in high seismic zones. The equivalent monolithic bridge bent dissipated a large amount of hysteretic energy, four and one-half times larger than the hybrid system, but sustained large residual drifts and severe damage, which make it unusable after an earthquake. Similarly, the bridge bent with PT bars only, displayed excellent self-centering properties, with five times less residual drift than the tested bridge bent. However, the lateral strength of the PT-only bent was reduced compared to the bridge bent tested; the hysteretic energy dissipation capacity was only one-third the capacity of the hybrid bridge bent. Given the observed residual displacement, self-centering, lateral strength, energy dissipation, and minimal damage of the tested hybrid bridge bent, it is recommended that it can be used in the construction of bridges in high seismic zones.

7.3 Recommendations for Further Research

Future research should focus more on the performance of the steel chairs and SLAs to improve existing knowledge of these connections between footings to columns and columns to cap beam. More research should be carried out on stretch length bolt connections with PT bars at a larger scale, with different loading protocols and shake table tests. It is recommended to use the height of steel jacket equal to two times the plastic hinge length, equivalent to one column diameter. It is recommended to carry out similar experiments using low-relaxation steel prestressing strands in place of PT bars. Experimental tests using a different combination of axial load, initial post-tensioning, and number of SLAs should be performed to improve the self-centering capacity of the specimen with minimal residual drift and higher energy dissipation. To improve construction efficiency, seven sides of the steel collar could be cast inside the forms — the eighth side would then be assembled using a plug weld and two side welds. Upset stretch length anchors could be used instead of the hexagonal couplers used in the present research to avoid issues with jammed anchors. Simplified design guidelines need to be developed to allow engineers to design precast PT bridge bents with these types of connections.

The analytical model developed in this research can be improved to capture the dynamic seismic behavior of similarly designed hybrid bridge bents, strength and stiffness degradation, and residual displacement of an actual bridge under seismic loads. Although columns of the tested specimen had an octagonal cross-section, the analytical model used an equivalent circular column because of the simpler fiber discretization available for the circular section in OpenSees. Though this might have little impact on the overall performance of the model, the improved model with an automated discretization of the typical concrete section can result in higher accuracy. Future analytical models should carry out incremental dynamic analyses to capture response of the bridge bent under near-field and far-field earthquakes. Future research must focus on simulating the rocking behavior of the PT column and the gap-opening phenomenon.

REFERENCES

Ameli, M. J. (2016). “Seismic Evaluation of Grouted Splic Sleeve Connections for Bridge Piers in Accelerated Bridge Construction.” PhD Dissertation, The University of Utah, Salt Lake City, UT.

Ameli, M. J., Brown, D. N., Parks, J. E., and Pantelides, C. P. (2016). “Seismic Column-to-Footing Connections Using Grouted Splice Sleeves.” *ACI Structural Journal*, 113(5), 1021–1030.

Ameli, M. J., and Pantelides, C. P. (2017). “Seismic Analysis of Precast Concrete Bridge Columns Connected with Grouted Splice Sleeve Connectors.” *Journal of Structural Engineering*, 143(2), 1–13.

Ameli, M. J., Parks, J. E., Brown, D. N., and Pantelides, C. P. (2015). “Seismic Evaluation of Grouted Splice Sleeve Connections for Reinforced Precast Concrete Column-to-Cap Beam Joints in Accelerated Bridge Construction.” *PCI Journal*, 60(2), 80–103.

Billington, S. L., and Yoon, J. K. (2004). “Cyclic Response of Unbonded Posttensioned Precast Columns with Ductile Fiber-Reinforced Concrete.” *Journal of Bridge Engineering*, 9(4), 353–363.

Bowman, B. W. (2016). “Modeling of Post-Tensioned Rocking Bridge Columns.” MS Thesis, University of Colorado, Boulder, CO.

Brenes, F. J., Wood, S. L., and Kreger, M. E. (2006). “Anchorage Requirements for Grouted Vertical-Duct Connectors in Precast Bent Cap Systems.” *Report No. FHWA/TX-06/0-4176-1*, Center for Transportation Research, University of Texas at Austin.

Cheng, X., Erochko, J. A., and Lau, D. T. (2017). “Improving the Seismic Performance of Existing Bridge Structures Using Self-Centering Dampers.” *Proceedings of 16th World Conference on Earthquake*, Santiago, Chile.

Chopra, A. K. (2007). *Dynamics of Structures, Theory and Application to Earthquake Engineering*. Pearson and Prentice Hall, Upper Saddle River, Nj.

Chou, C. C., and Chen, Y. C. (2006). “Cyclic Tests of Post-Tensioned Precast CFT Segmental Bridge Columns with Unbonded Strands.” *Earthquake Engineering and Structural Dynamics*, 35(2), 159–175.

Chowdhury, M. A. (2018). “Cyclic Performance of Self-Centering Post-Tensioned Steel Beam-Column Connections Using Shape Memory Alloy Energy Dissipators.” MS Thesis, The University of British Columbia, Vancouver, British Columbia.

Culmo, M. P. (2009). “Connection Details for Prefabricated Bridge Elements and Systems.” *Report No. FHWA-IF-09-010*, Federal Highway Administration, Virginia.

Currie, M. C. (2009). “Self-Centering Bridge Pier Columns with Structural Fuses.” MS Thesis, Iowa State University, Ames, Iowa.

Davoudi, R., Ghassemieh, M., and Khanmohammadi, M. (2014). “Seismic Performance of Self-Centering Bridge Pier using Seat Angles.” *International Journal for Engineering Modelling*, 27(1–2), 11–19.

Dutta, A., and Mander, J. B. (1999). “Seismic Fragility Analysis for Highway Bridges.” *Proc., Center-to-center Project Workshop on Earthquake Engineering in Transportation Systems*, 311–325.

El-sheikh, M. T., Sause, R., and Pessiki, S. (1999). “Seismic Behavior and Design of Unbonded Post-Tensioned Precast Frames.” *PCI Journal*, 44(3), 54–88.

ElGawady, M. A., and Sha’lan, A. (2010). “Seismic Behavior of Self-Centering Precast Segmental Bridge Bents.” *Journal of Bridge Engineering*, 16(3), 328–339.

Guerrini, G., Restrepo, J. I., Massari, M., and Vervelidis, A. (2014). “Seismic Behavior of Posttensioned Self-Centering Precast Concrete Dual-Shell Steel Columns.” *Journal of Structural Engineering*, 141(4), 04014115.

Guerrini, G., Restrepo, J. I., Vervelidis, A., and Massari, M. (2015). “Self-Centering Precast Concrete Dual-Steel-Shell Columns for Accelerated Bridge Construction : Seismic Performance, Aanalysis, and Design.” *PEER Report 2015/13*, Pacific Earthquake Engineering Research Center, University of California, Berkley, CA.

Guo, A., and Gao, H. (2016). “Seismic Behavior of Posttensioned Concrete Bridge Piers with External Viscoelastic Dampers.” *Hindawi Publishing Corporation*, 2016, 1–12.

Haber, Z. B., Saiid Saiidi, M., and Sanders, D. H. (2015). “Behavior and Simplified Modeling of Mechanical Reinforcing Bar Splices.” *ACI Structural Journal*, 112(2), 179–188.

Han, Q., Jia, Z., Xu, K., Zhou, Y., and Du, X. (2019). “Hysteretic Behavior Investigation of Self-Centering Double-Column Rocking Piers for Seismic Resilience.” *Engineering Structures*, Elsevier Ltd, 188, 218–232.

Haraldsson, O. S., Janes, T. M., Eberhard, M. O., and Stanton, J. F. (2013). “Seismic Resistance of Socket Connection between Footing and Precast Column.” *Journal of Bridge Engineering*, 18(9), 910–919.

Hewes, J. T., and Priestley, M. J. N. (2002). “Seismic Design and Performance of Precast Concrete Segmental Bridge Column.” *Report No. SSRP-2001/25*, University of California, San Diego, CA.

Jansson, P. o. (2008). “Evaluation of Grout-Filled Mechanical Splices for Precast Concrete Construction.” *Report No. R-1512*, Michigan Department of Transportation, Lansing, MI.

Khaleghi, B., Schultz, E., Seguirant, S., Marsh, L., Haraldsson, O., Eberhard, M., and Stanton, J. (2012). “Accelerated Bridge Construction in Washington State: From Research to Practice.” *PCI Journal*, 57(4), 34–49.

Lee, W. K., and Billington, S. L. (2009). “Simulation and Performance-Based Earthquake Engineering Assessment of Self-Centering Post-Tensioned Concrete Bridge Systems.” *PEER Report 2009/109*, Pacific Earthquake Engineering Research Center, University of California, Berkeley,CA.

Liu, R., and Palermo, A. (2017). “Quasi-Static Testing of a 1/3 Scale Precast Concrete Bridge Utilising a Post-Tensioned Dissipative Controlled Rocking Pier.” *Proceedings of 16th World Conference on Earthquake*, Santiago, Chile.

Makris, N., and Roussos, Y. (1998). “Rocking Response and Overturning of Equipment Under Horizontal Pulse-Type Motions.” *Report PEER-1998/05*, Pacific Earthquake Engineering Research Center, College of Engineering, University of California, Berkeley, CA.

Mander, J. B., and Cheng, C. T. (1997). “Seismic Resistance of Bridge Piers Based on Damage Avoidance Design.” *Technical Report NCEER-97-0014*, National Center for Earthquake Engineering Research,University at Buffalo, NY.

Marriot, D. (2009). “The Development of High-Performance Post-Tensioned Rocking Systems for the Seismic Design of Structures.” PhD Dissertation, University of Canterbury, Christchurch, New Zealand.

Marriott, D., Pampanin, S., and Palermo, A. (2009). “Quasi-Static and Pseudo-Dynamic Testing of Unbonded Post-Tensioned Rocking Bridge Piers with External Replaceable Dissipaters.” *Earthquake Engineering & Structural Dynamics*, 41(11), 1549–1568.

Marriott, D., Pampanin, S., and Palermo, A. (2011). “Biaxial Testing of Unbonded Post-Tensioned Rocking Bridge Piers with External Repalceable Dissipaters.” *Earthquake Engineering & Structural Dynamics*, 41(11), 1549–1568.

Mashal, M., and Palermo, A. (2019). “Low-Damage Seismic Design for Accelerated Bridge Construction.” *Journal of Bridge Engineering*.

Mashal, M., Palermo, A., and Chegini, Z. (2014). “Quasi-Static Cyclic Tests of Half-Scale Fully Precast Bridge Bents Incorporating Emulative and Post-Tensioned Low Damage Solutions.” *Proceedings of Second European Conference on Earthquake Engineering and Seismology*, Istanbul, Turkey.

McKenna, F., Scott, M. H., and Fenves, G. L. (2010). “Nonlinear Finite-Element Analysis Software Architectire Using Object Composition.” *Jounal of Computing in Civil Engineering*, 24(1), 95–107.

Mehrsoroush, A. (2014). “Experimental and Analytical Seismic Studies of Bridge Piers with Innovative Pipe Pin Column-Footing Connections and Precast Cap Beams.” PhD Dissertation, University of Nevada, Reno, NV.

Motaref, S., Saiidi, M. S., and Sanders, D. H. (2011). “Seismic Response of Precast Columns with Energy Dissipating Joints.” *Report No. CA12-1999*, Center for Civil Engineering Earthquake Research, Department of Civil Engineering, University of Nevada, Reno, NV.

New Zealand Concrete Society Inc. (2010). *PRESS Design Handbook*. Auckland, New Zealand.

Nikoukalam, M. T., and Sideris, P. (2017). “Resilient Bridge Rocking Columns with Polyurethane Damage-Resistant End Segments and Replaceable Energy-Dissipating Links.” *Journal of Bridge Engineering*, 22(10), 1–14.

Ou, Y.-C., Tsai, M.-S., Chang, K.-C., and Lee, G. C. (2010). “Cyclic Behavior of Precast Segmental Concrete Bridge Columns with High Performance or Conventional Steel Reinforcing Bars as Energy Dissipation Bars.” *Earthquake Engineering & Structural Dynamics*, 39, 1181–1198.

Ou, Y.-C., Wang, P.-H., Tsai, M.-S., Chang, K.-C., and Lee, G. C. (2009). “Large-Scale Experimental Study of Precast Segmental Unbonded Posttensioned Concrete Bridge Columns for Seismic Regions.” *Journal of Structural Engineering*, 136(3), 255–264.

Ou, Y. (2007). “Precast Segmental Post-Tensioned Concrete Bridge Coluymn for Seismic Regions.” PhD Dissertation, State University of New York, Buffalo, NY.

Palermo, A., and Mashal, M. (2012). “Accelerated bridge construction (abc) and seismic damage resistant technology: A new zealand challenge.” *Bulletin of the New Zealand Society for Earthquake Engineering*, 45(3), 123–134.

Palermo, A., Pampanin, S., and Marriott, D. (2007). “Design, Modeling, and Experimental Response of Seismic Resistant Bridge Piers with Post-Tensioned Dissipating Connections.” *Journal of Structural Engineering*, 133(11), 1648–1661.

Pang, J. B. K., Eberhard, M. O., and Stanton, J. F. (2010). “Large-Bar Connection for Precast Bridge Bents in Seismic Regions.” *Journal of Bridge Engineering*, 15(3), 231–239.

Parks, J. E., Pantelides, C. P., Ibarra, L., and Sanders, D. H. (2019). “Stretch Length Anchor Bolts Under Combined Tension and Shear.” *ACI Structural Journal*, 115(5), 1317–1328.

Priestley, M. J. N., Seible, F., and Calvi, G. M. (1996). *Seimic Design and Retrofit of Bridges*. John Wiley & Sons, Inc., New York.

Priestley, M. J. N., Sritharan, S. S., Conley, J. R., and Pampanin, S. (1999). “Preliminary Results and Conclusions from the PRESSS Five-Story Precast Concrete Test Building.” *PCI Journal*, 44(6), 42–67.

Raynor, D. J., Lehman, D. E., and Stanton, J. F. (2002). “Bond-Slip Response of Reinforcing Bars Grouted in Ducts.” *ACI Structural Journal*, 99(5), 568–576.

Restrepo, J. I., and Rahman, A. (2007). “Seismic Performance of Self-Centering Structural Walls Incorporating Energy Dissipators.” *Journal of Structural Engineering, ASCE*, 133(4), 484–494.

Routledge, P. J., Cowan, M. J., and Palermo, A. (2016). “Low-Damage Detailing for Bridges – A Case Study of Wigram-Magdala Bridge.” *Proceedings of 2016 NZSEE Conference*, New Zealand.

Sideris, P., Aref, A. J., and Filiatrault, A. (2014a). “Quasi-Static Cyclic Testing of a Large-Scale Hybrid Sliding-Rocking Segmental Column with Slip-Dominant Joints.” *Journal of Bridge Engineering*, 19(10).

Sideris, P., Aref, A. J., and Filiatrault, A. (2014b). “Quasi-Static Cyclic Testing of a Large-Scale Hybrid Sliding-Rocking Segmental Column with Slip-Dominant Joints.” *Journal of Bridge Engineering*, 19(10), 1–11.

Soules, J. G. (Greg), Bachman, R. E., and Silva, J. F. (2016). “Chile Earthquake of 2010: Assessment of Industrial Facilities around Concepcion.” ASCE/SEI, Reston, VA, 105.

Stanton, J., Stone, W. C., and Cheok, G. S. (1997). “A Hybrid Reinforced Precast Frame for Seismic Regions.” *PCI Journal*, 42(2), 20–32.

Steuck, K. P., Eberhard, M. O., and Stanton, J. F. (2009). “Anchorage of Large-Diameter Reinforcing Bars in Ducts.” *ACI Structural Journal*, 106(4), 506–513.

Tazarv, M., and Saiidi, M. S. (2015). “UHPC-Filled Duct Connections for Accelerated Bridge Construction of RC Columns in High Seismic Zones.” *Engineering Structures*, Elsevier Ltd, 99, 413–422.

Trautner, C. A., Hutchinson, T. C., and Grosser, P. R. (2014). “Cyclic Behavior of Structural Base Plate Connections with Ductile Fastening Failure: Component Test Results.” *Proceedings of 10th U.S. National Conference on Earthquake Engineering*, Earthquake Engineering Research Institute, Anchorage, AK.

Trautner, C., Hutchinson, T., Copellini, M., Grosser, P., Bachman, R., and Silva, J. (2017). “Developing Ductility Using Concrete Anchorage.” *ACI Structural Journal*, 114(1), 101–112.

Trono, W. D. (2014). “Earthquake Resilient Bridge Columns Utilizing Damage Resistant Hybrid Fiber Reinforced Concrete.” PhD Dissertation, University of California, Berkley, CA.

Wacker, J. M., Hieber, D. G., Stanton, J. F., and Eberhard, M. O. (2005). “Design of Precast Concrete Piers for Rapid Bridge Construction in Seismic Regions.” *Report No. WA-RD 629.1*, Washington State Transportation Center (TRAC), University of Washington, Seattle, WA.

Wang, J.-C., Ou, Y.-C., Chang, K.-C., and Lee, G. C. (2008). “Large-Scale Seismic Tests of Tall Concrete Bridge Columns with Precast Segmental Construction.” *Earthquake Engineering and Structural Dynamics*, 37(November 2007), 1449–1465.

Wang, Z., Li, T., Qu, H., Wei, H., and Li, Y. (2019). “Seismic Performance of Precast Bridge Columns with Socket and Pocket Connections Based on Quasi-Static Cyclic Tests: Experimental and Numerical Study.” *Journal of Bridge Engineering*, 24(11), 04019105.

White, S. (2014). “Controlled Damage Rocking Systems for Accelerated Bridge Construction.” MS Thesis, University of Canterbury, Christchurch, New Zealand.

White, S., and Palermo, A. (2016). “Quasi-Static Testing of Posttensioned Nonemulative Column-Footing Connections for Bridge Piers.” *Journal of Bridge Engineering*, 21(6), 04016025.

WisDOT. (2019). “WisDOT Bridge Manual.” Wisconsin Department of Transportation, WI, Wisconsin.

Yamashita, R., and Sanders, D. H. (2009). “Seismic Performance of Precast Unbonded Prestressed Concrete Columns.” *ACI Structural Journal*, 106(6), 821–830.